AD-A069 984 WESTINGHOUSE DEFENSE AND ELECTRONIC SYSTEMS CENTER B--ETC F/G 9/5
NEAR FIELD BLOCKAGE OF AN ULTRA LOW SIDELOBE ANTENNA (ULSA). PA--ETC(U)
DEC 77 S G WINCHELL, D DAVIS N00173-77-C-0106
UNCLASSIFIED 77-1070-PT-1 NL

1 OF 2
AD
A069984

AD A069984
DDC FILE COPY

N00173-77-C-0100-100

LEVEL II

NEAR FIELD BLOCKAGE OF AN ULTRA LOW SIDELOBE ANTENNA (ULSA)

PART 1

PT-2 B037 885L

Stephen G. Winchell
Daniel Davis
Westinghouse D&ESC
Systems Development Division
Baltimore, Maryland

DDC
RECEIVED
JUN 18 1979
C

December 1977

Final Report For Period May 1977-December 1977

Prepared For
Naval Research Laboratory
Washington, D.C.

This document has been approved for public release and sale; its distribution is unlimited.

79 03 23 043

UNCLASSIFIED

SECURITY CLASSIFICATION OF THIS PAGE (When Data Entered)

REPORT DOCUMENTATION PAGE

READ INSTRUCTIONS BEFORE COMPLETING FORM

1. REPORT NUMBER: N00173-77-C-01-6-100

2. GOVT ACCESSION NO.

3. RECIPIENT'S CATALOG NUMBER

4. TITLE (and Subtitle): Near Field Blockage of an Ultra Low Sidelobe Antenna (ULSA). Part 1.

5. TYPE OF REPORT & PERIOD COVERED: Final Report. May - Dec 77, 5/77 - 12/77

6. PERFORMING ORG. REPORT NUMBER: 77-1070-PT-1

7. AUTHOR(s): Stephen G. Winchell, Daniel Davis

8. CONTRACT OR GRANT NUMBER(s): N00173-77-C-0106

9. PERFORMING ORGANIZATION NAME AND ADDRESS: Westinghouse Defense & Electric Systems Center, Systems Development Division, Baltimore, Maryland

10. PROGRAM ELEMENT, PROJECT, TASK AREA & WORK UNIT NUMBERS

11. CONTROLLING OFFICE NAME AND ADDRESS: Naval Research Laboratory, 4555 Overlook Avenue S.W., Washington, D.C. 20375

12. REPORT DATE: December 1977

13. NUMBER OF PAGES: 104

14. MONITORING AGENCY NAME & ADDRESS (if different from Controlling Office): (12) 104p.

15. SECURITY CLASS. (of this report): Unclassified

15a. DECLASSIFICATION/DOWNGRADING SCHEDULE

16. DISTRIBUTION STATEMENT (of this Report): This document has been approved for public release and sale; its distribution is unlimited.

17. DISTRIBUTION STATEMENT (of the abstract entered in Block 20, if different from Report)

18. SUPPLEMENTARY NOTES: See Part 2 (Proprietary)

19. KEY WORDS (Continue on reverse side if necessary and identify by block number)

Near Field Blockage
Radiation Patterns
Antenna

20. ABSTRACT (Continue on reverse side if necessary and identify by block number)

Near field blockage of an ultra low sidelobe antenna (ULSA) by several frequently encountered obstacles is studied both experimentally and analytically to determine how the radiation characteristics of the antenna are affected. The results are generalized over a wide range of obstacle sizes and distances for aperture illuminations ranging from conventional reflector-type distributions to ultra low sidelobe distributions. These

DD FORM 1 JAN 73 1473 EDITION OF 1 NOV 65 IS OBSOLETE

UNCLASSIFIED

70 03 23 04 405 897

results demonstrate that the superior ECCM characteristics of the ULSA are maintained in the shipboard environment. Blockage reduction techniques and comprehensive antenna siting analyses are discussed as possible areas of future study.

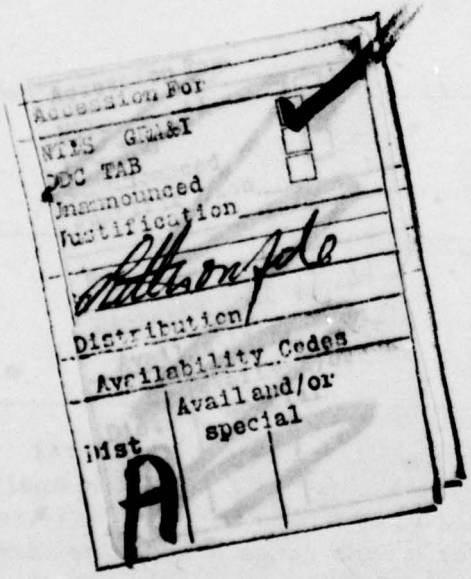

TABLE OF CONTENTS

		Page
1.	INTRODUCTION	7
2.	EXPERIMENTAL PHASE	11
2.1	X-Band Model	11
2.2	Experimental Setup	14
2.3	Obstacle Sizes and Placement	14
2.4	Results	16
3.	ANALYTICAL PHASE	19
3.1	Mast Blockage Analysis	19
3.1.1	Theoretical Background	21
3.1.2	Computer Simulation	23
3.1.2.1	Subaperture Size Considerations	24
3.1.2.2	Subaperture Illumination Functions	24
3.1.2.3	Bessel Function Upper Limit Determination	26
3.1.2.4	Experimental vs Theoretical Results	27
3.1.2.5	Reradiation of Scattered Fields	29
3.1.2.6	Blockage of the Scattered Fields by the Radiating Aperture	32
3.2	Yardarm Analysis	36
3.2.1	Theoretical Background	37
3.2.1.1	Normalization Approximation	37
3.2.1.2	Dual Beam Scattering	39
3.2.2	Computer Simulation	43
3.2.2.1	Normalization	43
3.2.2.2	Cylinder Illumination	43
3.2.2.3	Dual Beam Cylinder Radiation Patterns	44

TABLE OF CONTENTS (Continued)

		Page
3.2.2.4	Experimental vs Theoretical Results	45
3.3	Plate Blockage Analysis	49
3.3.1	Plate Geometry	51
3.3.2	Method of Calculation	51
3.3.3	Antenna Patterns	54
3.3.4	Blockage Region and Second Bounce Pattern Calculation	55
3.3.5	Grid Points and Grating Lobes	57
3.3.6	Experimental vs Theoretical Results	59
4.	GRAPHICAL SUMMARY OF RESULTS	67
4.1	Vertical Cylinder	67
4.2	Horizontal Cylinder	79
4.3	Flate Plate	85
5.	CONCLUSION	91
6.	RECOMMENDATIONS	93
	References	97
Appendix A	Measured Blockage Patterns	99
Appendix B	Mast/Yardarm Blockage Program - User Information	105
Appendix C	Flat Plate Blockage Program - User Information	147

LIST OF ILLUSTRATIONS

Figure		Page
1	L-Band Shipboard Blockage Environment	8
2	Stick Plane Radiation Pattern	12
3	Manifold Plane Radiation Pattern	13
4	Experimental Test Configuration	15
5	Rotating Antenna/Vertical Cylinder Blockage Geometry	20
6	Horizontal Line Source Blocked by a Vertical Cylinder	21
7	Subaperture Size Determination	25
8	Subaperture Illumination Functions	26
9	Vertical Cylinder Blockage, Obstacle Distance = 14 λ	28
10	Vertical Cylinder Blcokage, Obstacle Distance = 50 λ	30
11	Steered Beam Scattering Geometry	31
12	Vertical Cylinder Blockage-Horizontal Polarization	33
13	Vertical Cylinder Blockage-Vertical Polarization	34
14	Vertical Cylinder Blockage, Mast Bearing = -20°	35
15	Blockage of Scattered Energy from Vertical Cylinder	36
16	Rotating Antenna/Horizontal Cylinder Blockage Geometry	38
17	Normalization Geometry	40
18	Conical Scattering	41
19	Aperture and Cylinder Illumination Functions	42
20	Horizontal Cylinder Illumination Geometry	44
21	Dual Beam Geometry	45
22	Horizontal/Vertical Cylinder Blockage Geometry	47
23	Horizontal/Vertical Cylinder Blockage, Obstacle Bearing = 0°	48

LIST OF ILLUSTRATIONS (continued)

Figure		Page
24	Horizontal/Vertical Cylinder Blockage, Obstacle Bearing = -40°	50
25	Plate Geometry	51
26	Field Integration at Plate	52
27	Three Components of Resultant Pattern	53
28	Peak Directions of Radiation at Plate	55
29	Peak Direction of Second Bounce Off Antenna Face	57
30	Blockage Configuration Corresponding to Figure 32	59
31	Three Components of Plate Blockage Pattern of Figure 32	61
32	Computed and Measured Plate Blockage Patterns, Plate Bearing = -10°	63
33	Computed and Measured Plate Blockage Patterns, Plate Bearing = -20°	65
34	Vertical Cylinder Reference Blockage Configuration	68
35	Measured Vertical Cylinder Blockage, Obstacle Bearing = 0°	69
36	Measured Vertical Cylinder Blockage, Obstacle Bearing = -20°	70
37	Vertical Cylinder Blockage Dependence on Cylinder Diameter and Distance	71
38	Vertical Cylinder Blockage Dependence on Aperture Size and Illumination	72
39	Computed Rotating Antenna Pattern, 25 dB Taylor Distribution	76
40	Computed Rotating Antenna Pattern, 60 dB Taylor Distribution	77
41	Rotating Antenna Pattern Geometry	78
42	Horizontal Cylinder Reference Blockage Configuration	80
43	Measured Horizontal Cylinder Blockage, Obstacle Bearing = -40°	81

LIST OF ILLUSTRATIONS (continued)

Figure		Page
44	Horizontal Cylinder Blockage Dependence on Cylinder Diameter and Vertical Offset	82
45	Horizontal Cylinder Blockage Dependence on Cylinder Length and Distance	84
46	Plate Blockage Dependence on Aperture Illumination	86
47	Blocking Plate Clearing Critical Region	86
48	Plate Blockage Dependence on Plate Width and Bearing	88
49	Plate Blockage Dependence on Vertical Plate Offset and Separation	89
50	Blockage Reduction due to Absorber	95

1. INTRODUCTION

The purpose of this study was to determine whether or not an ultra low sidelobe antenna maintains significant EGCM characteristics in a shipboard environment. To answer this question, a two-phase study was proposed.

The experimental phase involved extensive measurements of the radiation patterns of an ultra low sidelobe antenna, blocked by several different types of near field obstacles. These measurements were made to determine the effect of the blockage on the sidelobe structure of the antenna.

The analytical phase of the study consisted of the development of several computer programs capable of computing the far field patterns of an antenna blocked by the same obstacles considered in the experimental phase.

Three different obstacles and their respective distances from the antenna were chosen to be representative of the situation that would be encountered by an L-band ultra low sidelobe antenna in a shipboard environment and are shown in figure 1. The mast is modeled by an infinite vertical cylinder located just outside the turning radius of the antenna. The yardarm passes through the center of the mast and is twice the length of the radiating aperture. It is simulated by a horizontal cylinder. Finally, another antenna is modeled by a flat plate located five aperture widths away from the antenna, and of the same size as the antenna.

The experimentally measured patterns will provide a wealth of information, and at the same time can be used to validate the analytical models. On the other hand, the analytical models can easily be used to analyze a wide range of blockage configurations that would be impossible to measure experimentally because of the limited nature of the study.

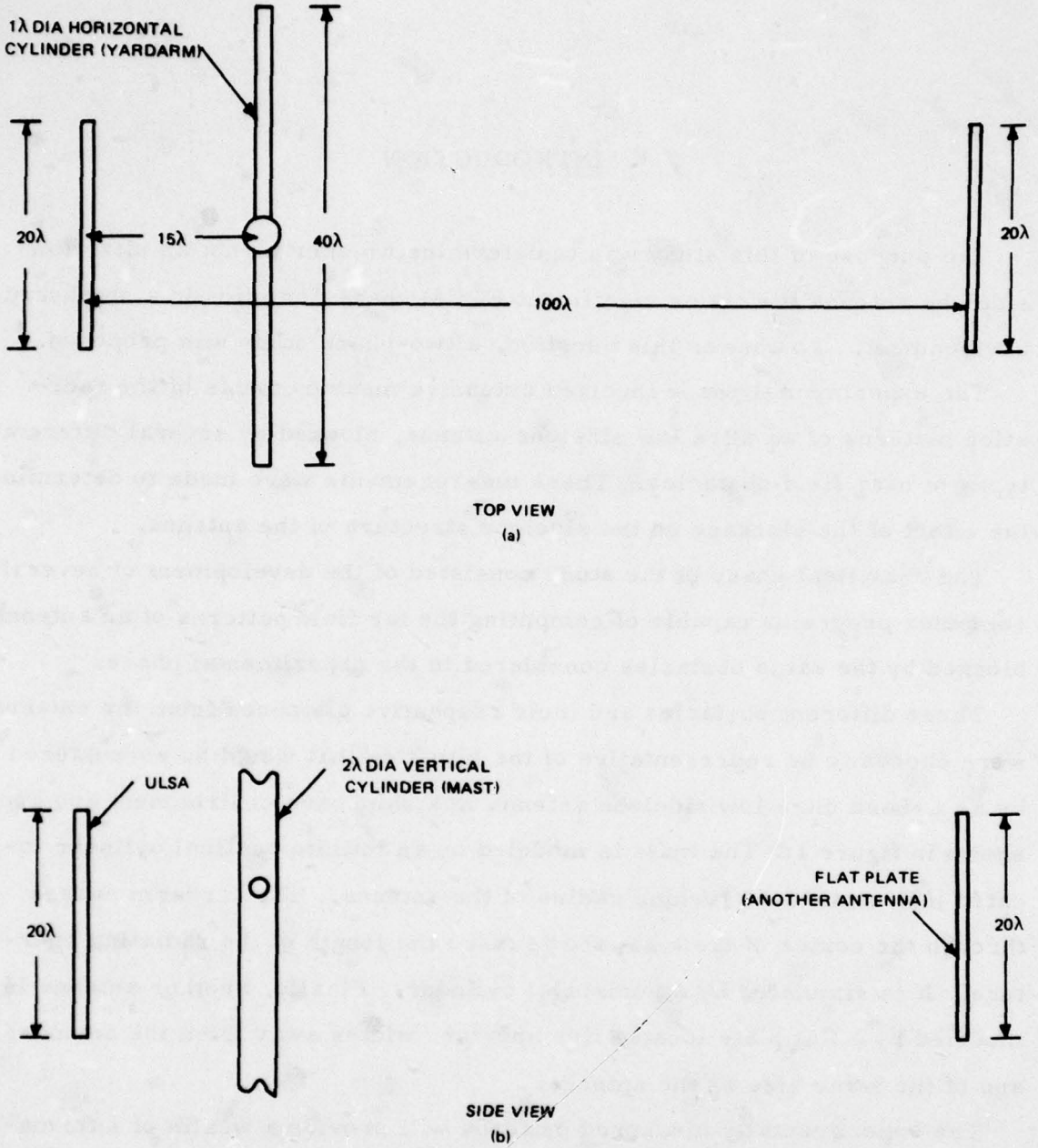

Figure 1. L-Band Shipboard Blockage Environment

Thus, by analyzing the near field blockage effects both experimentally and analytically, a comprehensive understanding of the blockage problem is attained, and the question of the effectiveness of an ultra low sidelobe antenna in a shipboard environment can be answered.

2. EXPERIMENTAL PHASE

An intensive experimental study was performed to determine the effects of near field blockage by three different types of obstacles: (1) a vertical cylinder, (2) a horizontal cylinder, and (3) a flat plate. Approximately 350 radiation patterns were recorded for a wide range of obstacle sizes and distances, and for both vertical and horizontal polarization. Selected cross-polarized blocked patterns were also measured. A complete list of all the configurations is included in Appendix A.

2.1 X-BAND MODEL

Duplicating the blockage configuration described in the introduction would be needlessly expensive. Aperture blockage effects are directly dependent on the wavelength of the radiated energy. As a result, the L-band blockage configuration can be exactly simulated at X-band by scaling all the lengths and distances accordingly.

The ultra low sidelobe antenna used for the blockage measurements was a pencil beam X-band resonant slotted waveguide array, approximately 18.5λ wide and 18.5λ high, radiating at 9.65 GHz. The illumination in both planes was designed to be a 42 dB Hamming function described by the function

$$f(x) = 0.08 + 0.92 \cos^2(x).$$

In the "stick plane," this illumination was successfully implemented, as shown by the measured radiation pattern in figure 2. However, in the "manifold plane," mutual coupling effects modified the distribution significantly, resulting in the measured pattern of figure 3. Consequently, the measured blockage results for vertical polarization must be interpreted accordingly.

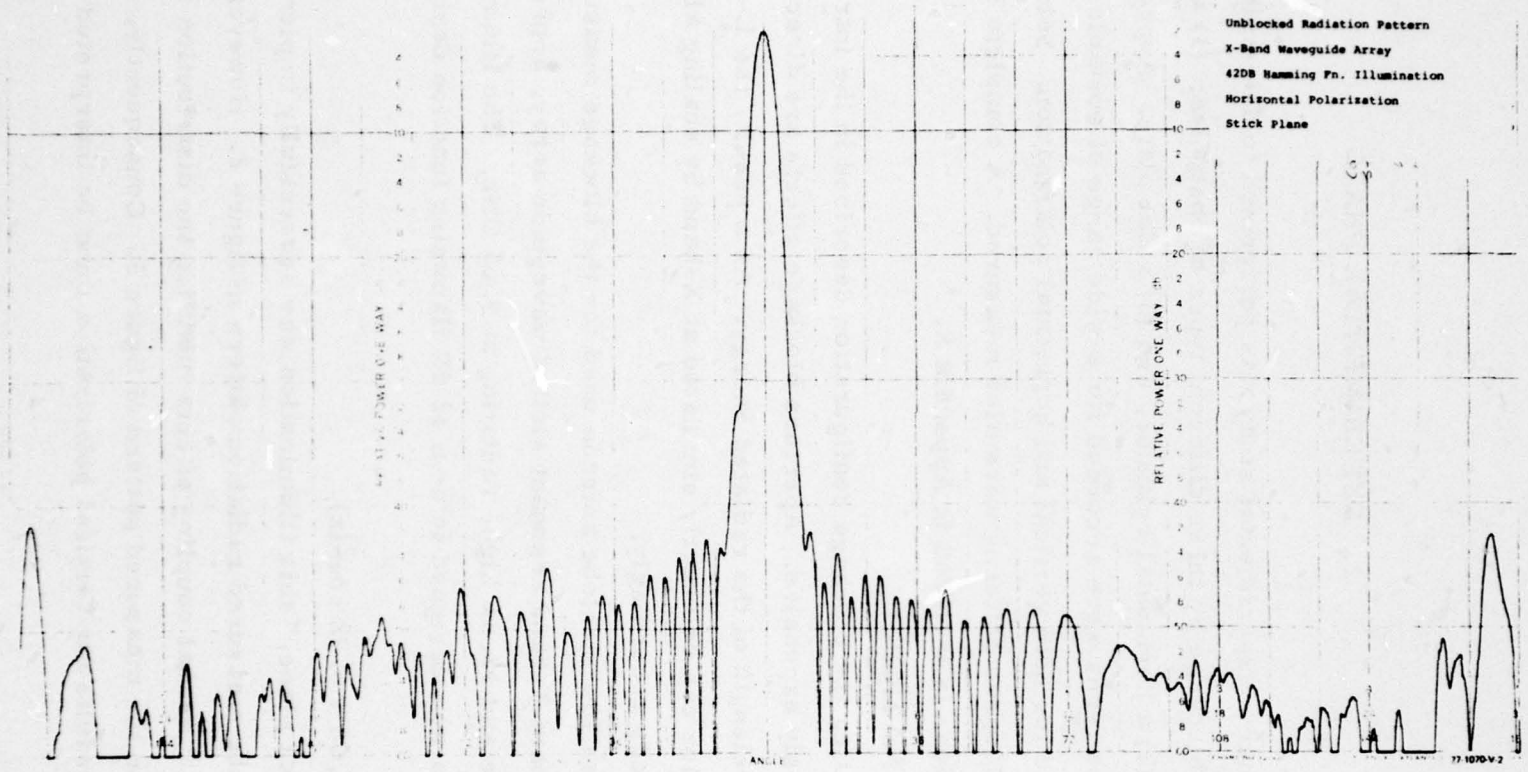

Figure 2. Stick Plane Radiation Pattern

77-1070

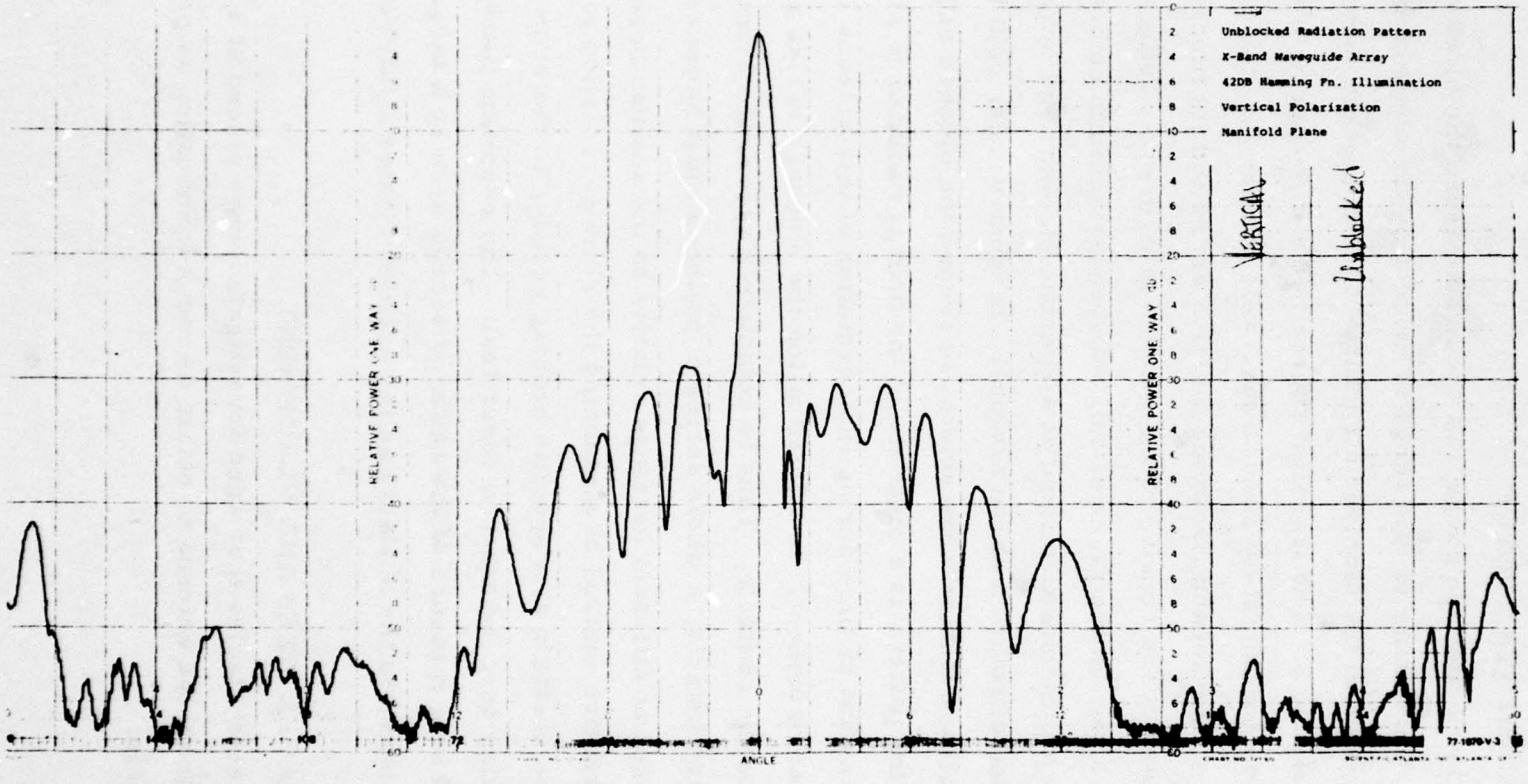

Figure 3. Manifold Plane Radiation Pattern

2.2 EXPERIMENTAL SETUP

A very low reflection range was used to measure the blocked radiation patterns. The quality of this range is evident by the absence of any significant reflections in the sidelobe structure of the unblocked measured radiation pattern of figure 2. The transmit source had a 2.9-degree beamwidth and was located approximately 200 ft away, well into the far field of the antenna under test. The X-band Hamming function array and its blockage fixture were mounted at the receive site as shown in figure 4. Using the 3-axis positioner shown in the picture, full 360-degree azimuth conical cuts were recorded with the obstacle fixed at a specific distance and bearing relative to the center of rotation of the antenna. In other words, both the antenna and the blockage fixture were rotated to record the blocked radiation pattern. The resulting pattern is a measure of the energy radiated in all directions at a fixed instant of time during the revolution of this antenna in an actual shipboard environment. In this situation the blockage varies as the antenna rotates past the obstacle. Thus to completely assess the blockage effects of a particular obstacle, a whole series of patterns must be measured with the obstacle fixed at different bearings relative to the antenna boresight.

An alternative method of measuring the blocked radiation pattern would be to fix the obstacle at a specific bearing relative to the source antenna, while rotating only the antenna under test. The resulting pattern in this case would be a measure of the radiated energy seen by a target at a fixed bearing relative to the obstacle as the antenna rotates a full revolution on its axis.

2.3 OBSTACLE SIZES AND PLACEMENT

The three obstacles that were investigated were placed at a number of distances from the antenna to obtain as much information as possible about each obstacle.

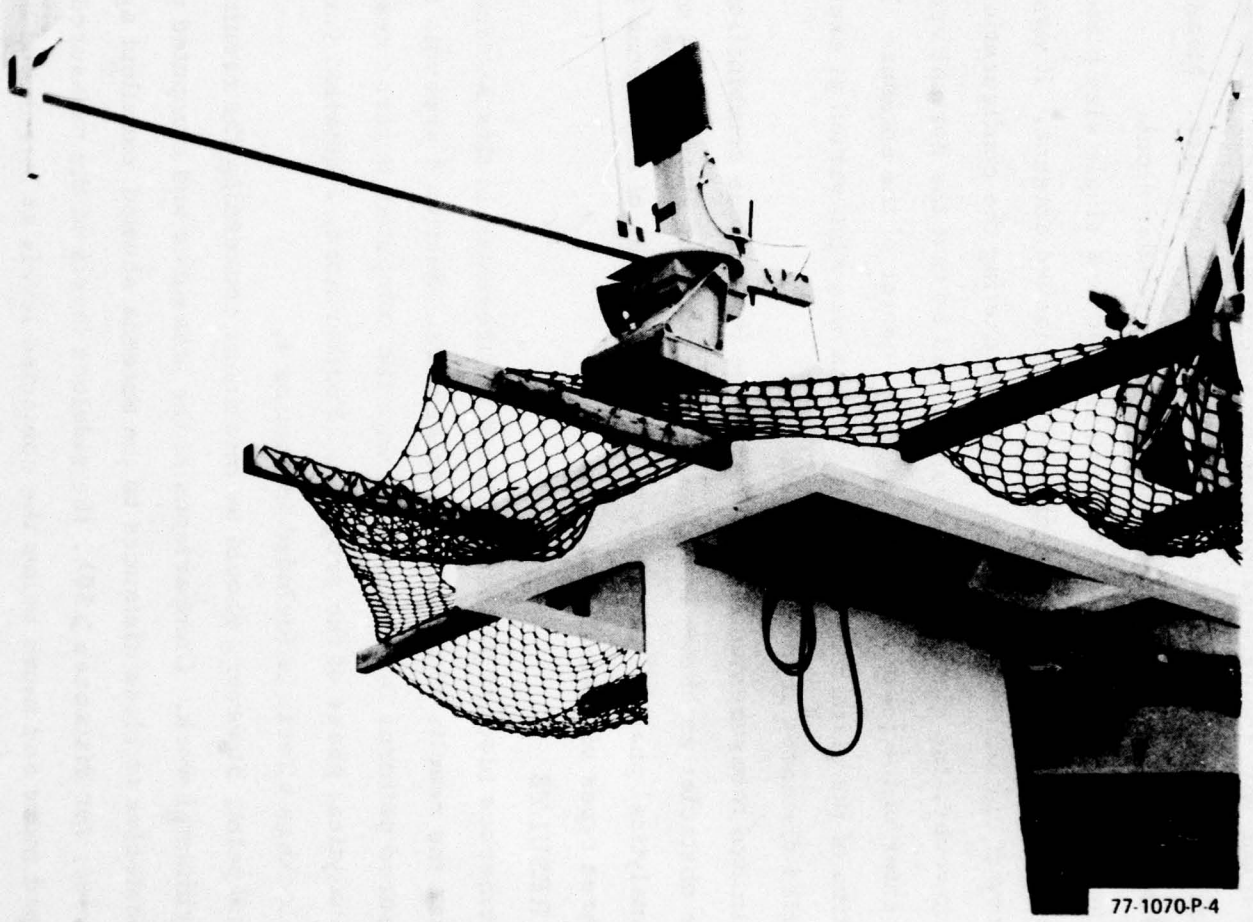

Figure 4. Experimental Test Configuration

Three different diameters were selected to bracket the configuration shown in figure 1, for both the vertical and horizontal cylinders. Measurements were made with the antenna blocked by a vertical cylinder alone and also by various combinations of a vertical and horizontal cylinder. Measurements were not made for blockage by a horizontal cylinder alone.

The flat plate measurements were limited to a single size plate, selected to be approximately the same size as the blocked antenna. It was fixed at a variety of distances from the antenna, bracketing the configuration of figure 1. However, the plate was always oriented so that the normal vector from the center of the plate passed through the center of the antenna. The vertical position of the plate relative to the antenna was also varied at each of the selected distances from the antenna.

Limited measurements were also made for various combinations of all three obstacles as shown in figure 4. However, no attempt was made during the analytical phase of the study to predict patterns of an antenna blocked by all three types of obstacles at once.

2.4 RESULTS

Numerous blocked patterns will not be presented in this section to summarize the results of the experimental work. Section 3 presents selected measured patterns for comparison with the computed patterns resulting from the analytical phase of the program. Furthermore, a detailed summary of the blockage effects is included in Section 4.

One point, however, should be mentioned concerning the results of the experimental work. Comparisons of the measured and computed patterns for obstacles at close distances to the antenna showed excellent agreement. However, for distances $\geq 50\lambda$, the sidelobe levels of the measured patterns dropped more and more below the computed levels at larger and larger angles from boresight. This descrepancy is attributed to the limited beamwidth of the source antenna. To minimize reflections from various areas of the receive site, the size of the transmit dish is normally chosen to have as

narrow a beamwidth as possible, while still maintaining less than 1/4dB amplitude taper across the aperture of the antenna under test. Since the antenna under test was a very low sidelobe antenna, minimizing extraneous reflections was especially important.

However, for the blockage measurements to be accurate, the antenna and the obstacle must be illuminated uniformly by the transmit dish. As the antenna and blockage fixture are rotated away from the source, the illumination on the obstacle gradually decreases relative to the illumination on the antenna, until at an angle of 90 degrees from the source, the difference in illumination is the greatest. With the obstacle located 14λ away from the antenna, this difference is only 0.25dB. As a result, the computed and actual blocked patterns agree very well over a full 360 degrees. But when the obstacle is located 50λ away, the illumination difference is 3.0dB; and at 100λ, the difference is 12.0dB. These values can be used to correct the measured blocked sidelobe levels at the angle where the obstacle is 90 degrees away from the source. Similar calculations were made to determine correction factors at other angles from boresight, and the corrected patterns were found to be in excellent agreement with the computed patterns.

3. ANALYTICAL PHASE

The analytical phase of the study consisted of the development of several computer programs capable of calculating the effects of selected near-field obstacles on the sidelobe structure of an ultra low sidelobe antenna. The specific obstacles were a vertical cylinder (mast), a horizontal cylinder (yardarm), and a flat plate (another antenna). The antenna is assumed to be a planar array with separable vertical and horizontal illumination functions. The computed patterns are limited to principal plane azimuth patterns so that the geometry can be simplified to a two-dimensional analysis.

The mast and yardarm analysis are included in one single main routine. Radiation patterns may be computed for either a mast or yardarm alone, or for the two obstacles together. The flat plate analysis, however, is handled in a separate program.

3.1 MAST BLOCKAGE ANALYSIS

To calculate the effects of a mast blocking the aperture of a radar antenna, the mast is assumed to be a vertical metalic cylinder of infinite length. The horizontal aperture is sub-divided into N subapertures, in such a way that the cylinder is in the far field of each subaperture. This technique then enables one to use the classical infinitesimal dipole and cylinder solutions for each subaperture to calculate the far field pattern of the cylinder when it is illuminated by the antenna.

The blocked radiation pattern is computed for a fixed angle of rotation of the antenna relative to the cylinder. Then, in order to obtain a complete description of the particular blockage configuration, a series of patterns must must be computed at various angles of rotation of the antenna as shown in figure 5. In effect, each one of these radiation patterns describes

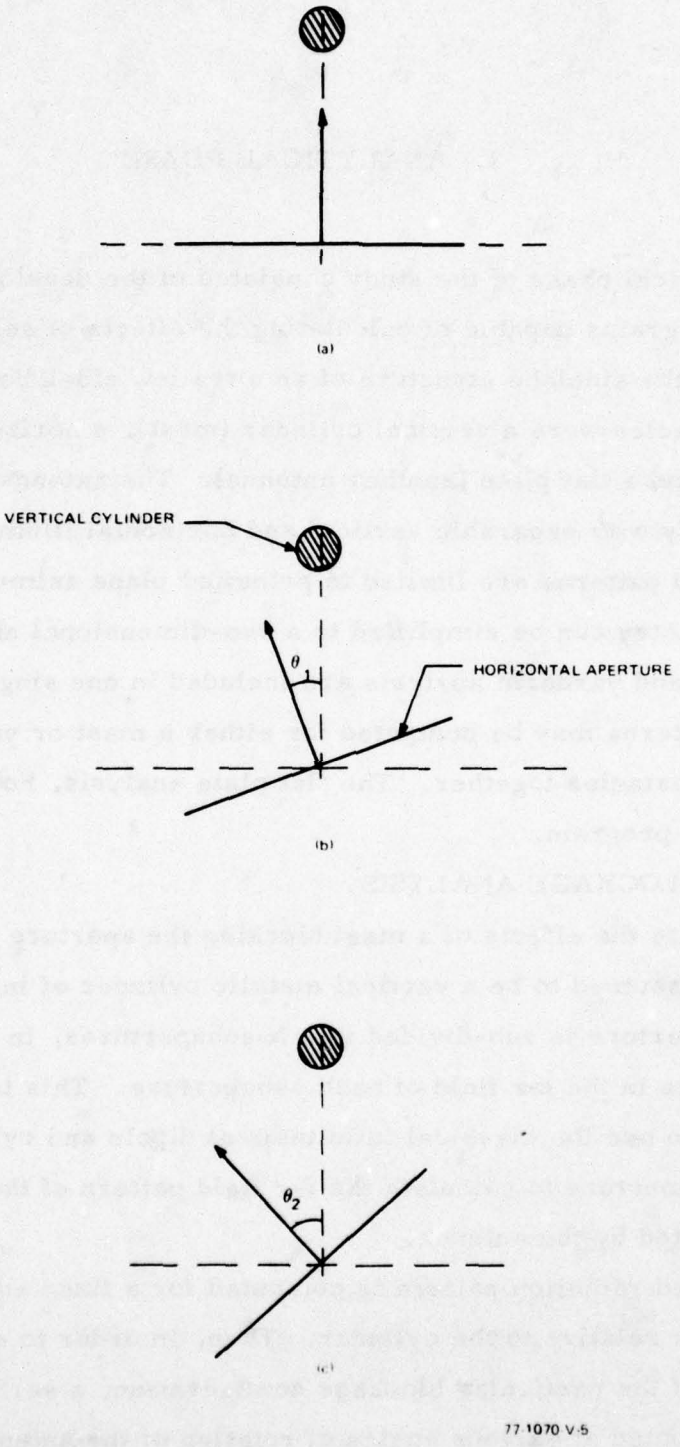

Figure 5. Rotating Antenna/Vertical Cylinder Blockage Geometry

the degraded performance of the antenna at a specific instant of time during its period of revolution.

3.1.1 Theoretical Background

Figure 6 shows the basic two-dimensional geometry for the infinitesimal dipole and cylinder solution. The horizontal aperture has been divided into N subapertures of such a size that the energy from any subaperature is a plane wave across the diameter of the mast.

For the case of a vertically polarized radiating element, the incident electric field is parallel to the axis of the cylinder and is propogating in the x' direction. Neglecting the time dependence, the plane wave from the mth radiating element can then be expressed as $E_{inc} = A_m e^{ikx'}$ which can be re-written in polar coordinates as:

$$E_{inc} = A_m e^{ikr\cos(\theta-\theta_m)} = A_m \left[\cos\left(kr\cos(\theta-\theta_m)\right) + i\sin\left(kr\cos(\theta-\theta_m)\right)\right]$$

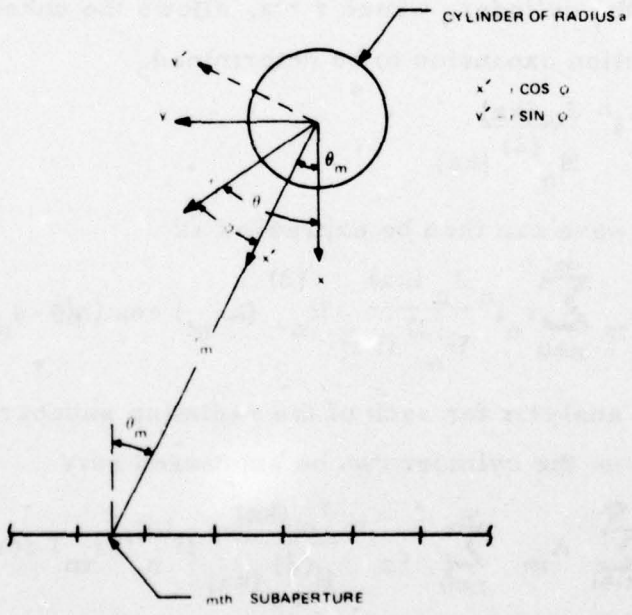

Figure 6. Horizontal Line Source Blocked by a Vertical Cylinder

Using the two identities[1]

$$\cos(Z\cos\theta) = J_o(Z) + 2\sum_{k=1}^{\infty}(-1)^k J_{2k}(Z)\cos(2k\theta)$$

$$\sin(Z\cos\theta) = 2\sum_{k=0}^{\infty}(-1)^k J_{2k+1}(Z)\cos\left((2k+1)\theta\right)$$

the incident electric field can be re-written as an infinite series of Bessel functions:

$$E_{inc} = A_m \sum_{n=0}^{\infty} \epsilon_n i^n J_n(kr)\cos\left(n(\theta-\theta_m)\right) \begin{cases} \epsilon_n = 1, & n = 0 \\ \epsilon_n = 2, & n \neq 0 \end{cases}$$

To fit the boundary conditions at the surface of the cylinder, an outward travelling cylindrical wave from the cylinder must be added of the form

$$E_{scat} = \sum_{n=0}^{\infty} B_n H_n^{(2)}(kr)\cos\left(n(\theta-\theta_m)\right)$$

Requiring the scattered wave to be equal and opposite to the incident wave at the surface of the cylinder, where r = a, allows the unknown coefficients of the Hankel function expansion to be determined.

$$B_n = -A_m \epsilon_n i^n \frac{J_n(ka)}{H_n^{(2)}(ka)}$$

The scattered wave can then be expressed as

$$E_{scat} = -A_m \sum_{n=0}^{\infty} \epsilon_n i^n \frac{J_n(ka)}{H_n^{(2)}(ka)} H_n^{(2)}(kr_m)\cos\left(n(\theta-\theta_m)\right)$$

Repeating this analysis for each of the radiating subapertures, the total scattered field from the cylinder can be expressed as:

$$E_{scat} = -\sum_{m=1}^{N} A_m \sum_{n=0}^{\infty} \epsilon_n i^n \frac{J_n(ka)}{H_n^{(2)}(ka)} H_n^{(2)}(kr_m)\cos\left(n(\theta-\theta_m)\right) \quad (1)$$

For the case of horizontally polarized radiating elements, the magnetic field is parallel to the axis of the cylinder, and the boundary conditions at the surface of the cylinder require the circumferential components of the

incident and scattered fields to cancel. Thus for the horizontally polarized elements, the coefficients are determined by

$$B_n = -A_m \epsilon_n i^n \frac{J_n'(ka)}{H_n^{(2)'}(ka)}$$

The total scattered field from a cylinder illuminated by a line source of horizontally polarized radiating elements is then:

$$H_{scat} = -\sum_{m=1}^{N} A_m \sum_{n=0}^{\infty} \epsilon_n i^n \frac{J_n'(ka)}{H_n^{(2)'}(ka)} H_n^{(2)}(k r_m) \cos\left(n(\theta-\theta_m)\right) \qquad (2)$$

The resultant far field radiation pattern of the blocked aperture at an angle θ can now be found. For each subaperture, a value of the direct (unblocked) field in the direction θ is calculated. To this value is added the scattered field from the cylinder at the angle θ resulting from the illumination by the subaperture. Summing the contributions from all the subapertures will then give the total blocked field at the angle θ.

$$E_{TOTAL} = E_{DIRECT} + E_{SCATTERED}$$

3.1.2 Computer Simulation

The basis for the implementation of the mast blockage analysis was a computer program written by A.J. Hissink.[2] Portions of the main routine have been modified or eliminated, while additional capabilities have been added to tailor the program to our needs. Nevertheless, the basic method of analysis and the associated geometry have been retained.

A major addition to the analysis, however, was the calculation of the energy scattered by the cylinder in the direction of the antenna. This energy is reradiated by the antenna to form a significant contribution to the total blocked pattern.

Three of Hissink's subroutines are used with only minor modifications. These include the Bessel function generator, the Lagrange 4-point interpolation routine, and the pattern printing routine.

A detailed explanation of the use of the mast blockage programs is included in Appendix B along with a complete description of the necessary input parameters, sketches of the basic geometry, and listings of the programs.

3.1.2.1 Sub-Aperture Size Considerations

When computing the radiation pattern of a linear array of elements, the aperture must first be divided into N sub-apertures. The execution time needed to compute the direct radiation pattern of the aperture is short even for large values of N. However, because of the Hankel and Bessel functions in equations (1) and (2), the time required to compute the scattered fields from the cylinder can become excessive, if the number of sub-apertures is not kept to a minimum.

The number of sub-apertures required to obtain an accurate representation of the scattered fields from the cylinder is determined by requiring the path length difference between L_1 and L_2 in figure 7 to be less than $\lambda/16$. This condition can be represented approximately by the expression

$$N \geq \frac{W}{\sqrt{4a^2 + \lambda/2\,(d-a)} - 2a} \qquad (3)$$

Hissink has shown that if this condition is met, then 92 percent of the scattered field points will be within 1 dB of the corresponding values had 2N subapertures been chosen, with the rest of the points being less than 2 dB in error.

Rather than requiring the user to determine the minimum number of sub-apertures for a particular blockage configuration, this determination is done automatically in the main routine. A Lagrange 4-point interpolation formula is then used to determine the value of the illumination function at each of the N sub-apertures from the values at each of the M sub-apertures input to the computer program. The user is then free to input the illumination to the program using any number of points which adequately describes the function.

3.1.2.2 Sub-Aperture Illumination Functions

In order to compute the radiation pattern of a linear array of elements having an arbitrary illumination function, f(x), the illumination across each

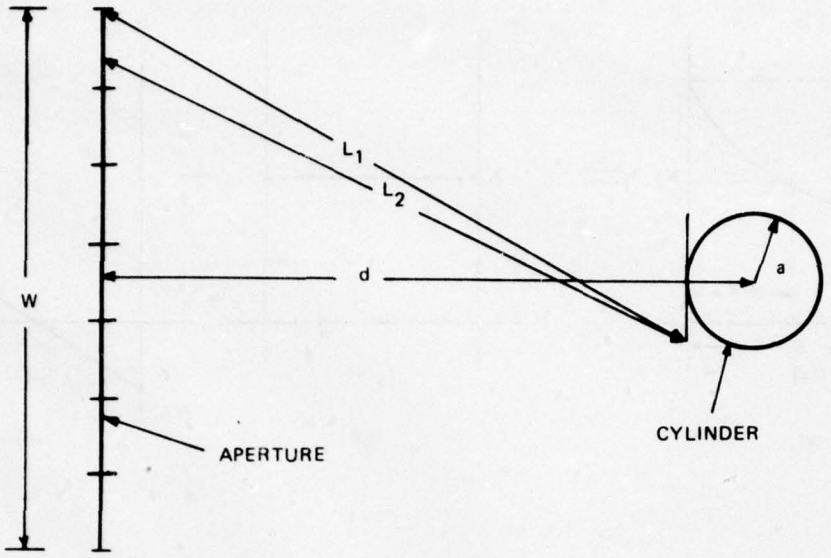

Figure 7. Subaperture Size Determination

subaperture is assumed to be uniform and equal to the value of f(x) at the center of the subaperture (figure 8 (b)). However, unless the size of the subaperture is less than $\lambda/2$, the calculation will produce grating lobes.

For most realistic blockage configurations, the criteria set forth in the previous section will result in a subaperture size that is much larger than $\lambda/2$. Unless the number of subapertures is increased, this method of analysis will not produce acceptable results.

However, a more efficient solution to the problem would be to add a skew-symmetric correction to the uniform illumination across each subaperture as shown in figure 8. Using the illumination information input to the program at M arbitrary points, the Lagrange interpolation routine generates values of the illumination function at the center and ends of each of the N subapertures determined by equation (3). The illumination function, f(x), can now be approximated by the sum of a uniform illumination, $f_1(x)$, and a tapered illumination, $f_2(x)$.

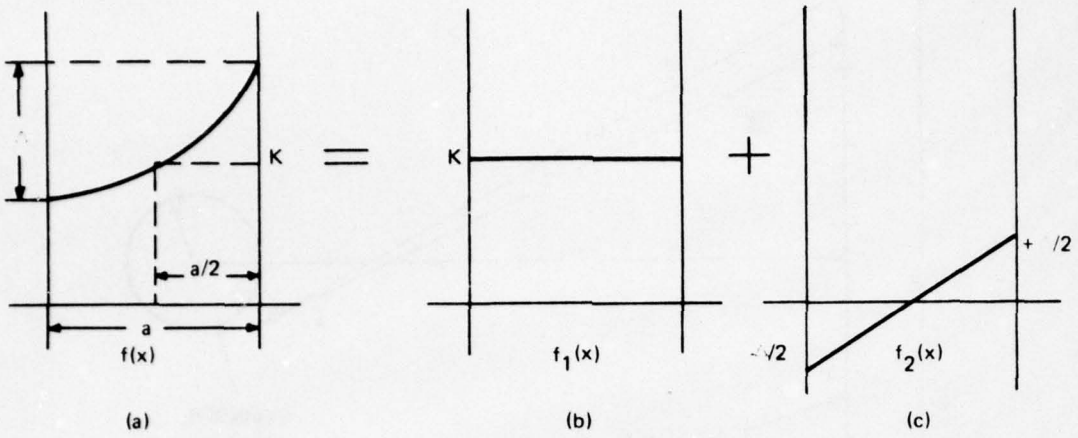

77-1070-V-8

Figure 8. Subaperture Illumination Functions

$$f(x) \approx f_1(x) + f_2(x)$$

The resulting far field radiation pattern is then approximated by

$$F(\theta) = F_1(\theta) + F_2(\theta)$$

$F_1(\theta)$ and $F_2(\theta)$ can easily be derived as

$$F_1(\theta) = K \int_{-a/2}^{+a/2} e^{i\frac{2\pi}{\lambda} x \sin\theta} dx = Ka\left[\frac{\sin(u)}{u}\right]$$

$$F_2(\theta) = \int_{-a/2}^{+a/2} \left(\frac{\Delta}{a} x\right) e^{i\frac{2\pi}{\lambda} x \sin\theta} dx = \frac{\Delta a}{2i}\left[\frac{\cos(u)}{u} - \frac{\sin(u)}{u^2}\right]$$

where $u = \pi a/\lambda \sin\theta$

The addition of a skew-symmetric correction to the uniform illumination across each subaperture allows a large subaperture size to be used without reducing the accuracy of the calculation significantly.

3.1.2.3 Bessel Function Upper Limit Determination

To evaluate the expressions for the scattered fields from the cylinder,

an upper limit must be determined at a point where succeeding terms in the summation are negligible. In developing an efficient Bessel function generator to evaluate these expressions, Hissink formulated an empirical expression describing this upper limit.[3]

$$NMAX = Z + 3.03 + 4.06\,(Z)^{1/3}$$

where Z is the argument of the Hankel function of the first or second kind:

$$H_n^{(1)}(Z) = J_n(Z) + i\,Y_n(Z)$$

$$H_n^{(2)}(Z) = J_n(Z) - i\,Y_n(Z)$$

The Bessel function subroutine returns values of the Hankel functions for all orders from zero to NMAX. Forward recurrence relations are used to calculate all the required orders of $Y_n(Z)$ and all orders of $J_n(Z)$ where $n<Z$. For higher orders of n, $J_n(Z)$ is a rapidly decreasing function, and the recurrence relation becomes unstable. These higher orders are determined, instead, by using a backward recurrence relation.

3.1.2.4 Experimental vs. Theoretical Results

During the experimental phase of the study, a significant discrepancy was observed between the measured radiation patterns and the patterns calculated using Hissink's formulation of the scattered fields from the cylinder.

Figure 9 shows both measured and computed radiation patterns for a blockage configuration that a horizontally polarized L-band ultra low sidelobe antenna might encounter in a shipboard environment. The 1.022 λ diameter cylinder (mast) is located 14 λ away (just outside the turning radius of the 18.4 λ wide aperture) and is directly in front of the antenna (O° angular offset).

Three separate radiation patterns are included in the figure. The computed pattern described by the discrete symbols O is the direct, or unblocked, pattern of the aperture, resulting from a 42-dB Hamming function illumination. The computed pattern described by the discrete symbols Δ is the total blocked pattern of the antenna. Superimposed on this computed pattern is

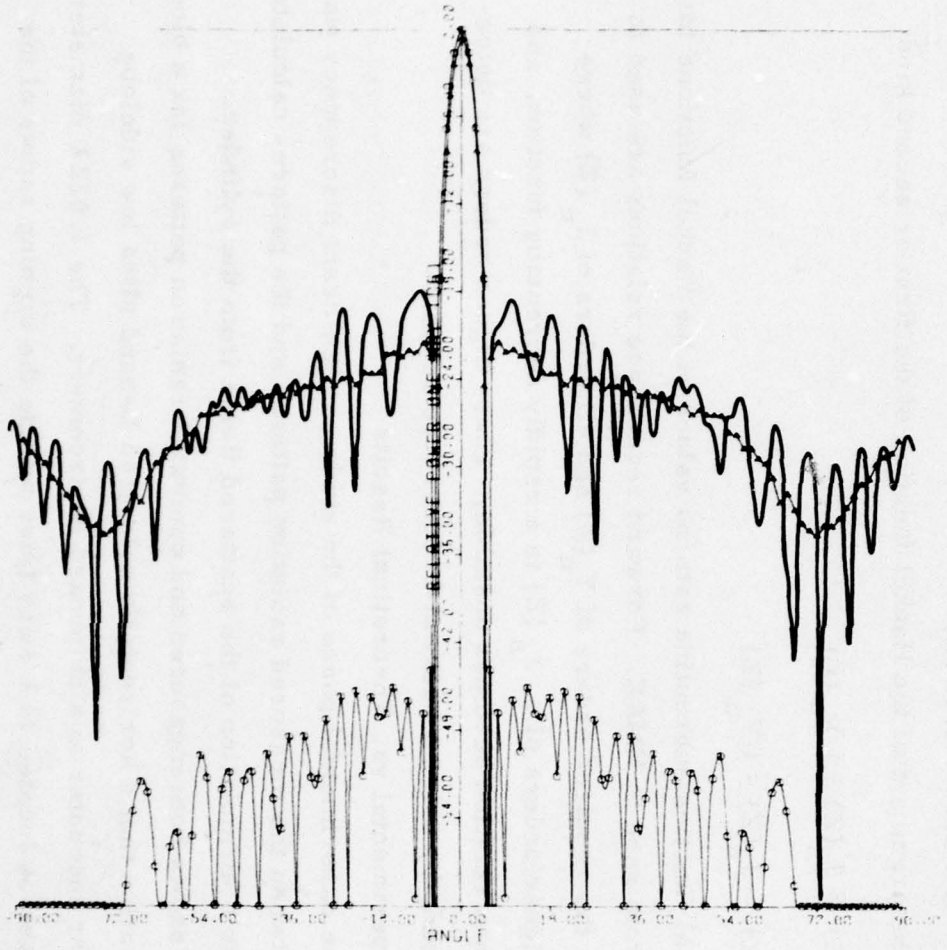

Figure 9. Vertical Cylinder Blockage, Obstacle Distance = 14λ

77-1070

the actual measured pattern corresponding to this blockage configuration. (A complete description of the expermintal phase of the study is included in Section 2). The computed pattern is a good first order approximation to the actual pattern; however, the measured pattern includes a second order perturbation not predicated by our model. The frequency of this perturbation was found to be proportional to the distance between the aperture and the cylinder as shown in figure 10, where the cylinder has been moved 50 λ away from the antenna.

3.1.2.5 Reradiation of Scattered Fields

Based on this aperature-to-cylinder distance dependence, the observed perturbations were attributed to a reradiation of the energy scattered by the cylinder in the direction of the aperture. This phenomenon will only be observed in situations where the energy radiated by the aperture is propogating in a direction normal to the axis of the cylinder. Antennas steered in elevation will not intercept the energy scattered by the cylinder(figure 11), and consequently, will not exhibit these second order effects. Such was the case for the antenna used by Hissink to verify his theoretical model.

Incorporating the second order perturbations into the pattern calculation is straightforward. However, instead of computing the resultant fluctuations of the total blocked pattern in detail, the maximum and minimum of the blocked signal are computed and plotted. There are several reasons for handling the calculation in this manner.

First of all, attempting to exactly describe a pattern such as the one in figure 10 is impractical because of the large number of closely spaced points that would be required. An envelope bounding the extent of the perturbations would be more informative. Furthermore, predicting the actual fluctuations would not be possible without a complete detailed description of the antenna under consideration, including actual dimensions of the power division network feeding the radiating elements. Without this information, the phase of

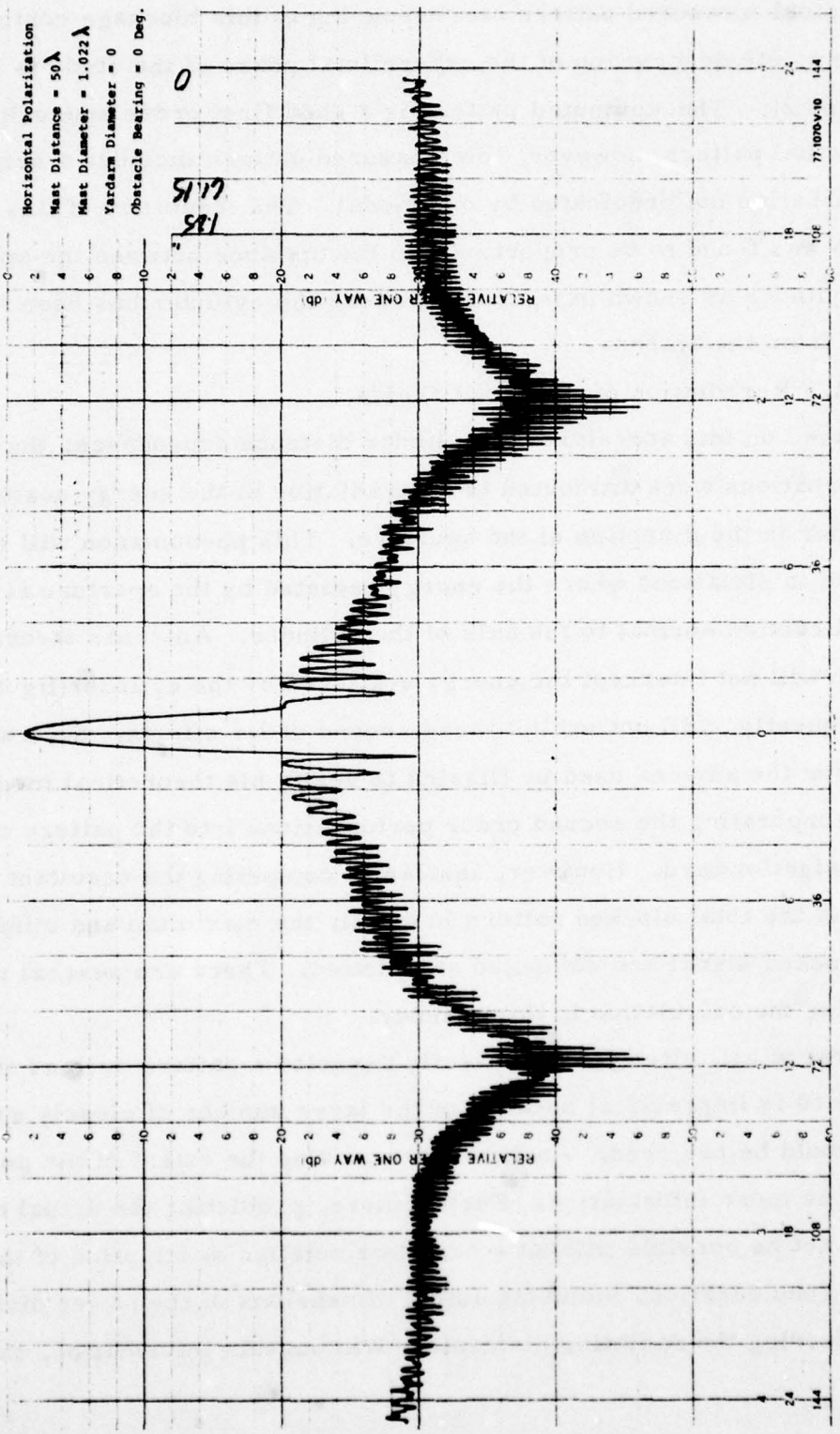

Figure 10. Vertical Cylinder Blockage, Obstacle distance = 50 λ

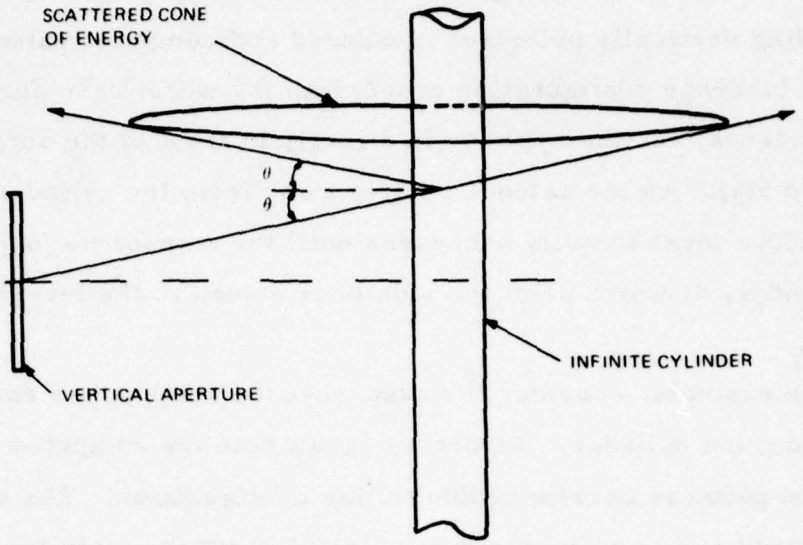

77-1070-V-11

Figure 11. Steered Beam Scattering Geometry

the reradiated energy from any element cannot be calculated. Expanding the model to handle detailed descriptions of this type for an "arbitrary" antenna would obviously be impractical.

The analysis routine has been set up to compute the second order perturbations only for antennas not having steered beams in elevation. However, if the user is not interested in the second order effects for an antenna of this type, a small elevation squint may be input to the program which will eliminate the calculation of the reradiated energy from the cylinder, and not otherwise affect the result.

Figure 12 shows the result of including the reradiated energy from the cylinder for the blockage configuration corresponding to figure 9. As before, the computed unblocked pattern is included as a reference. The computed upper limit of the blocked pattern is described by the symbols Δ, whereas the lower limit is represented by the symbols +. The actual measured blocked pattern is superimposed over the computed upper and lower limits

as a comparison, and the agreement is excellent. Figure 13 shows the corresponding vertically polarized measured and computed patterns.

This blockage configuration represents the worst case during the rotation of the antenna, for the cylinder is directly in front of the antenna as shown in figure 5(a). As the antenna rotates away from the cylinder (figure 5(b)), the sidelobe level steadily decreases until the antenna no longer illuminates the cylinder, at which point the sidelobes return to the level of the unblocked pattern.

As an example, consider the case when the antenna has rotated 20 degrees away from the cylinder. Figure 14 shows both the computed and measured radiation patterns corresponding to this configuration. The sidelobe level has dropped and is no longer symmetrical about the main beam. By the time the antenna has rotated 40 degrees, the blockage effects are negligible because the cylinder is on the edge of the projected aperture of the antenna. Thus, for the particular blockage configuration chosen here as an example, the total angular region during which the sidelobe levels of the antenna will be significantly increased is approximately 60 degrees. Or equivalently, during 83 percent of the time, the radiated far field pattern will approach the unblocked pattern of the antenna.

The extent of this blocked angular region is dependent on the blockage geometry, particularily on the width of the aperture and the distance to the cylinder. Section 4 presents a graphic summary of the behavior of the blocked rms sidelobe level as a function of the various blockage variables.

3.1.2.6 Blockage of the Scattered Fields by the Radiating Aperture

A vertical cylinder illuminated by a rectangular aperture radiates approximately omni-directionally. However, beyond some angle θ, the scattered energy will be blocked by the aperture and the sidelobe level in this region will rapidly decrease. The effect is not evident in the radiation patterns of figures 9 and 12 because for this configuration, the blockage does not begin

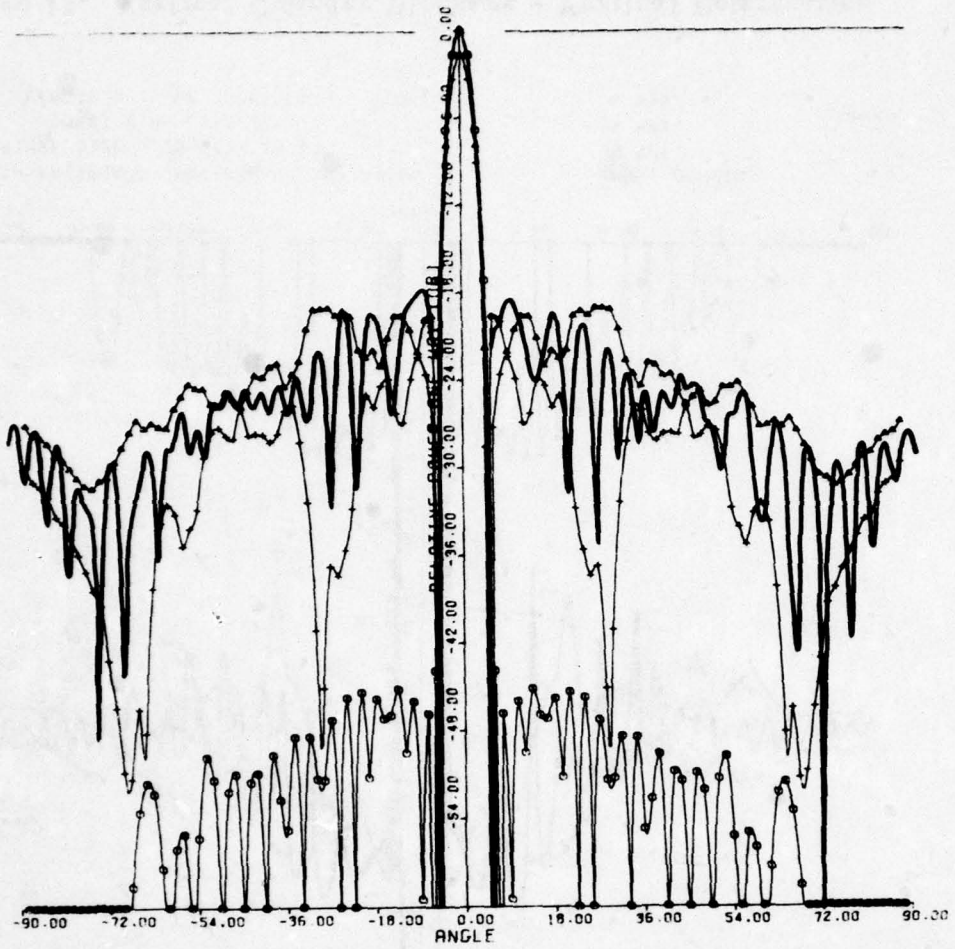

THIS PAGE IS BEST QUALITY PRACTICABLE
FROM COPY FURNISHED TO DDC

Figure 12. Vertical Cylinder Blockage - Horizontal Polarization

THIS PAGE IS BEST QUALITY PRACTICABLE
FROM COPY FURNISHED TO DDC

THIS PAGE IS BEST QUALITY PRACTICABLE
FROM COPY FURNISHED TO DDC

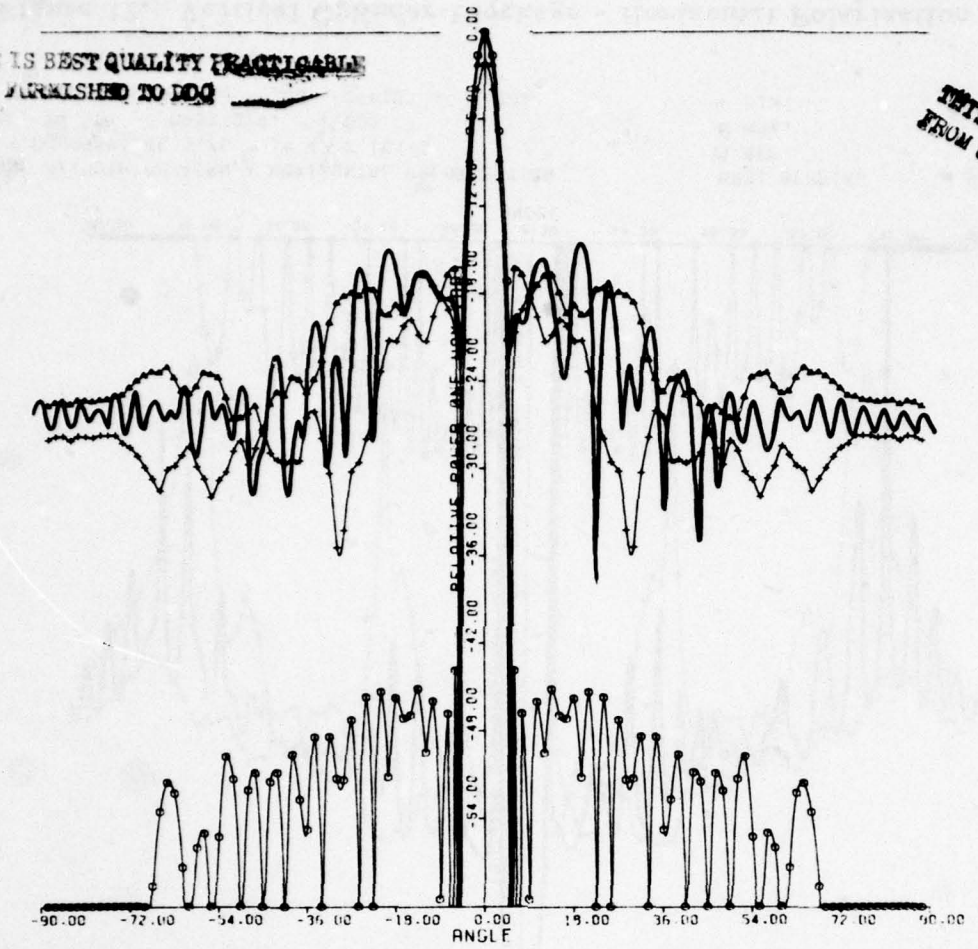

PRINCIPAL PLANE AZIMUTH PATTERN - VERTICAL POLARIZATION
WAVELENGTH = 1.000APERTURE SIZE = 18.43 X 18.45
MAST DISTANCE = 14.00 MAST DIA. = 1.022
YARDARM DIA. = .000 LENGTH = .00 OFFSET = .00

MAST BEARING = .0 DEG.
⊙ REF.
△ MAX.
+ MIN.

77-1070-V-13

Figure 13. Vertical Cylinder Blockage - Vertical Polarization

77-1070

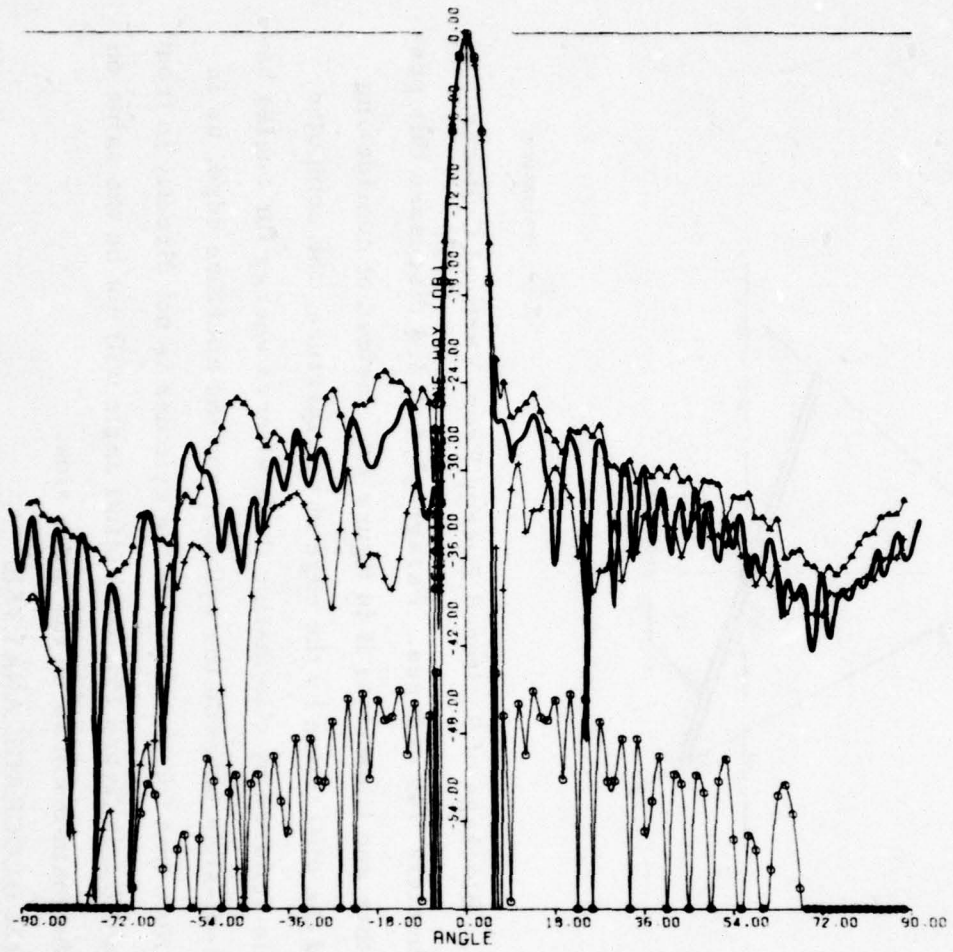

THIS PAGE IS BEST QUALITY PRACTICABLE
FROM COPY FURNISHED TO DDC

Figure 14. Vertical Cylinder Blockage, Mast Bearing = -20°

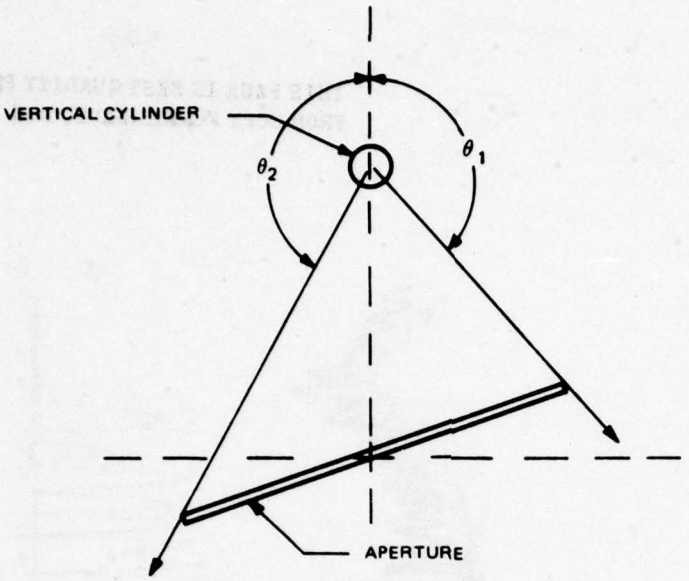

77-1070-V-15

Figure 15. Blockage of Scattered Energy From Vertical Cylinder

until approximately 140 degrees. Paragraph 3.2.2.4 discusses this phenomenon further and illustrates it in figure 23. Instead of considering the details of the diffraction by the edge of the aperture, the computed blockage is determined by eliminating the scattered energy for angles beyond the line-of-sight between the cylinder and the aperture edge, as in Figure 15. Note that for cases where the cylinder is not directly in front of the aperture (as in figure 15), the cuttoff angle will not be the same on one side of the main beam as on the other side.

3.2 YARDARM BLOCKAGE ANALYSIS

The yardarm analysis uses many of the techniques developed for the mast analysis. Therefore, it is combined with the mast analysis in one main program. Patterns can be computed for the mast or yardarm alone, or for various mast/yardarm combinations, within the geometrical limits of the model. Refer to Appendix B for details on the use of the mast/yardarm computer program.

3.2.1 Theoretical Background

The yardarm is modeled as a horizontal cylinder of finite length L and distance D from the center of the aperture as shown in figure 16. For a fixed angular position of the antenna, the total blocked radiation pattern is computed by subtracting the pattern radiated by the cylinder from the direct (unblocked) pattern of the antenna. The techniques used to calculate the patterns are in many ways similar to the ones used in the mast blockage analysis and are discussed in paragraph 3.2.2. However, unlike the vertical cylinder analysis, the horizontal cylinder analysis is not an exact solution. Several approximations are made in determining the normalization of the energy scattered from the cylinder. However, the resulting loss in accuracy is insignificant when compared to the reduction in computation time, as explained in the following section.

3.2.1.1 Normalization Approximation

The basic theory of the scattering from an infinite cylinder (paragraph 3.1.1) can be used to determine the elevation pattern of an antenna blocked by a horizontal cylinder. Since we are concerned only with the principal plane azimuth pattern, this model will be used only to determine the reduction in power of the pattern radiated by the cylinder when it is illuminated by the aperture. The procedure is essentially the same as the method used to calculate the scattered fields from the vertical cylinder. However, in this case, we are concerned with the vertical aperture of the antenna, rather than the horizontal aperture. The entire aperture of the antenna is divided into N columns, each having the same vertical illumination. For the case of figure 16(a) the columns are all the same distance from the cylinder, and the scattering from the cylinder can be exactly computed, as was done in paragraph 3.1. But, when the antenna is rotated an angle θ relative to the cylinder as in figure 16(b), the cylinder is no longer parallel to the aperture. Now, each column will illuminate the cylinder in a different manner, depending on its distance from the cylinder. An exact analysis of the situation

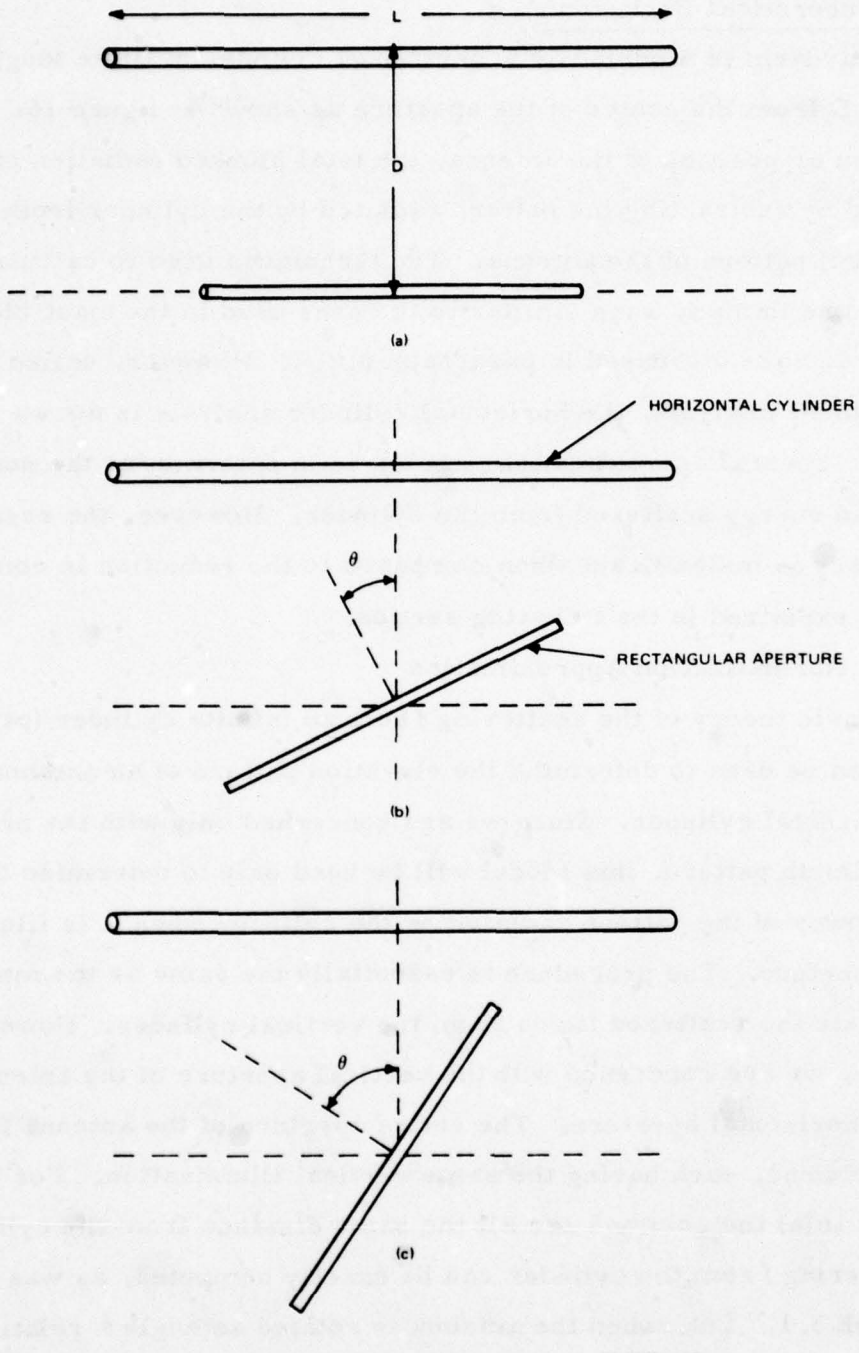

Figure 16. Rotating Antenna/Horizontal Cylinder Blockage Geometry

would involve a calculation of the type described in paragraph 3.1.1 for each column. This information could then be used to normalize the scattered fields from the cylinder in the azimuth plane relative to the directly radiated fields from the antenna. However, implementing this calculation would increase the execution time of the program tremendously.

A more practical solution would be to determine an average separation distance between the aperture and the cylinder as shown in figure 17. The effect of the vertical aperture on the level of the scattered energy from the cylinder can then be calculated using one representative column of radiating elements. Note that this realignment of the cylinder is only done to simplify the normalization calculation, and is not used in the actual pattern computation geometry discussed in paragraphs 3.2.2.2 and 3.2.2.3.

3.2.1.2 Dual Beam Scattering

When a horizontal cylinder is illuminated by a rectangular aperture oriented parallel to the axis of the cylinder, as in figure 16(a), the scattered energy lies primarily in a plane perpendicular to the axis of the cylinder. But when the antenna has rotated to a position where it is no longer parallel to the cylinder, the scattered energy forms a cone as in figure 18. Effectively, in the principal azimuth plane, two beams are formed.

The magnitude of these beams, relative to the direct radiation from the antenna, is dependant on several variables, including (1) the diameter of the cylinder relative to the size of the vertical aperture, (2) the distance of the cylinder from the aperture, (3) the vertical offset of the cylinder relative to the center of the vertical aperture, and (4) the angular offset of the aperture from the cylinder. These values are an integral part of the normalization calculation discussed in the previous section. It should be noted that separate normalization factors are needed for each beam.

The forward beam will combine with the main beam from the antenna

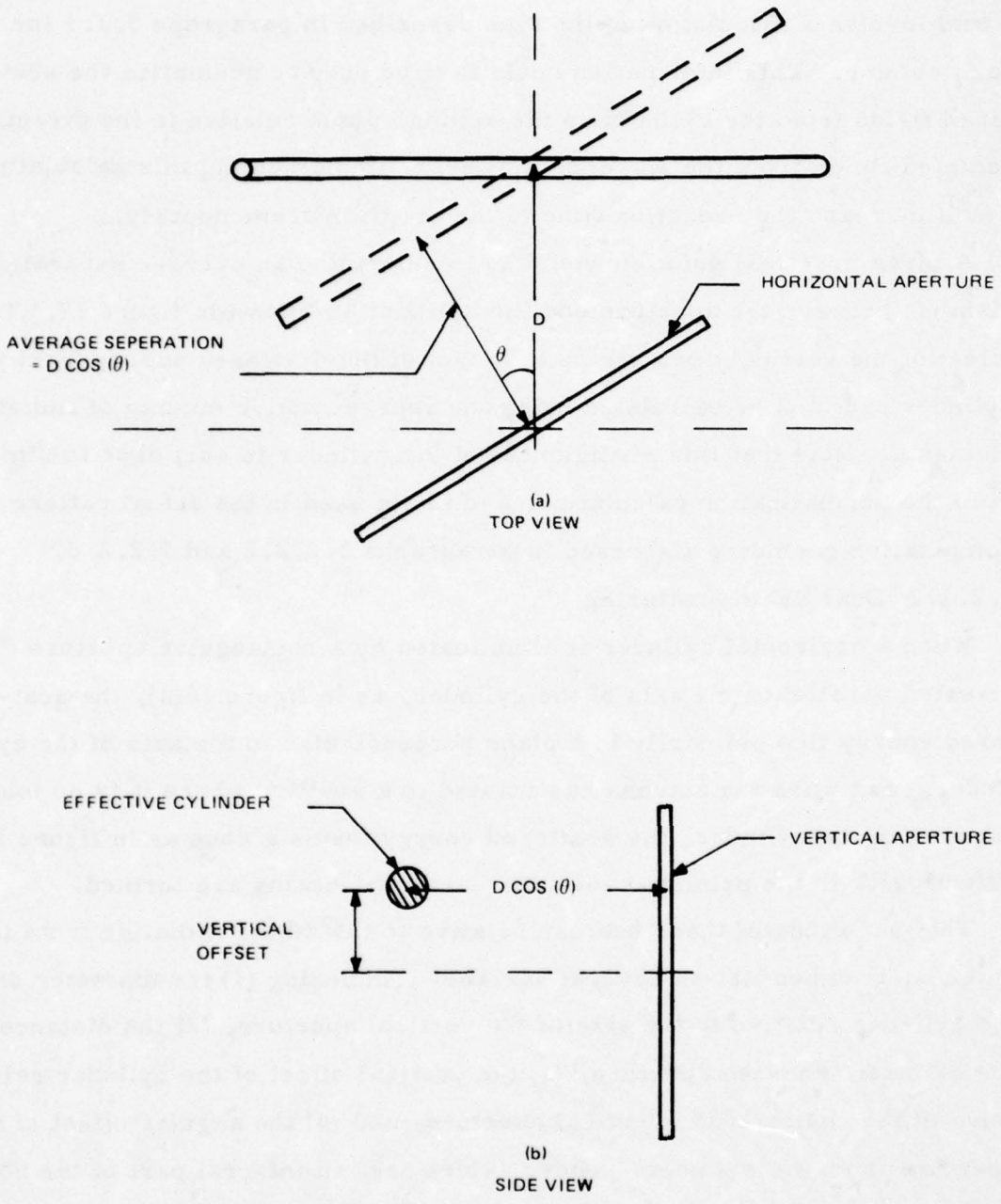

Figure 17. Normalization Geometry

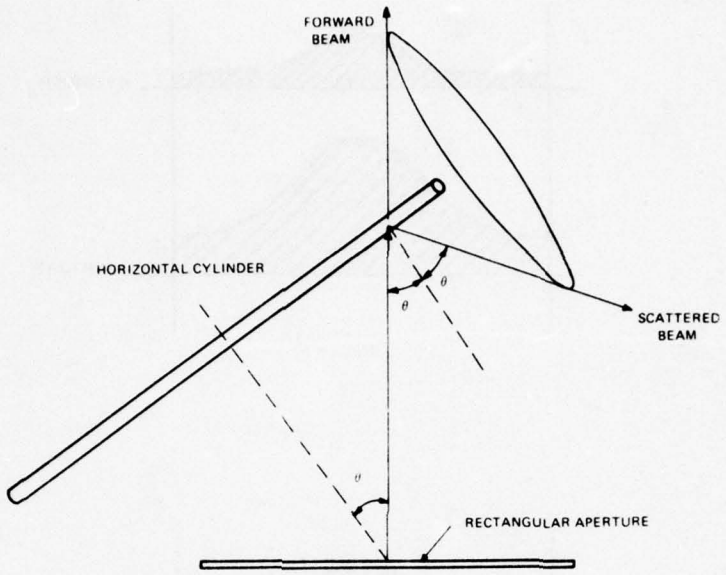

Figure 18. Conical Scattering

to determine the gain of the blocked aperture. The reflected beam, however, will show up as broad sidelobe (having approximately the same beamwidth as the unblocked aperture) at an angle of $180^{\circ} - 2\theta$.

The distribution of fields along the cylinder, resulting from the horizontal illumination function of the aperture, determines the azimuth radiation pattern of the two scattered beams. As long as the cylinder extends completely across the projected horizontal aperture of the antenna, the cylinder will radiate an azimuth pattern identical to the unblocked pattern of the antenna. But as the antenna continues rotating to a position where the cylinder extends only partially across the projected aperture, as in figure 16(c), the illumination on the cylinder no longer matches the illumination function of the antenna (figure 19). The azimuth pattern of the two scattered beams will begin to deteriorate and exhibit rapidly decreasing gain.

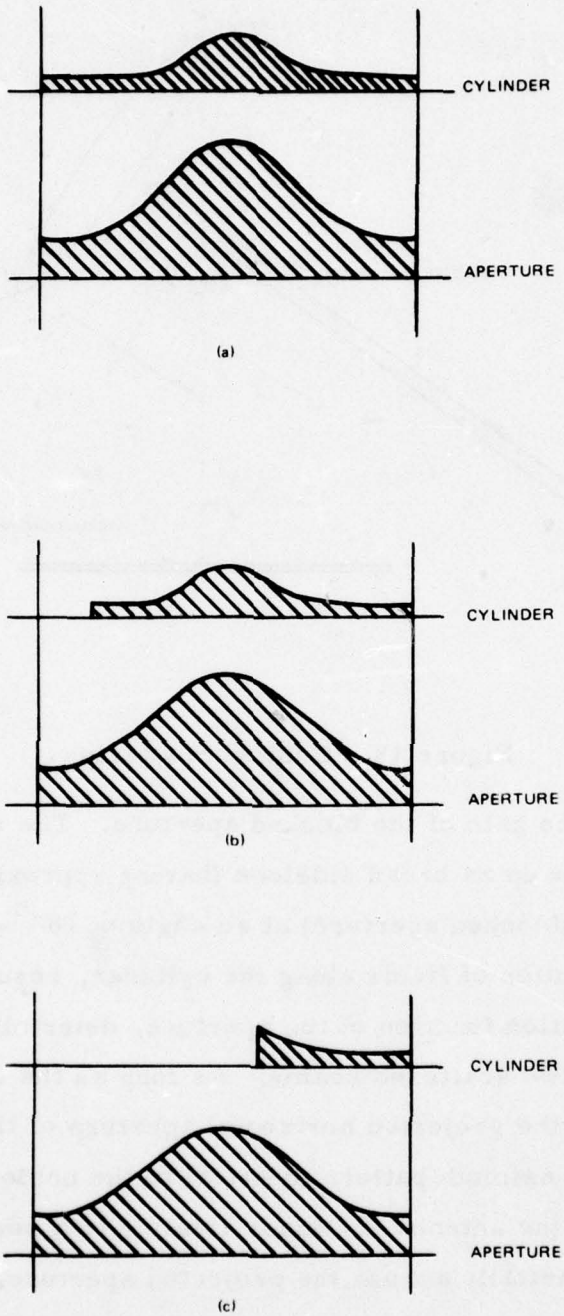

Figure 19. Aperture and Cylinder Illumination Functions

3.2.2 Computer Simulation

The implementation of the horizontal cylinder blockage was broken down into three parts: (1) normalization of the scattered beams due to the vertical aperture distribution, (2) calculation of the fields on the cylinder due to the horizontal aperture distribution, and (3) calculation of the dual beam azimuth pattern of the cylinder.

3.2.2.1 Normalization

The normalization of the horizontal cylinder pattern was implemented by considering the elevation radiation pattern of the cylinder. If the blockage configuration is viewed from the side, as in figure 17, the geometry appears identical to the vertical cylinder blockage configuration of paragraph 3.1. The very same analysis is then used to calculate the pattern of the cylinder due to the vertical illumination of the aperture. However, only two angles are of interest, corresponding to the two beams of figure 18.

3.2.2.2 Cylinder Illumination

To determine the illumination on the cylinder, the horizontal aperture of the antenna is first subdivided into N subapertures so that any point on the cylinder is in the far field of the subapertures. The same techniques described in paragraphs 3.1.2.1 and 3.1.2.2 are used to make the size of the subapertures as large as possible, while still retaining good accuracy.

While the illumination across any antenna subaperture is assumed to be the sum of a uniform illumination and a tapered illumination, the cylinder subapertures will be assumed to have only a uniform illumination. As a result, the size of the cylinder subapertures is made less than $\lambda/2$ to eliminate grating lobes from the calculation.

To determine the fields on the m^{th} cylinder subaperture, the contributions from each of the N antenna subapertures are summed vectorally, as shown in figure 20. Repeating this procedure for each of the M cylinder subapertures determines the total illumination on the cylinder.

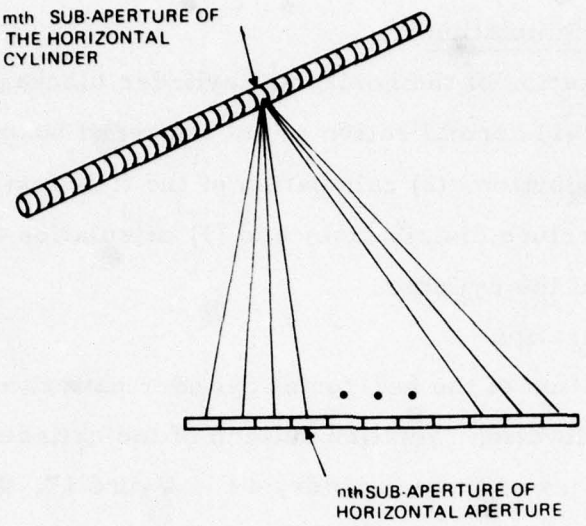

77-1070-V-20

Figure 20. Horizontal Cylinder Illumination Geometry

3.2.2.3 Dual Beam Cylinder Radiation Patterns

Combining the two radiated beams from the cylinder is accomplished using the geometry shown in figure 21. If d is the size of the cylinder subapertures, and SQNT is the azimuth squint angle of the antenna, then the forward beam radiated from a typical subaperture at an angle θ is

$$\sin(X1)/X1$$

where

$$X1 = \frac{\pi d}{\lambda}(\sin(PHI - \theta) - \sin(SQNT - \theta))$$

Setting PHIR = PHI - π, the scattered beam radiating from the subaperture is sin (X2)/X2 where

$$X2 = \frac{\pi d}{\lambda}(\sin(PHIR - \theta) - \sin(\theta - SQNT))$$

Summing the contributions from each subaperture on the cylinder, and phasing the fields to a common phase center gives the complete azimuth pattern of the horizontal cylinder.

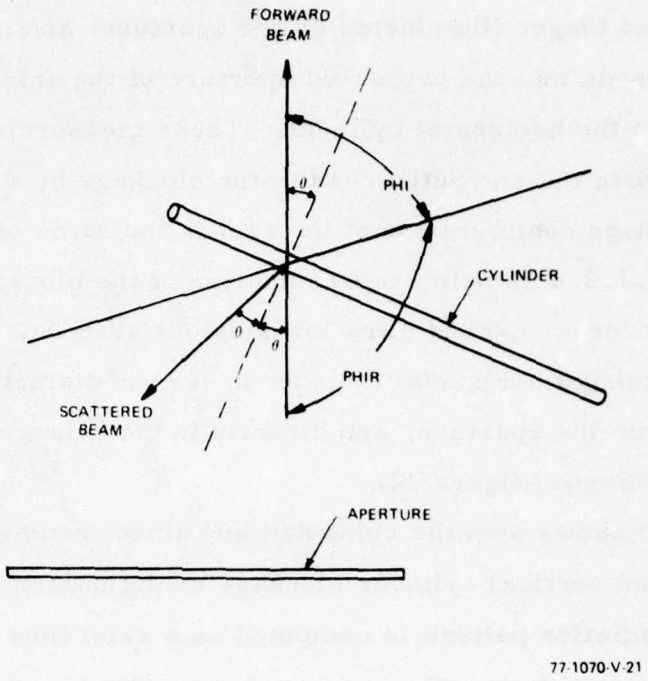

Figure 21. Dual Beam Geometry

To complete the horizontal cylinder analysis, the blockage of the scattered beam by the antenna must be considered. For small angular offsets of the cylinder relative to the antenna, the scattered beam is blocked by the aperture. Rather than performing a detailed reradiation analysis, as in paragraph 3.1.2.4, the scattered beam is simply eliminated from the calculation in these situations. (Diffraction effects from the edge of the aperture are beyond the scope of this study). The scattered beam is only included for angular offsets where less than half the projected cylinder aperture is blocked by the antenna, and eliminated otherwise.

3.2.2.4 Experimental vs Theoretical

Radiation patterns of an antenna blocked by a horizontal cylinder alone were not measured during the experimintal phase of the study. However, blockage measurements were made for various combinations of horizontal and vertical cylinders (section 2). At angular offsets where the vertical

cylinder is no longer illuminated by the aperture, and only the horizontal cylinder extends into the projected aperture of the antenna, the blockage is due totally to the horizontal cylinder. These measurements can thus be used to validate the computed results for blockage by a horizontal cylinder.

The blockage configuration of interest is the same one described in paragraph 3.1.2.4 as being representative of the blockage in a shipboard environment for an L-band ultra low sidelobe antenna. But in this case, we are including a horizontal cylinder 0.409 λ in diameter, 29.44 λ long, located 14 λ from the aperture, and directly in the center of the vertical aperture of the antenna (figure 22).

Figure 23 shows both the computed and actual radiation patterns of the horizontal and vertical cylinder blockage configuration of figure 22(a). The unblocked radiation pattern is computed as a reference and is designated by the discrete symbols 0. The upper and lower limits of the computed blocked pattern are designated by the discrete symbols Δ and + respectively. (see paragraph 3.1.2.4 for a discussion of these limits.) Several points should be made about this pattern.

First of all, the agreement between the measured and computed patterns is excellent. The rapid reduction in power at approximately 140 degrees is due to the blockage by the antenna of the scattered energy from the vertical cylinder as described in paragraph 3.1.2.6. The descrepancy between the measured and acutal patterns in this region is attributed to the diffraction of the scattered energy by the edge of the aperture.

Secondly, the pattern of the antenna blocked by the combination of a vertical and horizontal cylinder (figure 23) is virtually identical to the pattern of the antenna blocked by vertical cylinder alone (figure 12). This result was not unexpected, since the scattered beam from the horizontal cylinder is being blocked by the antenna and does not show up in the sidelobe region. The differences between the computed patterns for the two cases results from the fact that the point spacing used to calculate patterns to $\pm$ 180 degrees

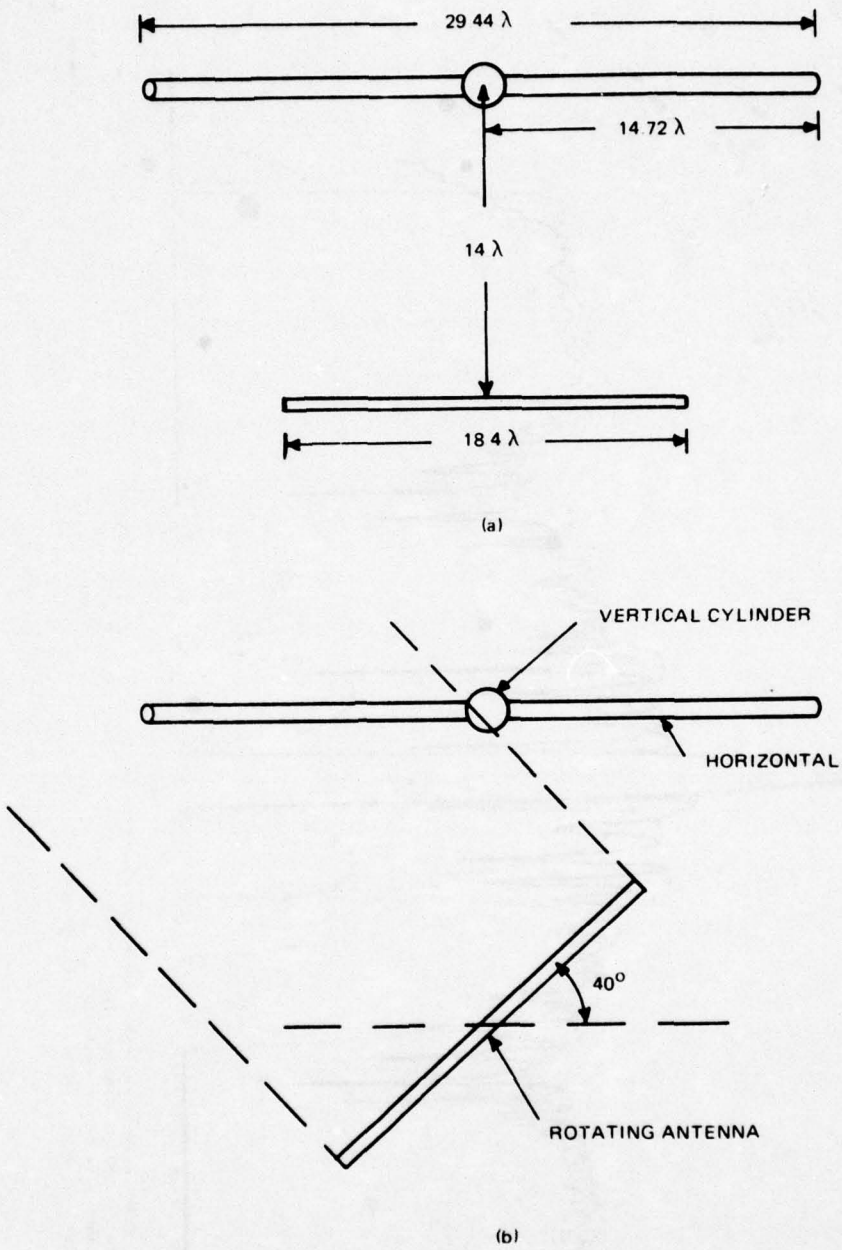

Figure 22. Horizontal and Vertical Cylinder Blockage Geometry

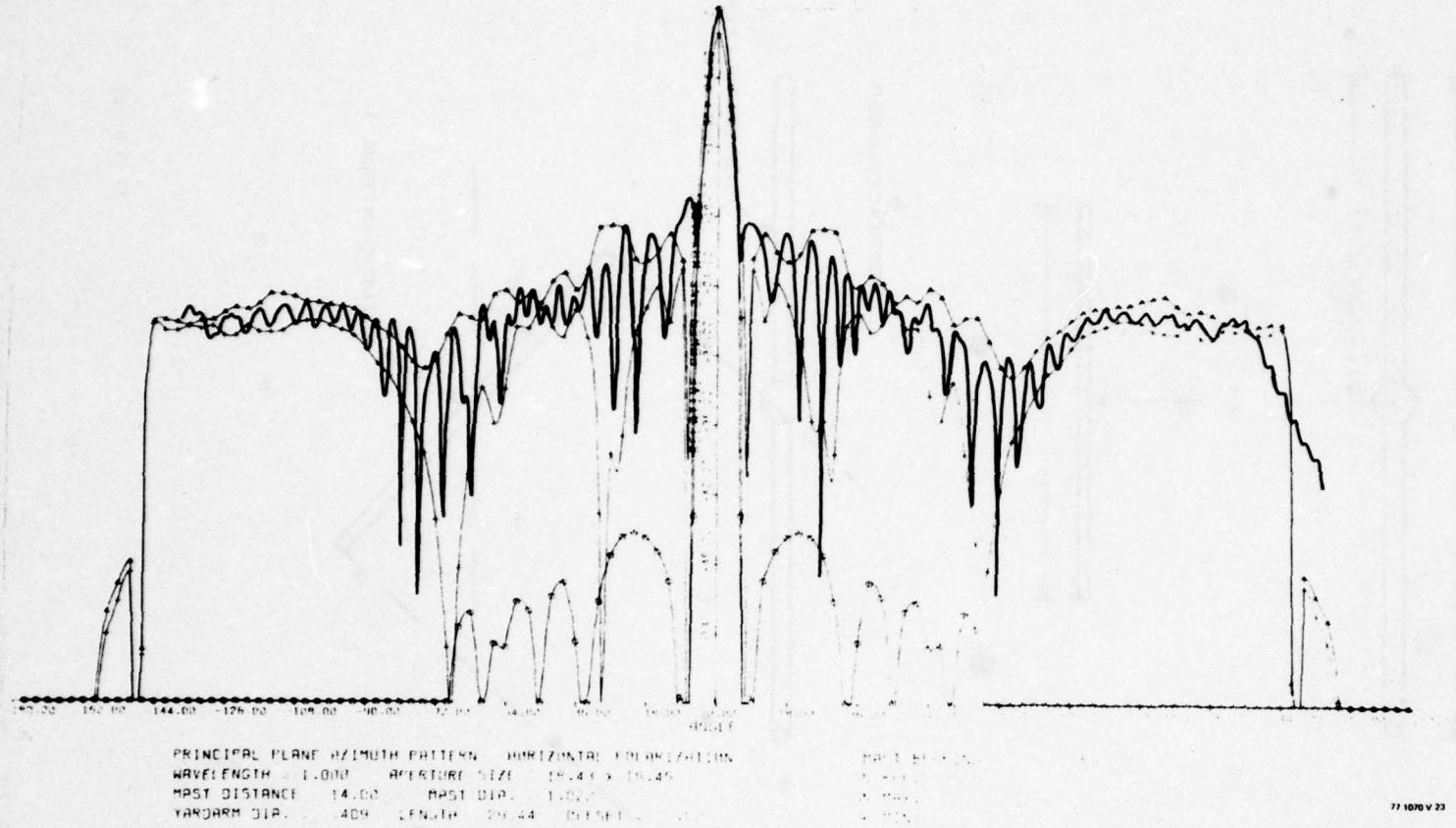

Figure 23. Horizontal/Vertical Cylinder Blockage, Obstacle Bearing = 0°

is twice that used for $\pm$ 90 degrees, and the plotting routine connects the points differently for the two cases. The minor differences between the measured pattern for the two cases can only be attributed to the reradiation by the antenna of the scattered beam from the horizontal cylinder.

As the antenna rotates away from the on-boresight blockage configuration of figure 22(a), the blockage due to the vertical cylinder steadily decreases, because it is no longer being illuminated by the center of the aperture where the illumination is a maximum. Simultaneously, the scattered beam from the horizontal cylinder is directed away from 180 degrees according to the relation $\phi = 180 - 2\theta$ until it is no longer blocked by the aperture and appears in the far out sidelobes of the antenna.

When the antenna has rotated 40 degrees to the position shown in figure 22(b), the blockage effects of the vertical cylinder are negligable, and the blocked pattern of the antenna is due to the scattering from the horizontal cylinder. Figure 24 verifies this fact. Here the blocked pattern was calculated assuming that only the horizontal cylinder was blocking the aperture. As expected, the blocked pattern has dropped to the level of the unblocked pattern at all angles except near $100° = 180 - 2(40)$, where the scattered beam from the horizontal cylinder rises up above the sidelobes of the antenna. For comparison, the measured pattern has been plotted in this region, showing good agreement. (The complete measured pattern is shown in figure 43.) The slight angular offset between the two patterns can be attributed to the angular tolerance of the test fixture used to position the obstacle relative to the antenna.

A graphical summary of the level of the scattered beam as a function of various blockage variables is presented in Section 4.

3.3 PLATE BLOCKAGE ANALYSIS

In this section, we shall discuss the theoretical basis and technique for calculating low sidelobe antenna patterns, with a thin rectangular plate in the near field. Three patterns are computed: (1) the direct pattern,

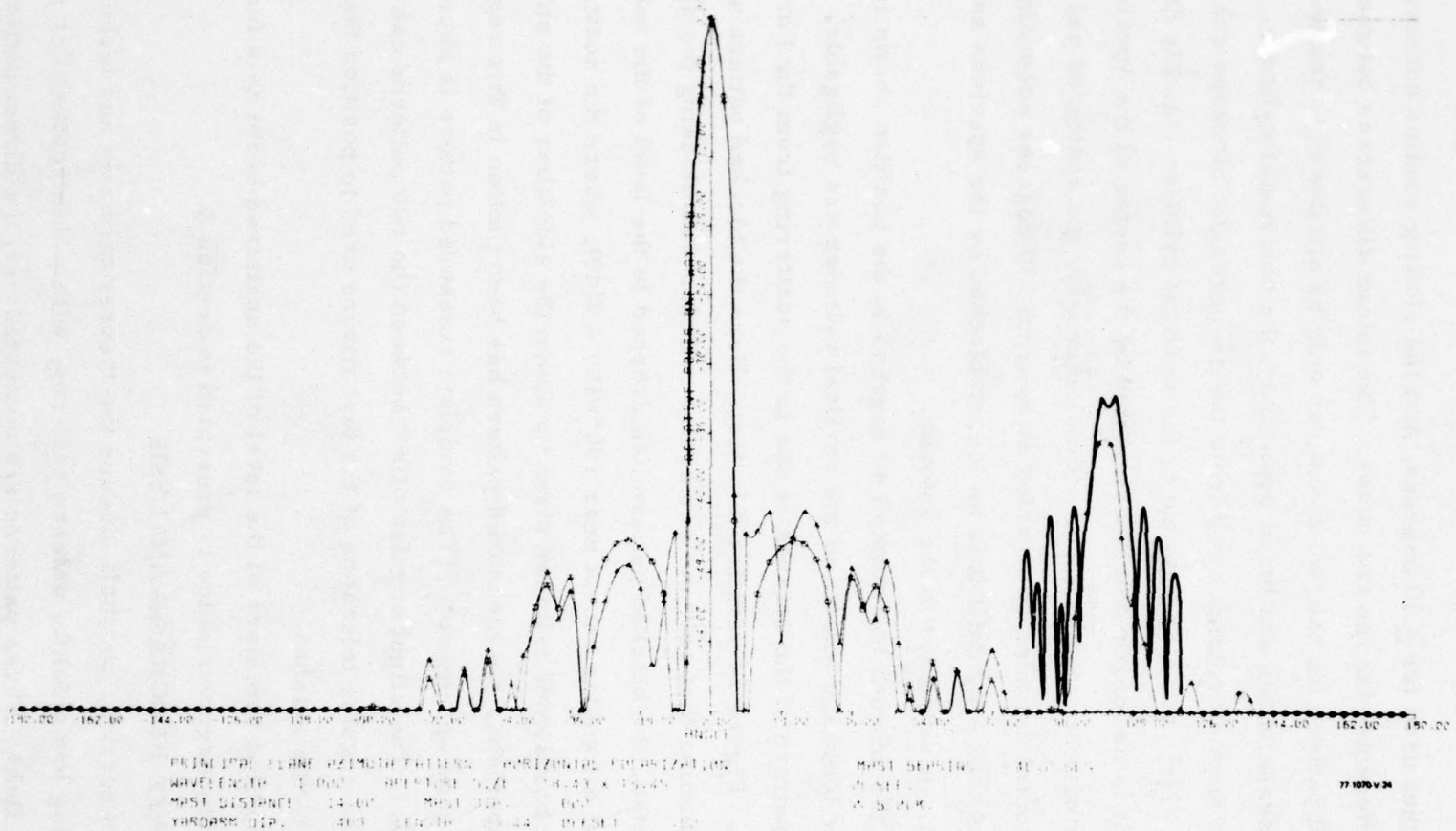

77-1070

Figure 24. Horizontal/Vertical Cylinder Blockage, Obstacle Bearing = -40°

computed as if there were no blockage at all; (2) the pattern of the energy blocked by the plate, which is removed from the direct pattern; (3) the pattern caused by energy reflecting back from the plate, bouncing off the antenna face. Before getting into the analytical details, a description of the geometry and an overview of the calculation will be helpful.

3.3.1 Plate Geometry

The geometrical configuration is shown in figure 25. The plate axis is parallel to the antenna axis. The two axies are separated by an arbitrary range and angle, and the centers may be displaced in height. The plate may be rotated about its own axis.

3.3.2 Method Of Calculation

The radiated fields of an antenna can be projected to a surface, some distance away from the antenna. If all the fields are then reradiated from that surface, the total pattern will be produced. Blockage can be taken into account by not including the radiation from the blocked area. The direct or

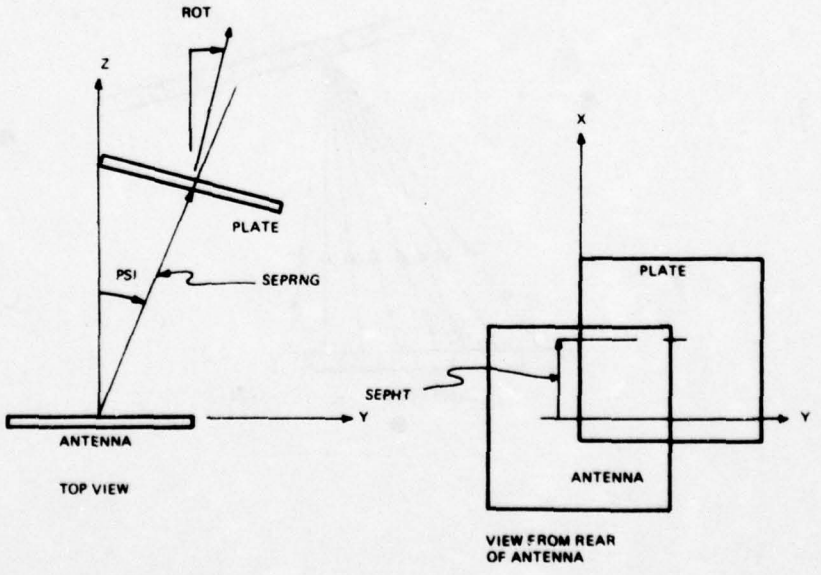

Figure 25. Plate Geometry

unblocked pattern is equivalent to the total pattern from a surface completely enclosing the antenna. The equivalent of this is achieved by calculating the pattern due to the blocking area and subtracting its pattern from the direct pattern. This is similar to the aperture blocking technique presented by Silver 4 which is commonly used to account for horn blockage.

To calculate the portion of the pattern blocked by the plate, the plate is divided into small regions and the radiation from the antenna at each region is integrated (see figure 26). Subapertures of the antenna are chosen small enough to ensure that the subregion of the plate will be in the far field of each antenna section. The far field pattern of these fields is computed and subtracted from the direct radiation.

A second bounce signal, that is, the reflection off the plate and back off the antenna face, has been identified as a major contributor to the final

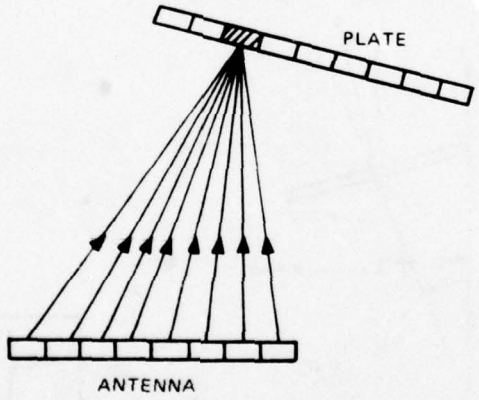

77-1070-V-26

Figure 26. Field Integration at Plate

patterns. Thus after deriving the plate fields, the currents on the antenna face, received from the plate, are determined and the pattern they cause is added to the total pattern.

The three patterns used in deriving the resultant pattern are shown symbolically in figure 27. The computer program developed to analyze this problem prints out these three primary contributors to each pattern relative to the direct pattern. These patterns are applicable to the two-dimensional case, in other words, the antenna and the blocker may as well be infinite in height at this point. The program then goes on to print out the resultant pattern, taking into account heights and offsets. Two additional patterns, the maximum and minimum or envelope due to the second bounce, are also printed. This is desirable because of the extreme sensitivity to position tolerance. This will be explained later.

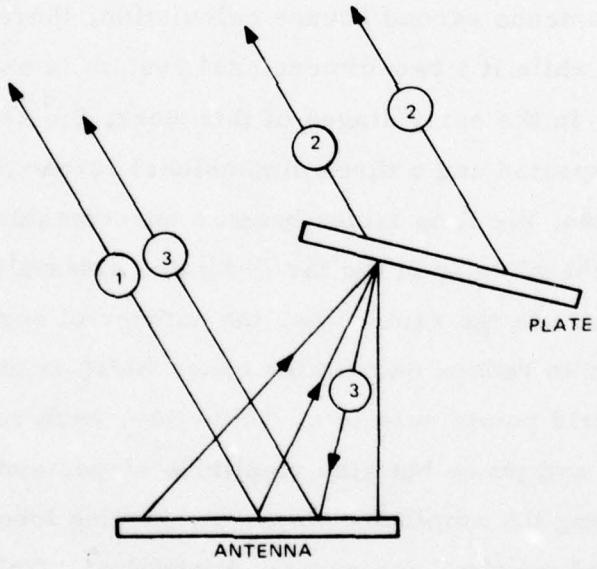

77-1070-V-27

Figure 27. Three Components of Resultant Pattern
(1-Direct, 2-Plate Blocked, 3-Second Bounce)

3.3.3 Antenna Patterns

The antenna is assumed to be rectangular with independent distributions in the azimuth and elevation planes. The distributions are configured as the sum of a series of cosine illuminations on a pedestal. The azimuth distribution may be tilted about broadside as a travelling wave array would steer, with a uniform phase front. These restrictions make it possible to use fewer sample points on the antenna, thus shortening the computation time without impairing accuracy.

The elevation system is intentionally kept simple, being used to determine gain functions and blockage factors. This is done in line with the intent of the study, that is, to examine azimuth sidelobe level as affected by blockage. It also reduces the computation time by several orders of magnitude. The field integration technique used involves many point-to-point calculations. Very simply in three dimensions, if NxN grid points are used in the antenna, the plate, and the antenna second bounce calculation, there are N^6 point-to-point calculations; while if a two-dimensional system is used, there are N^3 such calculations. In the early stages of this work, the second bounce calculation was not expected and a three dimensional calculation was reasonable but with its inclusion, the time factor became unacceptable.

To ensure that the plate is in the far field, the antenna is divided into small subapertures. At the same time, the number of regions must be minimized in order to reduce calculation time, which is mainly determined by the number of grid points selected. To do this, each region is assigned not only amplitude and phase but also amplitude slope, and peak direction of radiation. By adding the amplitude slope, the grating lobes, normally formed by wide grid spacing, are greatly diminished. This method is described in detail in paragraph 3.1.2.2.

Each subaperture field has a three-dimensional vector associated with it which accounts for the type element in the array. In the problem studied,

77-1070

the elements are either vertically or horizontally polarized slots. The fields determined in the antenna subaperture are carried throughout the calculation.

3.3.4 Blockage Region And Second Bounce Pattern Calculation

The surface currents at each plate grid point are calculated by integrating the contributions from each antenna subaperture. The computation uses the subaperture pattern in the direction of the plate grid point, and the cylindrical attenuation factor, the square root of the radial distance. Geometric optics approximations are introduced to account for the area blocked and the phase front across the region. The region is assumed to have the gain of a uniformly illuminated section.

The phase across the region determines the element pattern peak direction. In our analysis, the peak is determined from an optical approximation. Referring to figure 28, the region illuminated by the antenna, that is, where

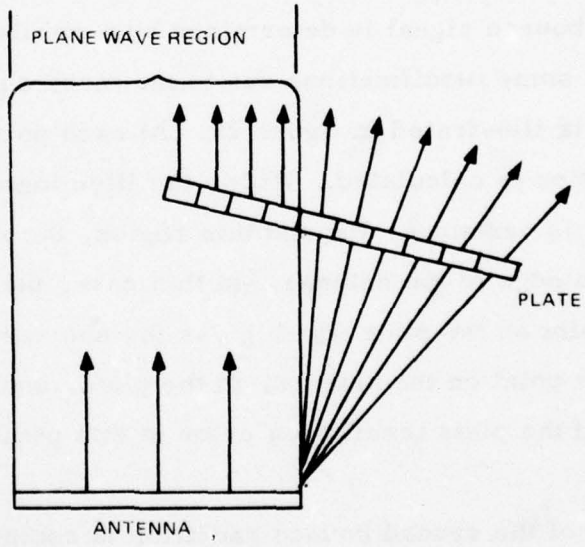

Figure 28. Peak Directions of Radiation at Plate

the projection of the antenna illumination hits the plate, the direction of the element pattern is the same as the antenna radiation. Outside this region, the direction is assumed to come from the edge of the antenna closest to the plate grid point.

The pattern of each blocked region is summed in the far field, and phased relative to the antenna axis. For this calculation, it is impractical to compute the amplitude slope for the plate subregions, therefore the grid points must be reasonably close, between 0.5 and 1 wavelength, to avoid grating lobes in this portion of the calculation.

The fields at the plate are also used to compute the fields reflected back to the antenna, resulting in the surface currents on the antenna face. This calculation is done in the same way as the antenna-to-plate calculation, except that the element peak direction is reflected about the normal to the plate in accordance with Snell's Law. Again, the illumination is assumed uniform, thus the grid points must be reasonably close. The peak radiation direction of this second bounce signal is determined by a similar mechanism to that of the plate, with some modifications due to the more complicated situation. The technique is illustrated in figure 29. At each point on the antenna face, a unique direction is calculated. Within the illuminated region, the plane wave direction is assumed. Beyond this region, the radiation is assumed to originate at the edge of the antenna. In this case, the path is determined by computing a point on the plate which gives the shortest round trip path length from the point on the antenna, to the plate, and back to the edge of the antenna. If the plate terminates prior to this point, the edge of the plate is assumed.

The pattern of the second bounce radiation is computed and also phased relative to the antenna axis. Plate blockage of this second bounce radiation is also accounted for, but in less elaborate fashion. In this case, the rays from each second bounce region which would hit the plate, are deleted from the summation. This is reasonable since the region where this signal is

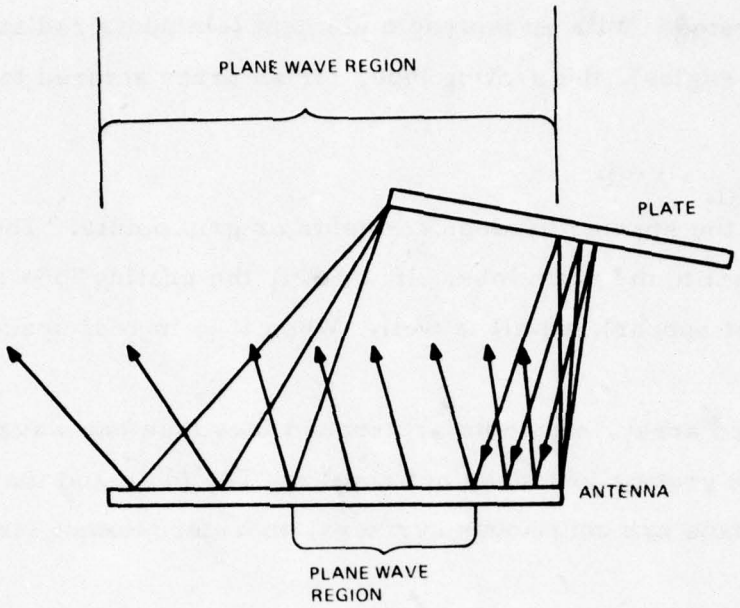

Figure 29. Peak Direction of Second Bounce Off Antenna Face

most apparent is at angles well away from the plate, that is, the plate and the second bounce are at equal but opposite angles from boresight.

This second bounce signal as calculated will be a little larger than in the actual case. This is because a small portion is absorbed by the antenna. The power absorbed by the antenna is a function of the feed network. In series feed networks, like the resonant or travelling wave array, fields which do not correlate or match the transmissions are reflected or reradiated. Were the antenna built with a hybrid coupling network, most of the second bounce power would be absorbed and for an array of ideal elements (with $\sqrt{\cos\theta}$ element patterns), the reflection coefficient would be $\sqrt{1-\cos\theta}$. In the experimental work a resonant array was used, thus most of the power is reflected and this factor is ignored.

3.3.5 Grid Points And Grating Lobes

A few additional words about this critical property of the solution implicated are in order. Grating lobes occur in an array when elements are

widely separated. With an isotropic element (elements radiating equal power at all angles), the grating lobe, for an array steered to boresight, appears at

$$\sin \theta_{GL} = \lambda/SP$$

where SP is the spacing between elements or grip points. The grating lobe is a lobe equal to the main lobe. If $\lambda/SP>1$, the grating lobe is outside real space (cannot appear) and all is well. When it is in real space, it is a problem.

In a slotted array, elements are spaced less than one wavelength apart, therefore the grating lobe does not appear. The plate and the reflection off the antenna face are continuous surfaces, therefore do not form grating lobes.

Inherent in the implemented solution are elements. Each surface is broken up into grid points representing the fields over a small region of that surface. If the grid points are widely separated, the grating lobes come into real space. To compute rms sidelobes, patterns were required to approach $\pm$ 90 degrees, thus the limits of real space.

Amplitude slope has been used, and is discussed earlier, to relieve some of this problem. But for plate positions to the sides of the antenna, a large grating lobe can fall on the plate distorting computed results. It is therefore recommended for wide coverage, to reduce the antenna grid point size to one wavelength or less.

The plate grid points actually have a phase shift as a function of rotation angle. This phase shift is negligable at boresight, but gets large as the obstacle is rotated. If the phase between plate grid points is represented by ϕ, and the grid point spacing on the plate by SPL, the grating lob relative to the plate from its pattern appears at

$$\sin \theta_{GL} = \lambda/SPL - \sin |\phi|$$

If the right-hand side of the equation is less than 1, a grating lobe will appear. This can be avoided if the grid point spacing on the plate is set to $\lambda/2$.

These grid point limits of λ on the antenna and $\lambda/2$ on the plate are not always necessary, but at times will be required. Therefore, it will be necessary for the user of this plate blockage program to consider grid point spacing and grating lobes.

3.3.6 Experimental vs Theoretical Results

Patterns were taken on slotted X-band antenna, blocked by a 19.624 wavelength square plate. The antenna and the test configurations are described in Section 2. In brief, the blocking plate was located 50 and 100 wavelengths from the antenna at a variety of angles and heights. The plate was mounted square on a long arm and the arm was moved radially about the antenna. This plate rotation angle corresponds to just about the worst case, in terms of second bounce radiation. In this case reflections off the plate always hit the antenna, and the second bounce signal is always large in all the measured patterns.

The configuration which best displays the workings of this program is shown in figure 30. The plate is 50 wavelengths from the antenna, -10 degrees off boresight, rotated -10 degrees from boresight, and the heights are equal. In this case, the antenna is slightly more than half blocked. The

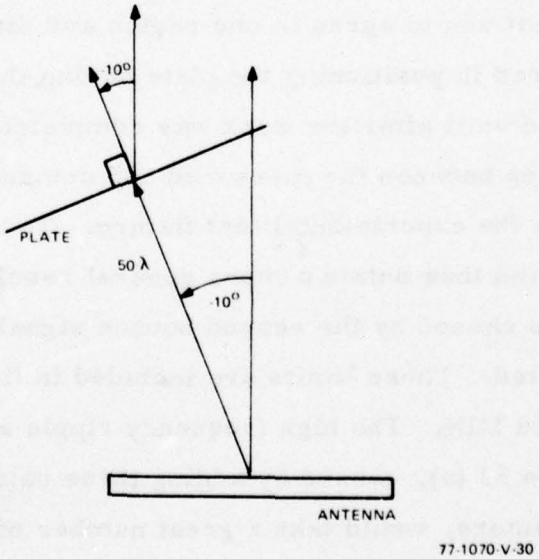

Figure 30. Blockage Configuration Corresponding to Figure 32.

three patterns, the direct or unblocked pattern, the blocked pattern, and the pattern formed by energy bounced off the antenna face, which are added vectorially to make up the resultant pattern are shown in figure 31. They are labeled DIRECT, BLKAGE, and BOUNCE in the figure. These three patterns are part of the normal program output and should be helpful in evaluating blockage problems.

The measured pattern and computed resultant pattern (labeled PATTRN) are shown in figure 32. Comparing these patterns, the computed pattern power falls off from boresight in the same manner as the measured pattern. On the right side of both patterns there is a high frequency ripple caused by the second bounce reflection adding and cancelling with the direct-blocked pattern. Synchronizing these patterns if difficult, in that extreme precision is required in setting up the experiment. An error of 0.25 wavelengths in 50 wavelengths in range separation is enough to rotate the second bounce 180 degrees in phase. This has the effect of interchanging peaks and nulls in the region where the two power levels are comparable. Angular position and rotational angle of the plate shifts the phase of the second bounce pattern relative to the blocker pattern. This type of error will cause the pattern to agree in one region and disagree in another. The accuracy required in positioning the plate during the experimental phase was not realized until after the work was completed. As a result, most of the discrepancies between the measured and computed patterns are due to tolerances in the experimental test fixture. To avoid these tolerance type problems and thus obtain a more general result, the maximum and minimum limits caused by the second bounce signal adding in and out of phase is computed. These limits are included in figure 32(b) and are labeled MAX and MIN. The high frequency ripple seen on the measured pattern of figure 32 (a), caused by adding three patterns with greatly displaced phase centers, would take a great number of sample points to precisely reproduce.

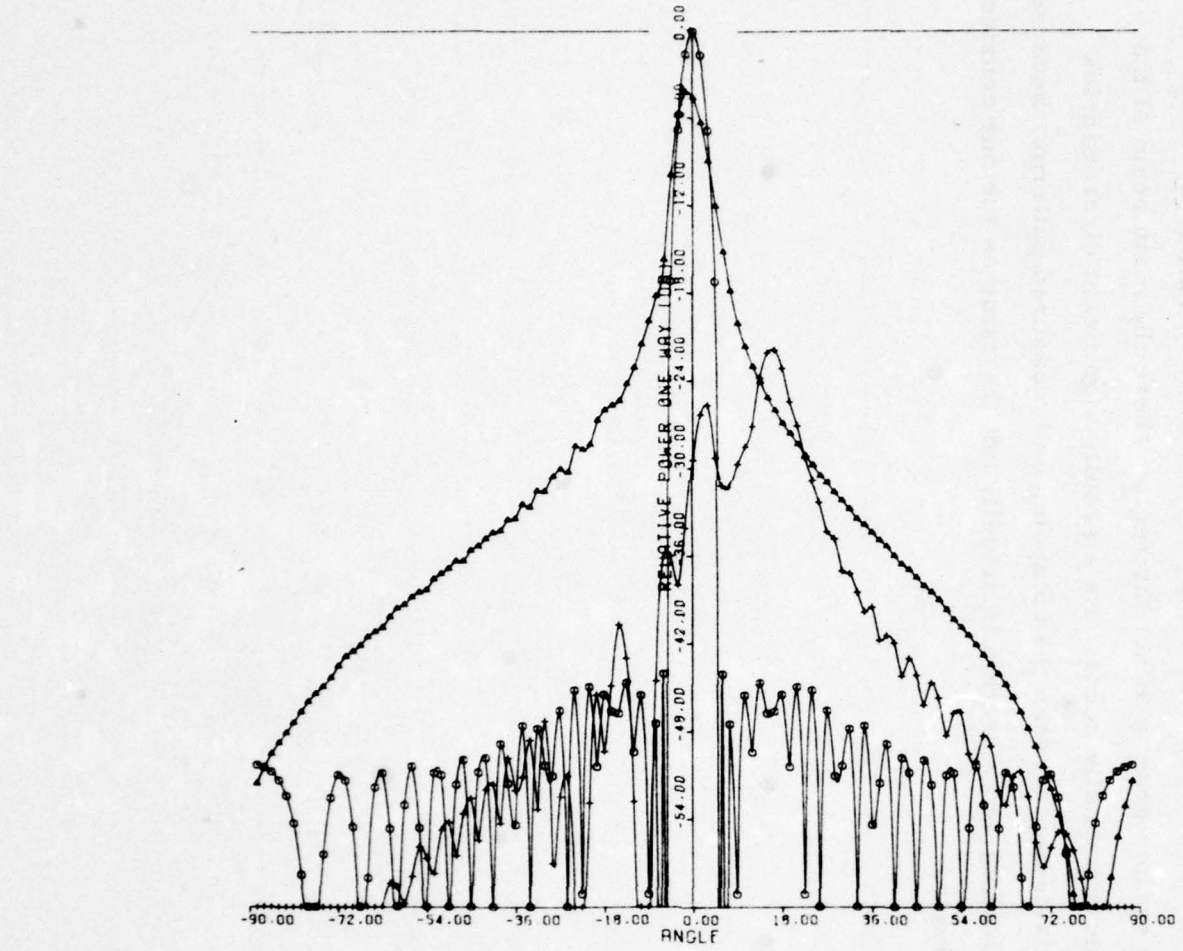

Figure 31. Three Components of Plate Blockage Pattern of Figure 32

77-1070

When the antenna has rotated to a position 20 degrees away from the plate, the blockage has decreased significantly, as shown in figure 33. Again, the comparison between the computed and measured patterns is very good. This type of agreement is typical of nearly all the flat plate configurations that were measured, with one exception. When the plate is located directly in front of the antenna, the positioning tolerances mentioned earlier greatly affect the region where the main beam of the antenna would normally occur. As a result, significant discrepancies exist in this region between the computed and measured patterns, because the experimental configuration is actually not the same as the one considered in the analysis.

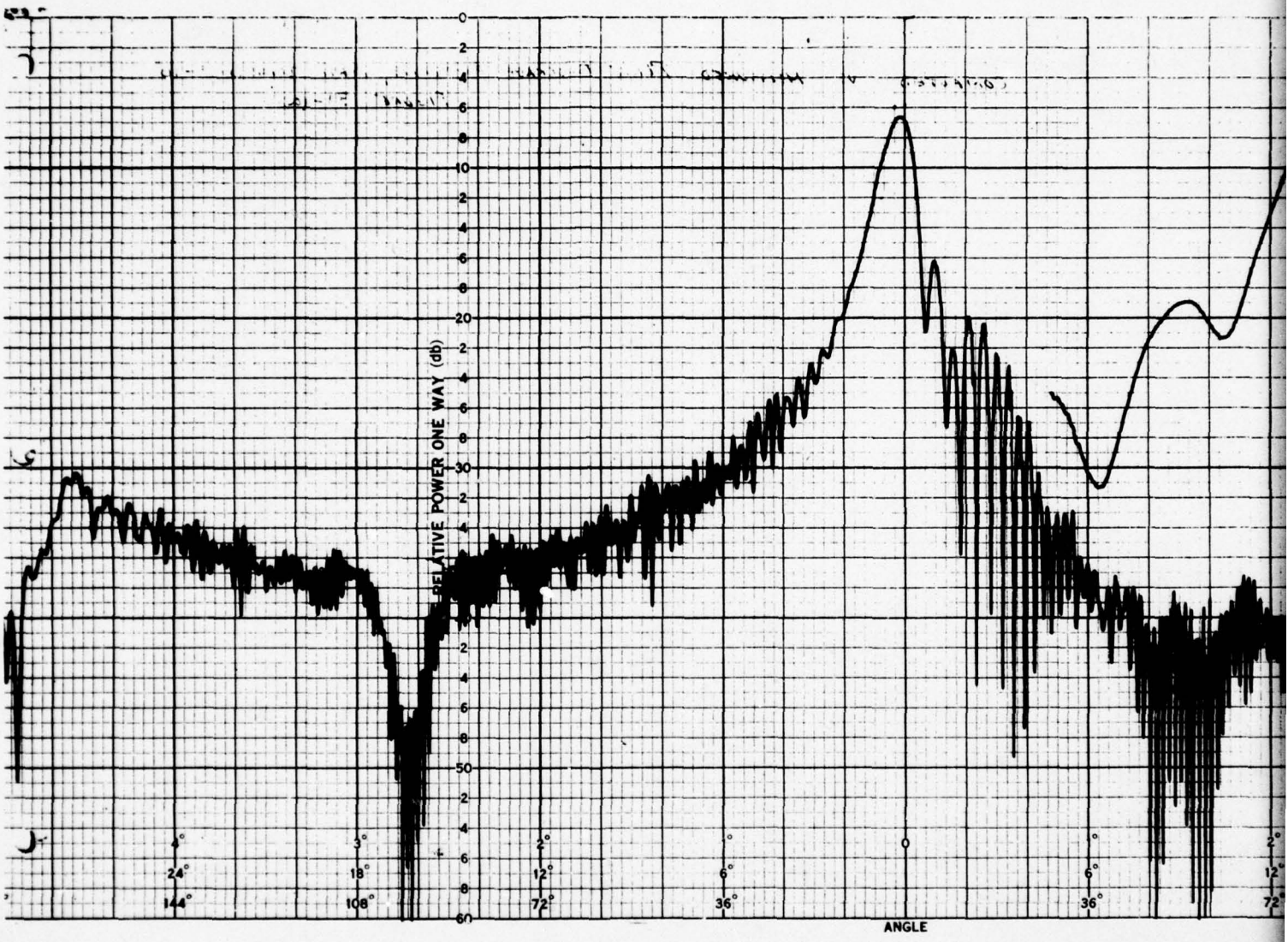
RELATIVE POWER ONE WAY (db)
0
2
4
6
8
10
2
4
6
8
20
2
4
6
8
30
2
4
6
8
50
2
4
6
8
60
4°
24°
144°
3°
18°
108°
2°
12°
72°
6°
36°
0
6°
36°
2°
12°
72°
ANGLE

(A)

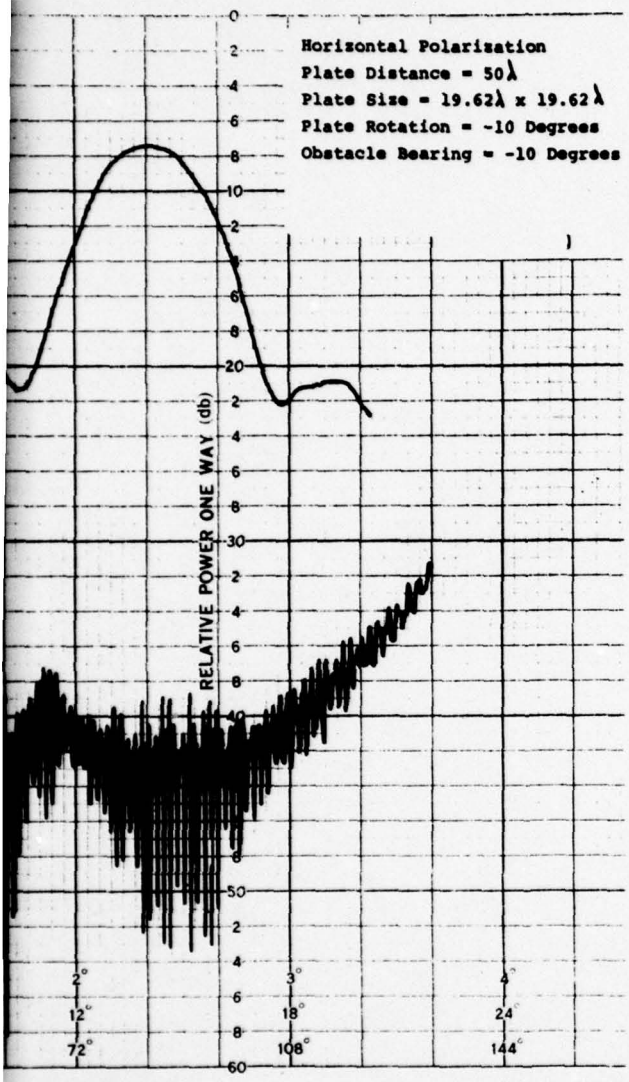

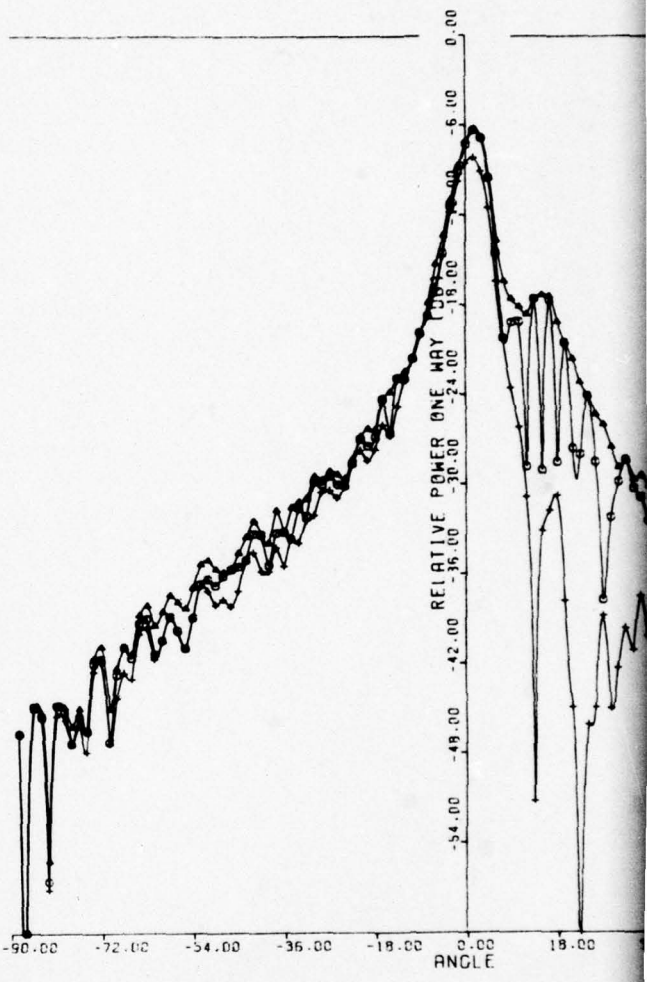

EXP. ANTENNA-HAMMING DIST. HORIZONTAL POLARIZATION
ANTENNA 18.434X 18.453 WL PLATE 19.624X 19.624 WL
PLATE POSITION 50.000 WL, -10 000 DEG. ROTATED -10 000 DEG
PLATE HEIGHT 000 WL

(B)

Figure 32. Computed and Measured Plate Blockage Pa
Bearing = -10°

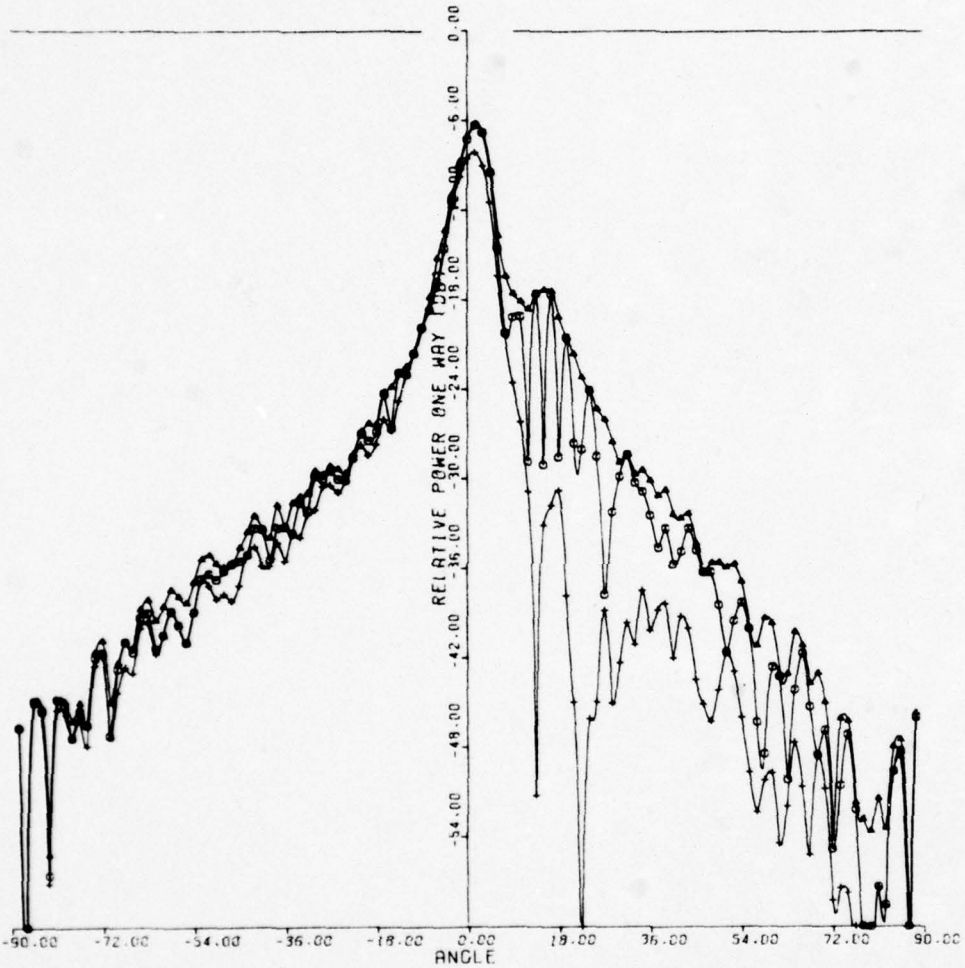

NTENNA-HAMMING DIST. HORIZONTAL POLARIZATION
P 18.434X 18.453 WL PLATE 19.624X 19.624 WL
POSITION 50.000 WL -10 000 DEG. ROTATED -10 000 DEG
HEIGHT 000 WL

PATTERN SYMBOLS
⊙ PATTRN
△ MAX
+ MIN

(B) 77-1070-V-31

Figure 32. Computed and Measured Plate Blockage Patterns, Plate Bearing = -10°

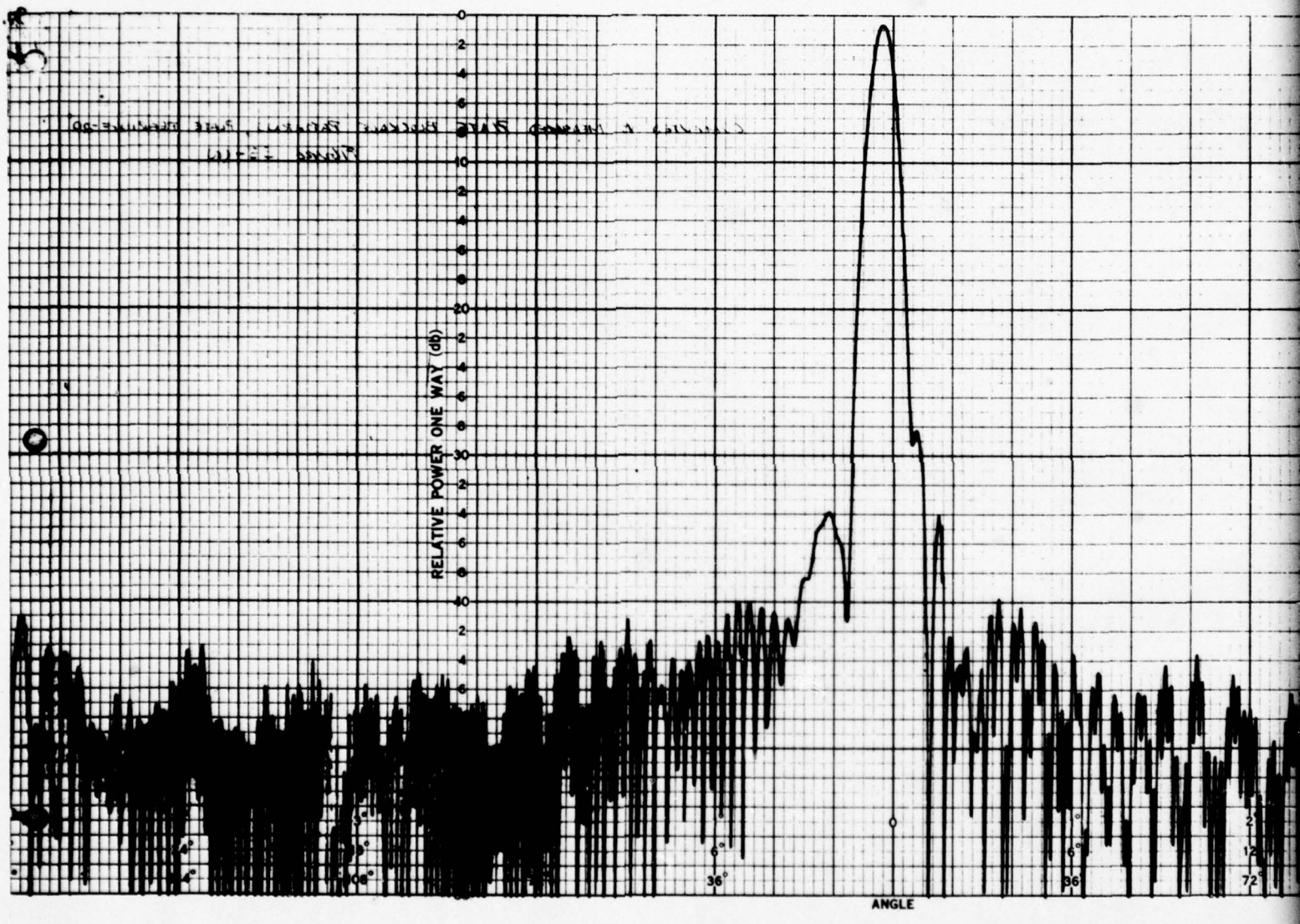
RELATIVE POWER ONE WAY (db)
0
2
4
6
8
10
2
4
6
8
20
2
4
6
8
30
2
4
6
8
40
2
4
6
36°
0
36°
72°
ANGLE

(A)

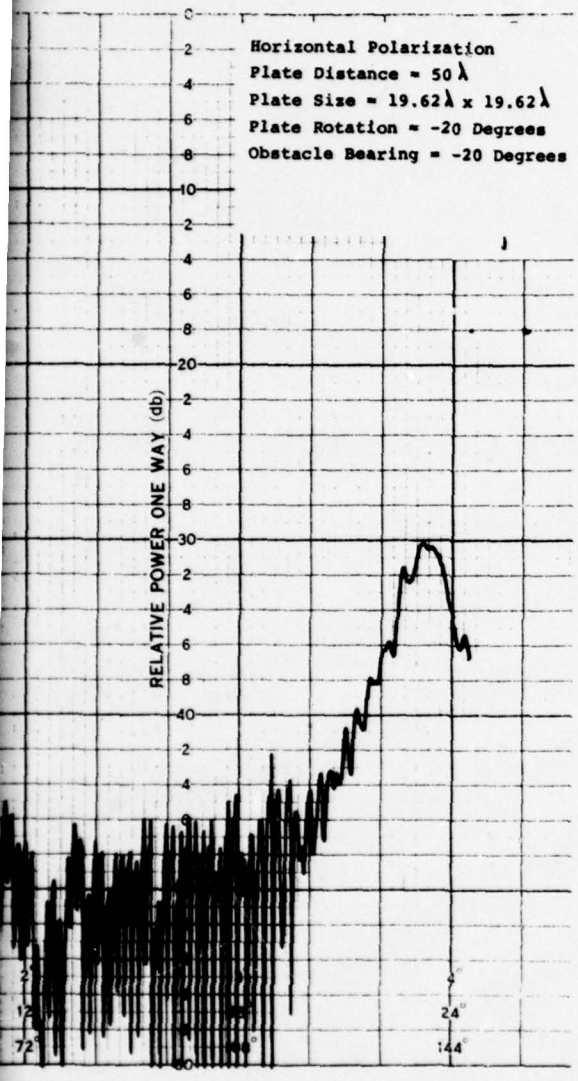

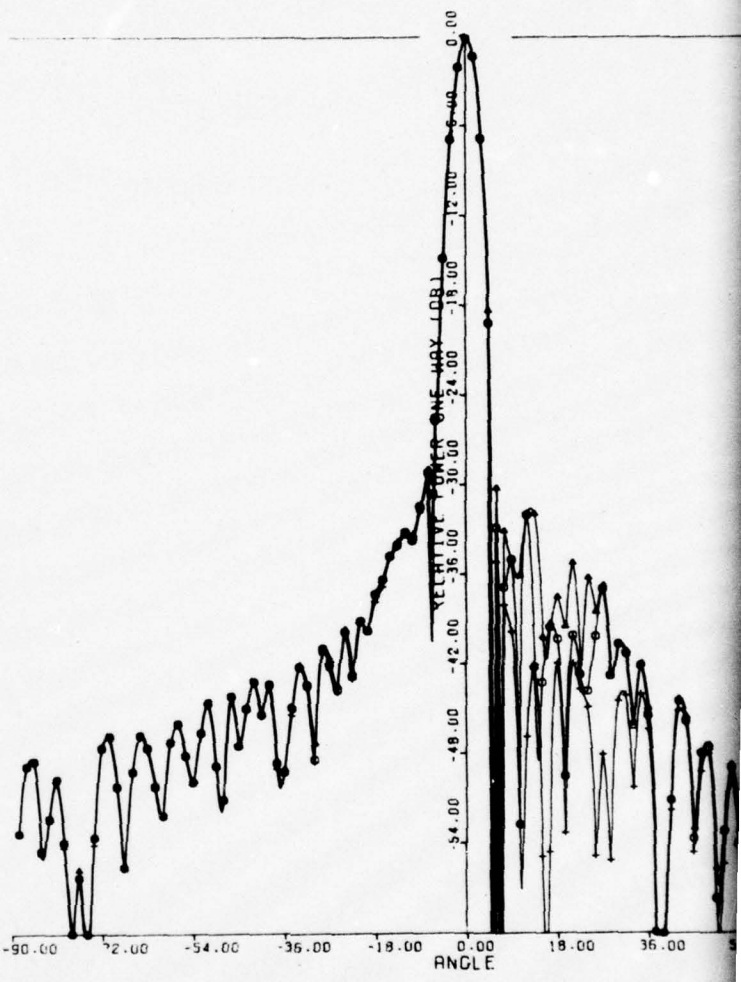

(B)

Figure 33. Computed and Measured Plate Blockage Patter
Bearing = -20°

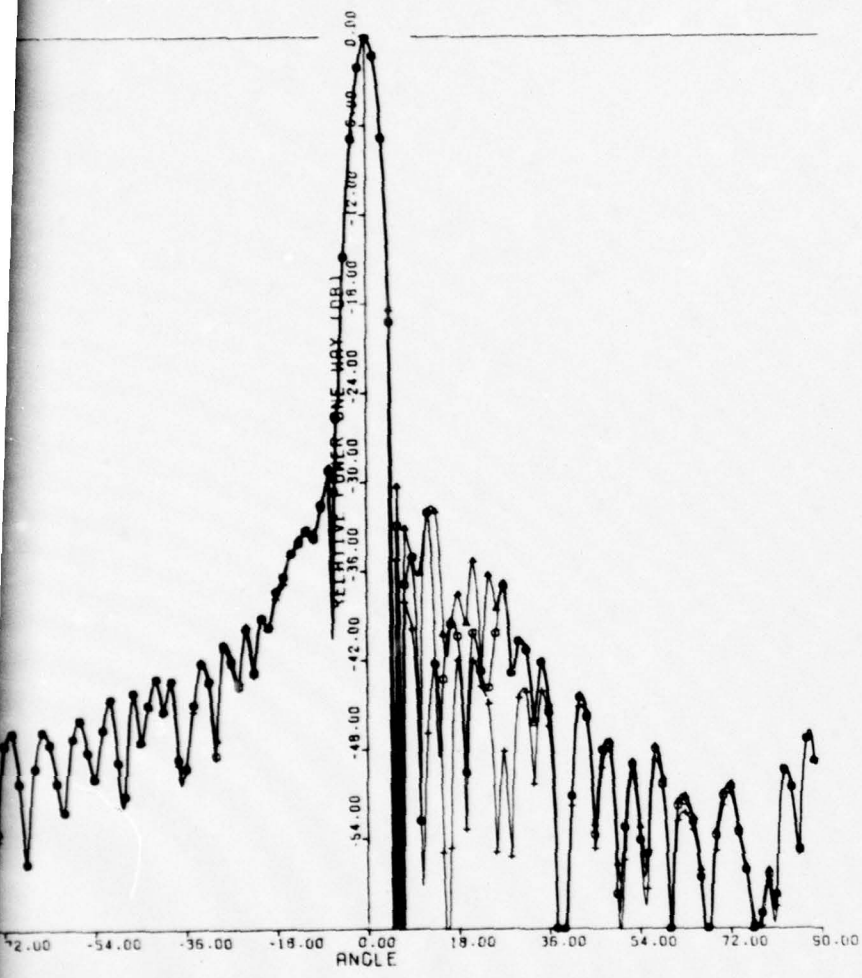

HORIZONTAL POLARIZATION
PLATE 19.624X 19.624 WL
.-20.000 DEG. ROTATED -20.000 DEG

PATTERN SYMBOLS
⏲ PATTRN
△ MAX
+ MIN

(B)

77-1070-V-60

nputed and Measured Plate Blockage Patterns, Plate
ring = -20°

4. GRAPHICAL SUMMARY OF RESULTS

To convey as much information as possible about the results of the experimental and analytical phases of the program, a graphical summary will be used to analyze the effects of selected variables on the sidelobe structure of the blocked radiation patterns for each of the three obstacles. The computational models developed to analyze the various obstacles have been validated by comparison to actual measured patterns in Section 3, and these models are used to generate the results presented in this section. Using these models allows results to be presented for a whole spectrum of blockage configurations beyond those chosen for the experimental phase of the program.

Each of the obstacles that were studied produced different effects on the sidelobe structure of the blocked aperture. Consequently, different parameters are used to generalize the results for each case. The results are presented for horizontal polarization only. Any differences for vertical polarization are described in the text that accompanies each of the plots.

For each obstacle, a typical configuration is chosen as a reference. By varying the individual blockage variables independently, the dependence of the blocked pattern on these variables is determined.

4.1 VERTICAL CYLINDER

The reference blockage configuration for the vertical cylinder is shown in figure 34, where the aperture illumination is determined by a 42 dB Hamming function.

In general, the blockage is a maximum when the bearing of the antenna from the cylinder, θ, is zero. In this case, the cylinder is located in the center of the projected aperture where the illumination is the greatest. The blocked radiation pattern of figure 35 is a good example of this situation.

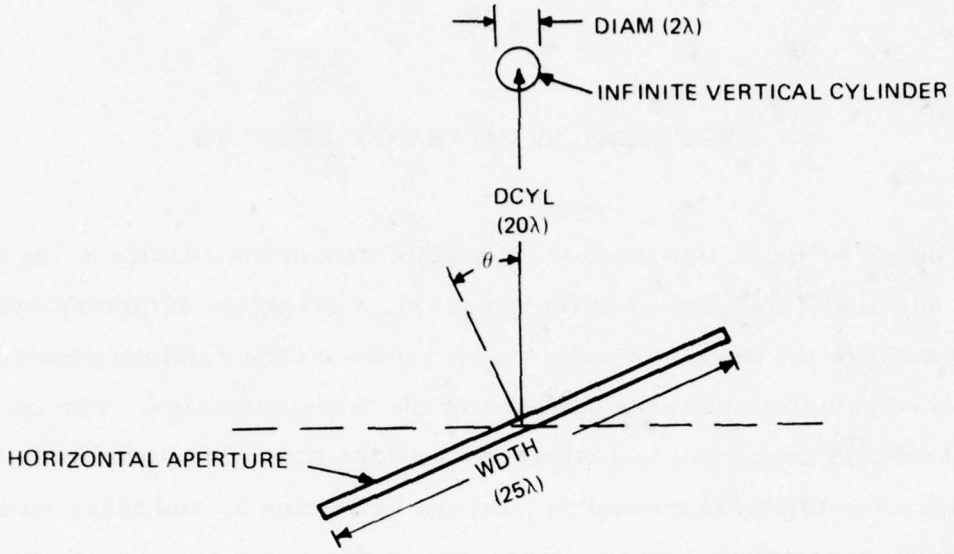

Figure 34. Vertical Cylinder Reference Blockage Configuration

Notice that the cylinder radiates approximately omnidirectionally (except near 180 degrees where the scattered energy is blocked by the aperture), and the total blocked pattern is symmetrical.

As the antenna rotates away from the cylinder, the level of the energy scattered by the cylinder begins to decrease, and the blocked pattern becomes slightly asymmetric as shown in figure 36, where the bearing of the cylinder from boresight is -20 degrees. Soon the antenna will have rotated to a position where the cylinder is no longer in the projected aperture of the antenna, and the effects of the cylinder blockage are negligible. The angular extent of the region during which the cylinder is within the projected aperture thus determines the fraction of time during which the far field pattern of the antenna will be degraded, and is designated as the "critical region."

The graphs in figures 37 and 38 show the magnitude of this degradation as a function of the bearing of the cylinder from the antenna boresight, θ. For vertically polarized radiating elements, the rms values are approximately

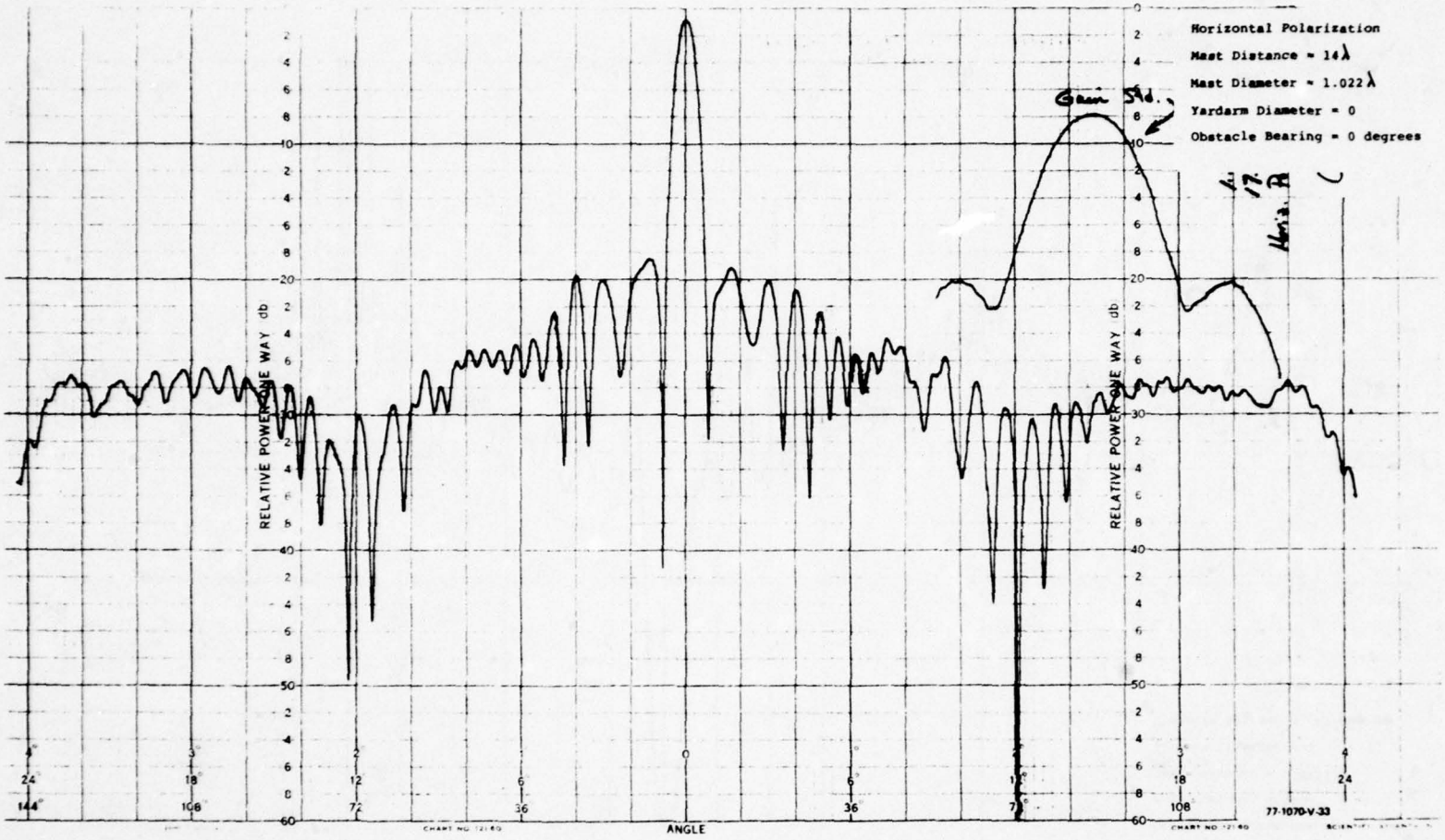

Figure 35. Measured Vertical Cylinder Blockage, Obstacle Bearing = 0°

77-1070

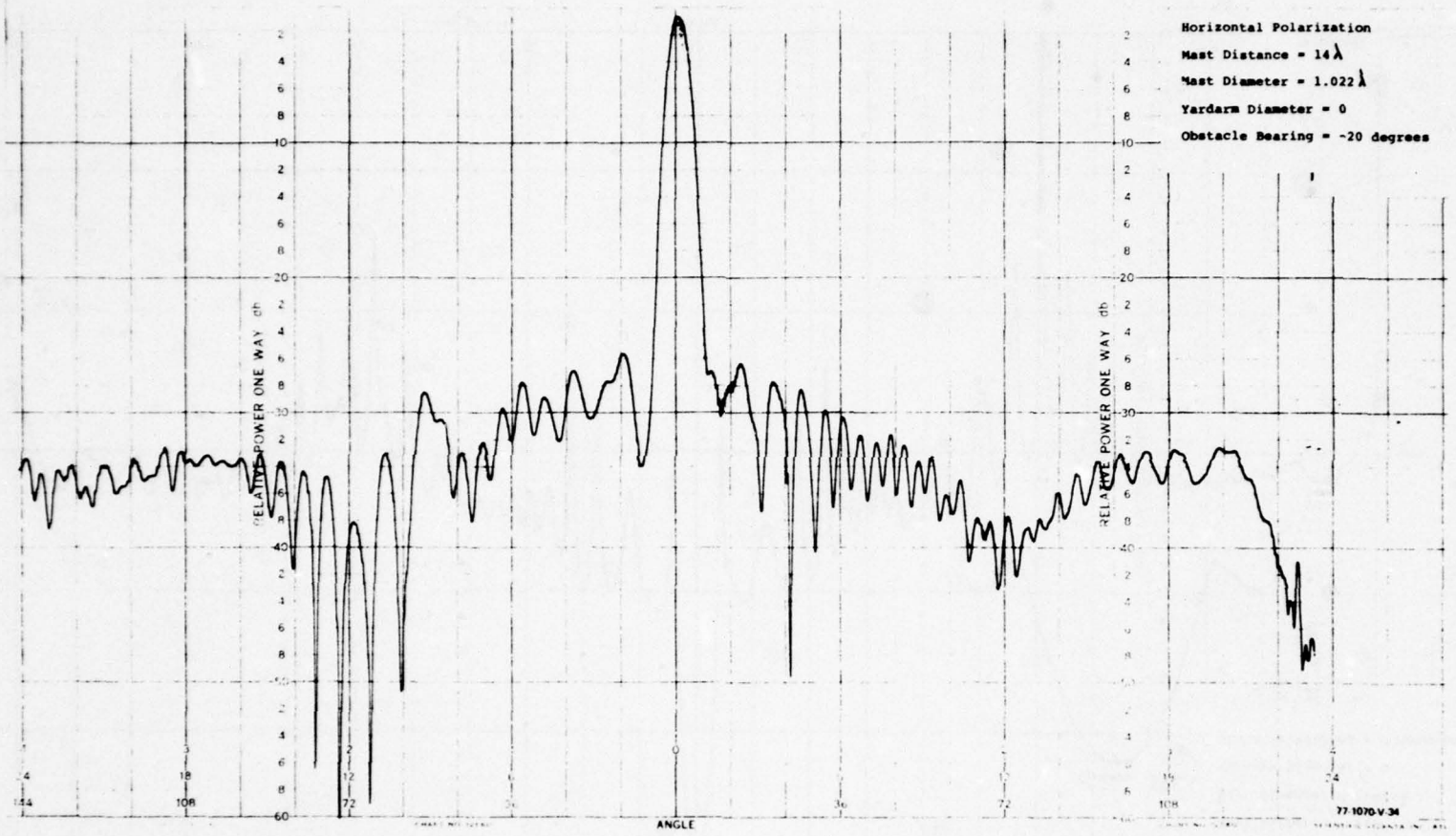

Figure 36. Measured Vertical Cylinder Blockage, Obstacle Bearing = -20°

77-1070

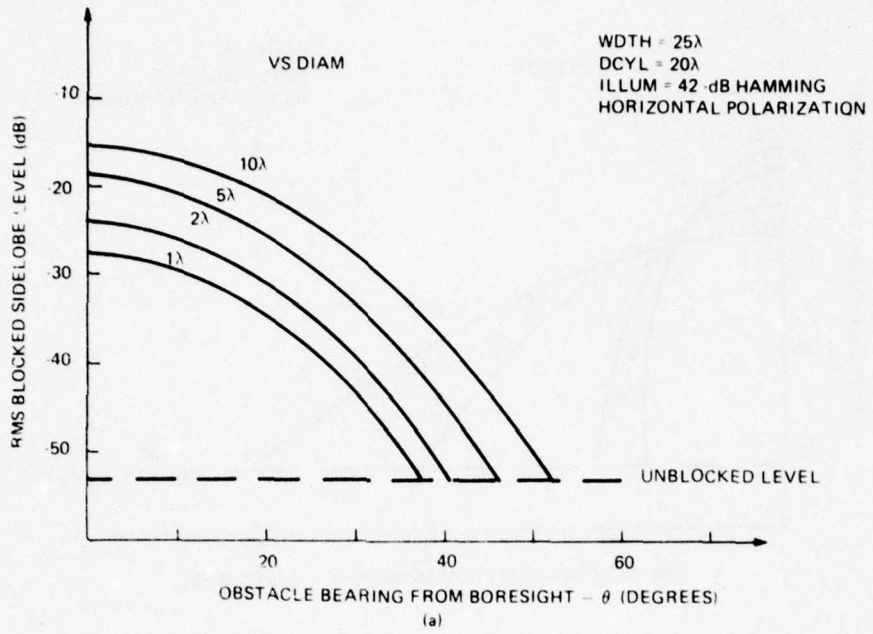

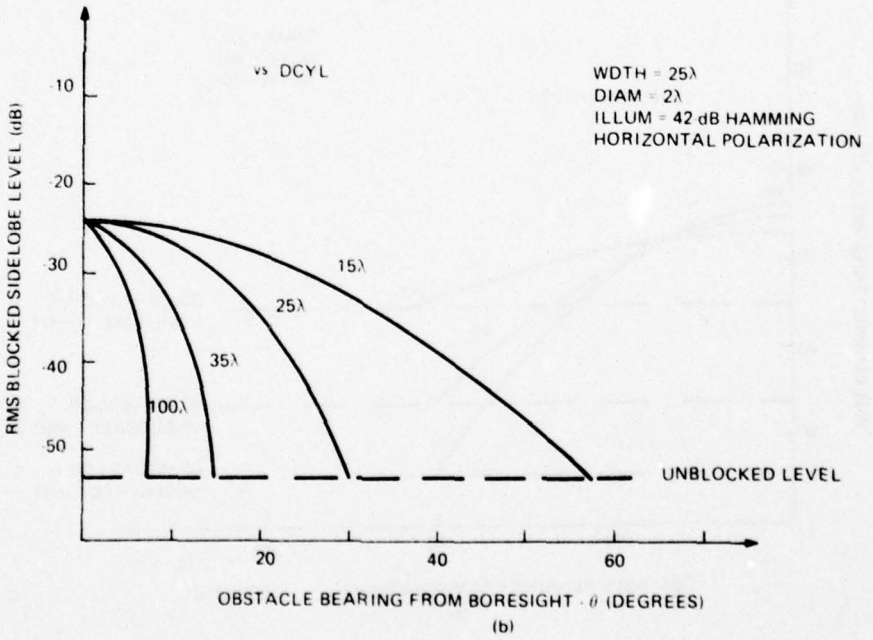

Figure 37. Vertical Cylinder Blockage Dependence on Cylinder Diameter and Distance

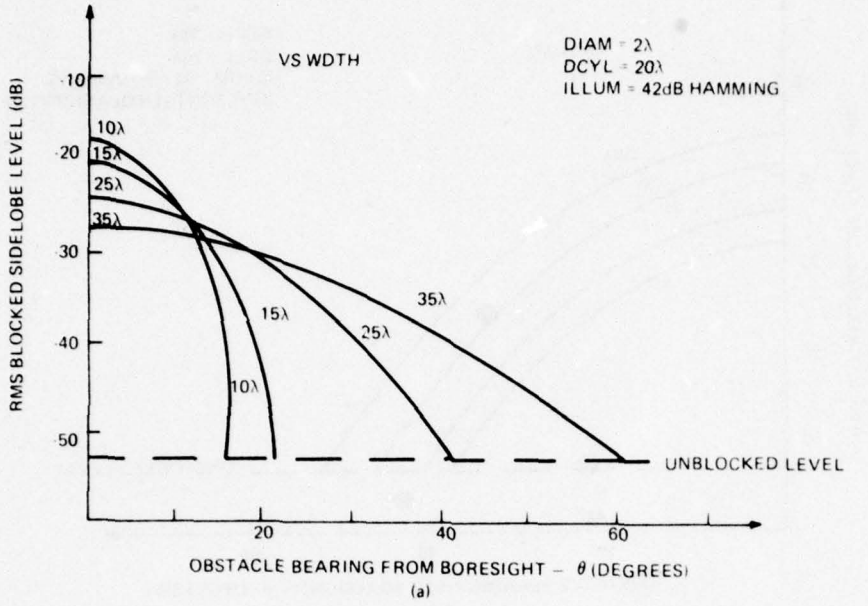

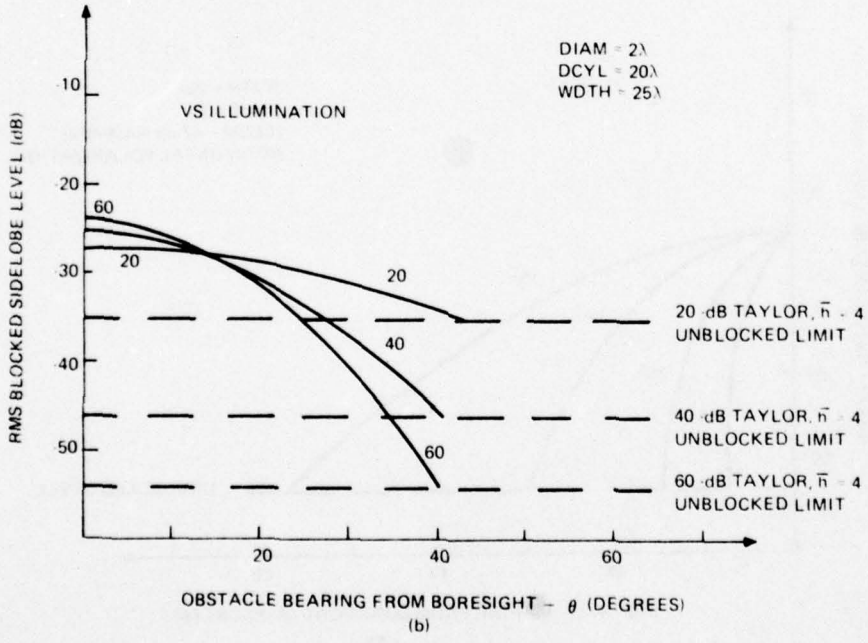

77-1070-V-36

Figure 38. Vertical Cylinder Blockage Dependence on Aperture Size and Illumination

1.5 to 3 dB higher. In each of the four graphs, a different variable is parameterized to determine the dependence of the blocked pattern on these variables. A good measure of the degradation of the sidelobes due to the vertical cylinder blockage is the rms blocked sidelobe level, defined as

$$\text{rms}_{\text{block}} = 20 \log_{10} \sqrt{\frac{\Sigma V^2}{N}}$$

where the v's are the amplitudes of the radiated energy (in volts) at N evenly spaced angles.

Since the blocked sidelobe level is approximately the same at all angles (figure 35), the rms can be taken over any reasonable interval, and the result will be representative of the average sidelobe level at any angle. For the graphs of figures 37 and 38, the rms blocked sidelobe level is measured over ±90 degrees.

Figure 37(a) shows how the rms blocked sidelobe level varies as a function of the cylinder bearing from boresight, for the reference blockage configuration of figure 34. Varying the critical blockage variables will shift the curve up and down, as in figure 37(a), or distort the curve as in figure 37(b), but the dependence is always a smooth steadily decreasing function of θ.

The effects of varying the diameter of the vertical cylinder are shown in figure 37(a), where, as expected, increasing the size of the cylinder increases the rms blocked sidelobe level. Also the extent of the critical region increases significantly for larger diameters.

In figure 37(b), the effects of varying the distance between the antenna center of rotation and the axis of the cylinder, DCYL, are presented. This graph dramatically shows the dependence of the extent of the critical region on this distance. This dependence was not unexpected, since for greater distances, the cylinder will be outside the projected aperture of the antenna much sooner. For most realistic blockage configurations, the angle through

which the antenna must turn before the cylinder is no longer illuminated by the aperture, is approximately

$$\theta_{c/2} = \text{ARCSIN}\left(\frac{\text{WDTH}/2}{\text{DCYL}}\right)$$

where θ_c is the total extent of the critical region. Note that for the case where the cylinder is directly in front of the center of the aperture ($\theta = 0^{\circ}$), the rms blocked sidelobe level is only slightly dependent on the distance to the cylinder.

Figure 38(a) shows the results of varying the width of the aperture, WDTH. Increasing the width causes the extent of the critical region to increase according to the approximation presented in the last paragraph. In addition, the rms blocked sidelobe level for a cylinder bearing of 0° decreases as the size of the aperture is increased. Comparing the graphs of figure 37(a) and 38(a) reveals why decreasing the diameter of the cylinder is not equivalent to increasing the size of the aperture.

To determine whether an ultra low sidelobe antenna is affected any differently from a conventional reflector antenna confronted with the same blockage configuration, the aperture illumination was varied as shown in figure 38(b). This graph reveals several very important facts.

First of all, for the worst case configuration where the cylinder bearing from boresight is 0°, an ultra low sidelobe antenna will have an rms blocked sidelobe level that is approximately 3-dB higher than a conventional reflector antenna. This trend is reasonable, since an ultra low sidelobe antenna has a more sharply peaked illumination function than a conventional antenna does. In other words, a larger fraction of the total illumination is concentrated in the central area of the aperture.

However, the initial difference in the rms blocked sidelobe level soon disappears. For, as the antenna begins to rotate away from the cylinder, the rms blocked sidelobe level of the ultra low sidelobe antenna decreases much more rapidly than that of the conventional antenna. Eventually the

blocked sidelobe levels for the two types of antennas reach the levels of the respective unblocked radiation patterns at the same bearing, θ. That is to say that both the ultra low sidelobe antenna and the conventional antenna have the same size critical region. However, for angles outside this region, the rms sidelobe level of the conventional antenna remains at a level of 35-40 dB, compared to a level of 55-60dB for the ultra low sidelobe antenna.

The information contained in the graph of figure 38(b) can be more fully understood by considering the blocked radiation patterns of figures 39 and 40. These radiation patterns present the vertical cylinder blockage information in an entirely different format than the one used throughout this report for each of the three obstacles.

The patterns discussed in Sections 2 and 3 showed the resulting blocked radiation pattern with the antenna fixed at a specific bearing from the cylinder. In other words, this type of pattern, of which figures 35 and 36 are examples, describes the blocked pattern at a fixed instant of time during the rotational period of the antenna.

For our reference blockage configuration, the radiation patterns of figures 39 and 40 describe the radiated energy seen by a target (jammer) at a specific bearing from the cylinder, $\theta = 60^{\circ}$, as the antenna rotates about its axis (figure 41). These patterns will be referred to as "rotating" patterns in contrast to the fixed position patterns of figure 35. For the computed patterns, the direct, or unblocked, radiation pattern of the antenna is designated by the symbols 0, and is included as a reference. The blocked radiation pattern for the configuration described at the bottom of the plot is designated by the symbols Δ.

The only difference between figures 39 and 40 is the aperture illumination. Figure 39 shows the computed blocked radiation pattern seen by a target 60 degrees away from the cylinder, when the aperture is illuminated by a 25-dB Taylor distribution (simulating a conventional reflector antenna). In figure 40, the illumination has been changed to a 60-dB Taylor distribution to

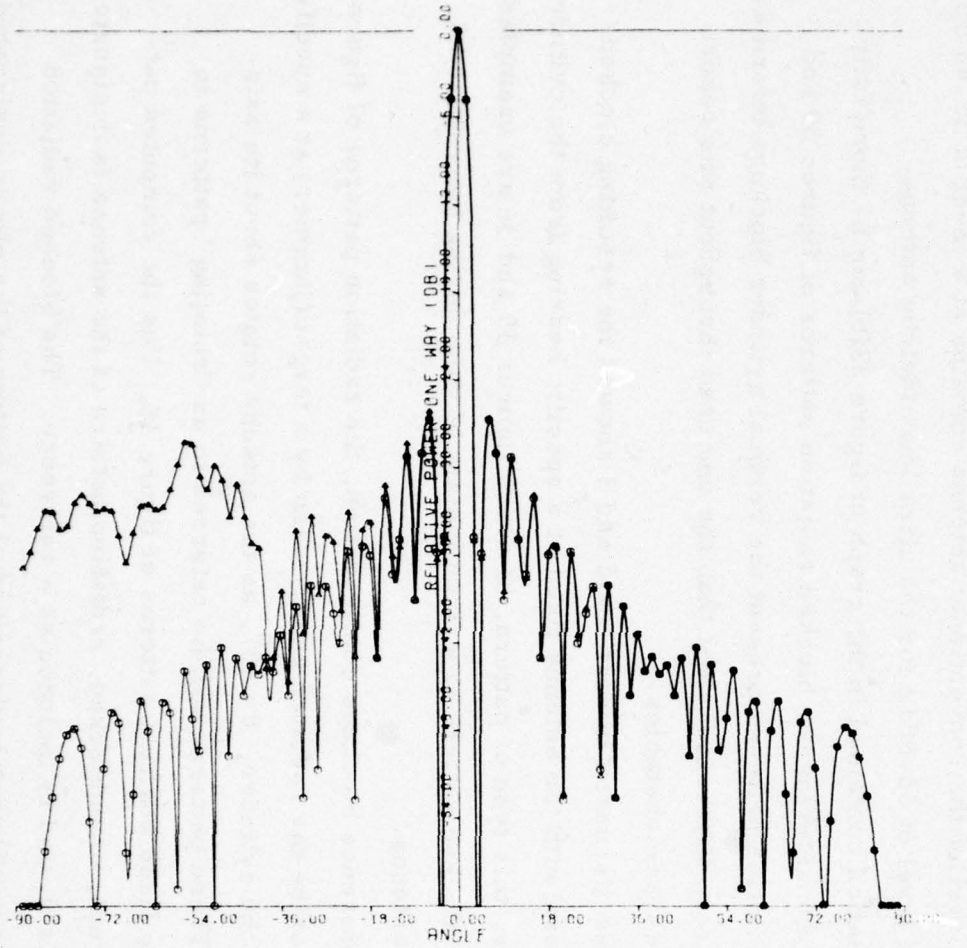

Figure 39. Computed Rotating Antenna Pattern, 25 dB Taylor Distribution

77-1070

77-1070

77

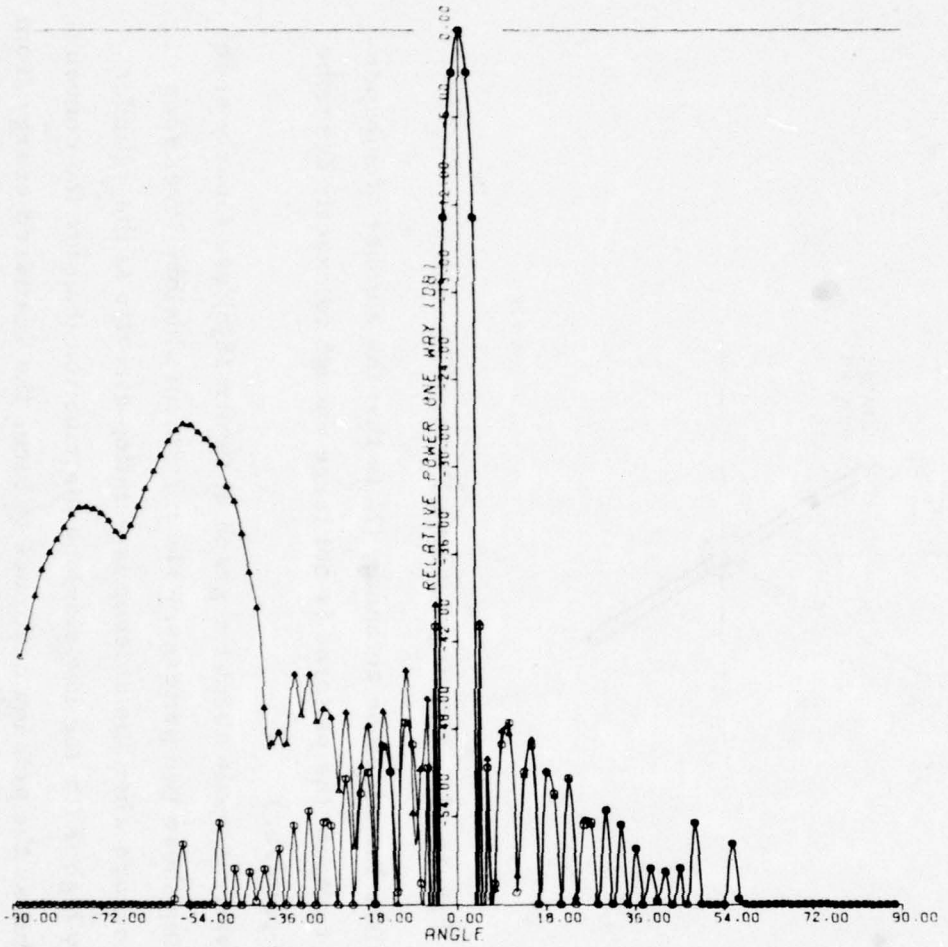

77-1070

Figure 40. Computed Rotating Antenna Pattern, 60 dB Taylor Distributon

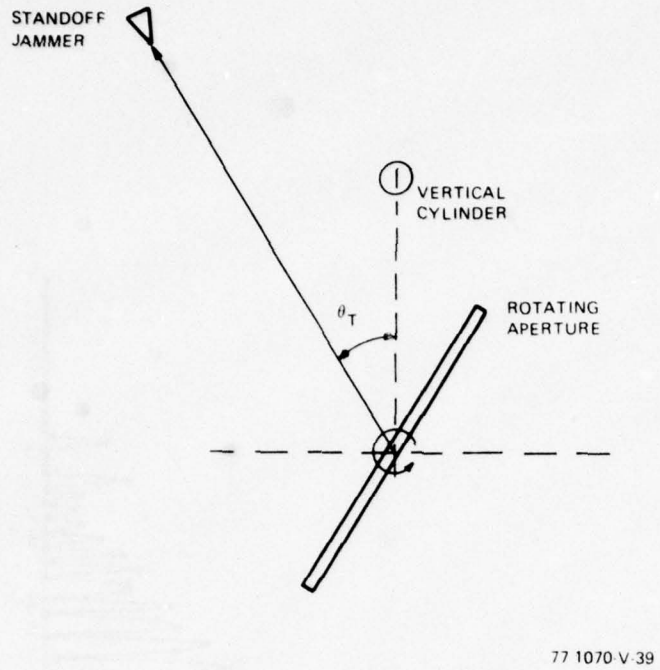

Figure 41. Rotating Antenna Pattern Geometry

simulate an ultra low sidelobe antenna. (Note that the number of subapertures used to compute the patterns is not large enough to exactly describe the unblocked pattern.)

The observations made about the graph of figure 38(b) are clearly seen when comparing these two patterns. The maximum sidelobe level seen by the target occurs when the antenna is pointing directly at the cylinder and is slightly higher for the low sidelobe distribution than for the conventional one. But as the antenna continues to turn, the scattered energy from the cylinder falls off faster in the case of a low sidelobe antenna than for a conventional antenna, soon reaching the sidelobe levels of the unblocked antennas. Obviously, the ultra low sidelobe antenna is far superior to the conventional antenna outside the critical region, as expected. However, we have also shown quantitatively that it is significantly better within the critical region when the cylinder is illuminated by the antenna.

The program used to compute the rotating patterns is not the same as the one used to compute the fixed position patterns. Details for the use of both programs and complete program listings are presented in Appendix B.

4.2 HORIZONTAL CYLINDER

The reference blockage configuration for the horizontal cylinder is shown in figure 42, where the vertical offset of the cylinder relative to the center of the vertical aperture of the antenna, YOFF, is 5λ. The illumination function for both the vertical and horizontal apertures is a 42-dB Hamming function.

The scattered energy from the horizontal cylinder effectively forms two beams in the principal azimuth plane as discussed in paragraph 3.2. One beam is scattered in the direction of the main beam of the antenna, while the other is scattered at an angle of $180-2\theta$ from the main beam. Both beams are small compared to the main beam, and as a result, the forward beam causes a change in gain, while the scattered beam shows up as a very wide sidelobe, as shown in figure 43. As the antenna continues to rotate away from the center of the cylinder, the scattered beam moves closer to the main beam and begins to rapidly decrease in magnitude as soon as the cylinder is not illuminated by the entire aperture of the antenna.

Looking at figure 43, one might be led to believe that the effects of blockage by a horizontal cylinder are almost insignificant, especially when compared to the effects of blockage by a vertical cylinder. However, this assumption is incorrect. For antennas without steered beams in elevation, the vertical cylinder radiates nearly omnidirectionally in the principal azimuth plane. But the horizontal cylinder scatters the incident energy in the shape of a cone, and thus directs energy over a wide region of space.

Nevertheless, the remainder of this section will attempt to generalize the results obtained in the principal azimuth plane. The parameter which best describes the effects of blockage by a horizontal cylinder is the peak level of the scattered beam shown in figure 43. It is this level which will be

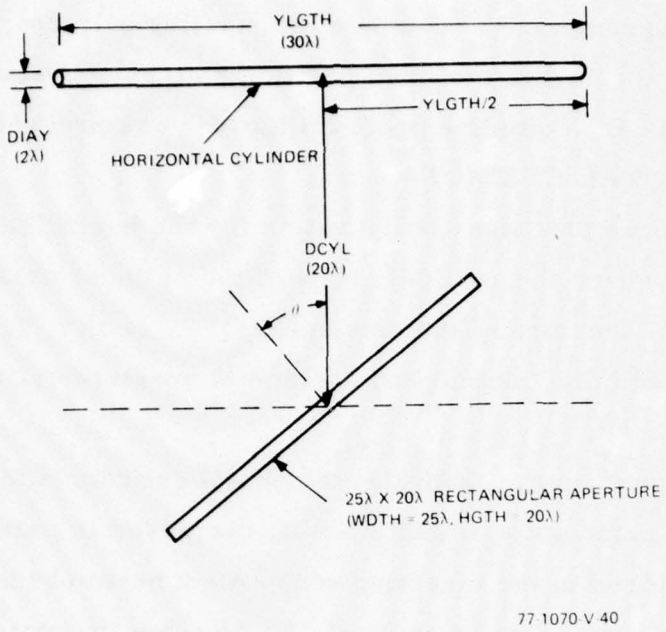

Figure 42. Horizontal Cylinder Reference Blockage Configuration

analyzed to determine the effects of changing the critical blockage variables of figure 42.

Figure 44(a) shows how the peak of the scattered beam varies as a function of the cylinder bearing from boresight for the reference blockage configuration of figure 42. Note that the scattered beam is blocked by the antenna for obstacle bearings close to boresight. The approximate bearing at which the effect no longer occurs is dependent on the geometry of the blockage configuration. One would expect the level of the scattered beam to be approximately constant for increasingly larger obstacle bearings from boresight, until the cylinder is no longer illuminated by the entire projected aperture of the antenna. From this point on, the scattered beam should rapidly decrease in magnitude.

Also, for identical blockage configurations, the magnitude of the scattered beam from a horizontal cylinder at a bearing of zero degrees should be

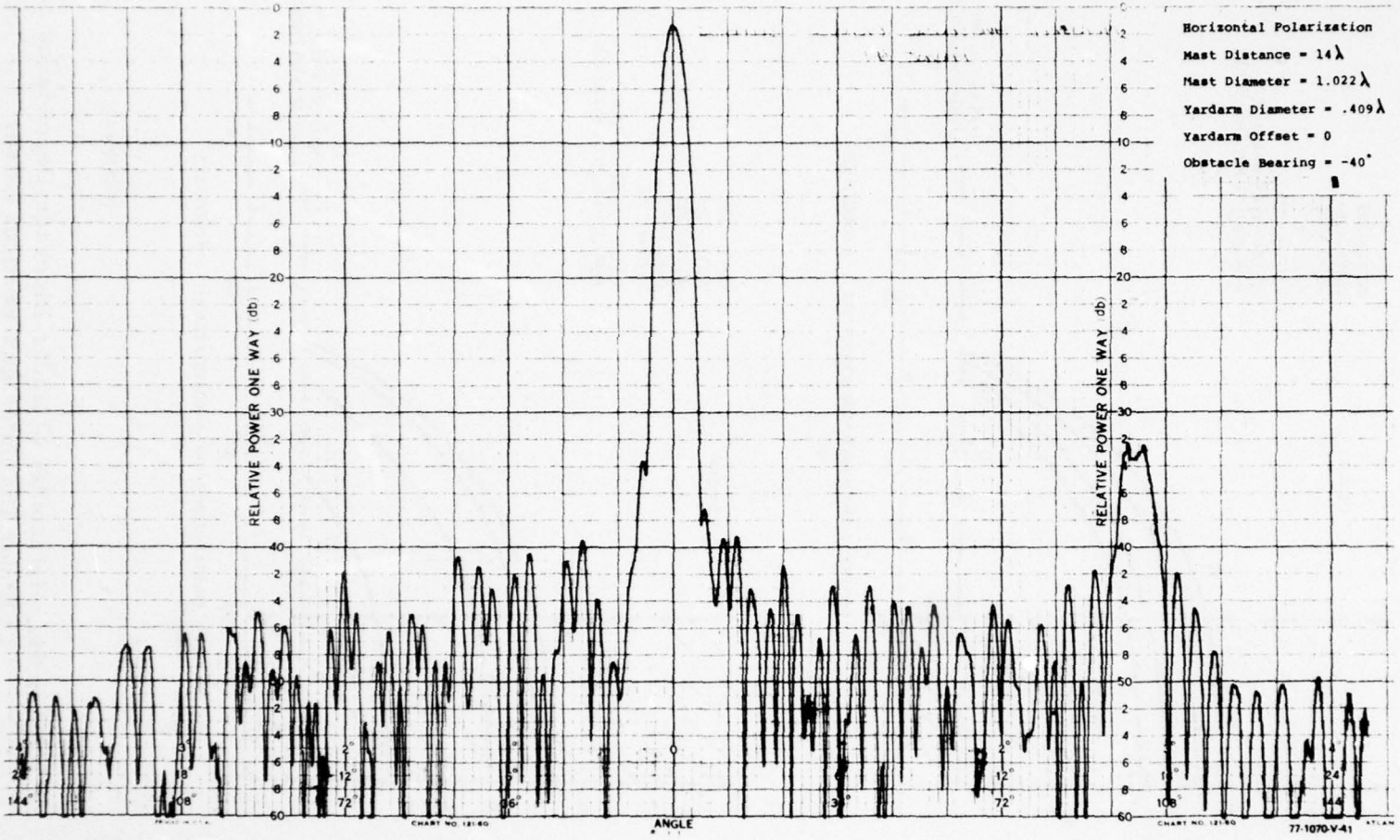

Figure 43. Measured Horizontal Cylinder Blockage, Obstacle Bearing = -40°

77-1070

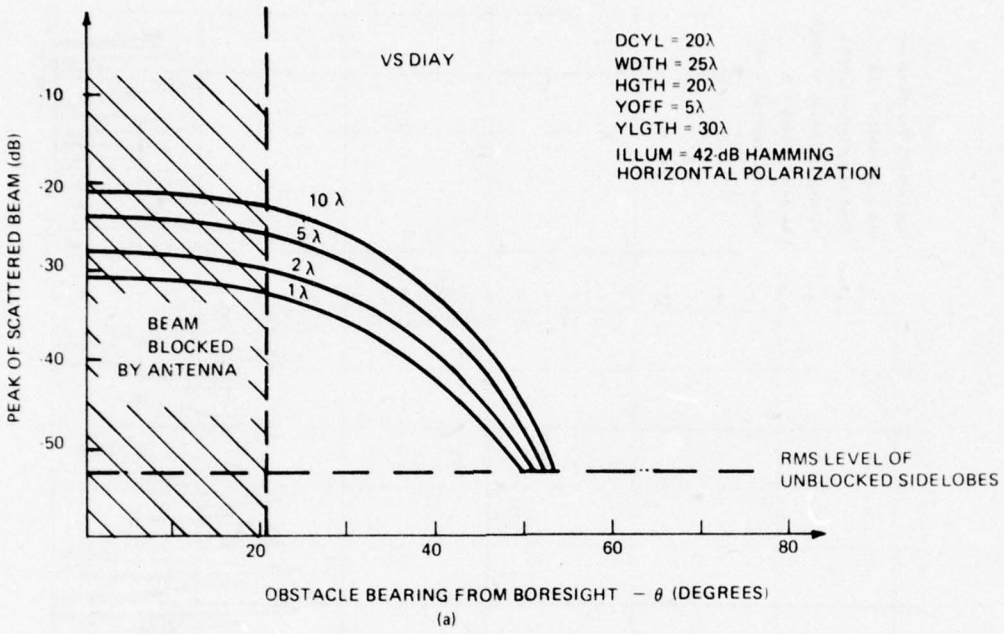

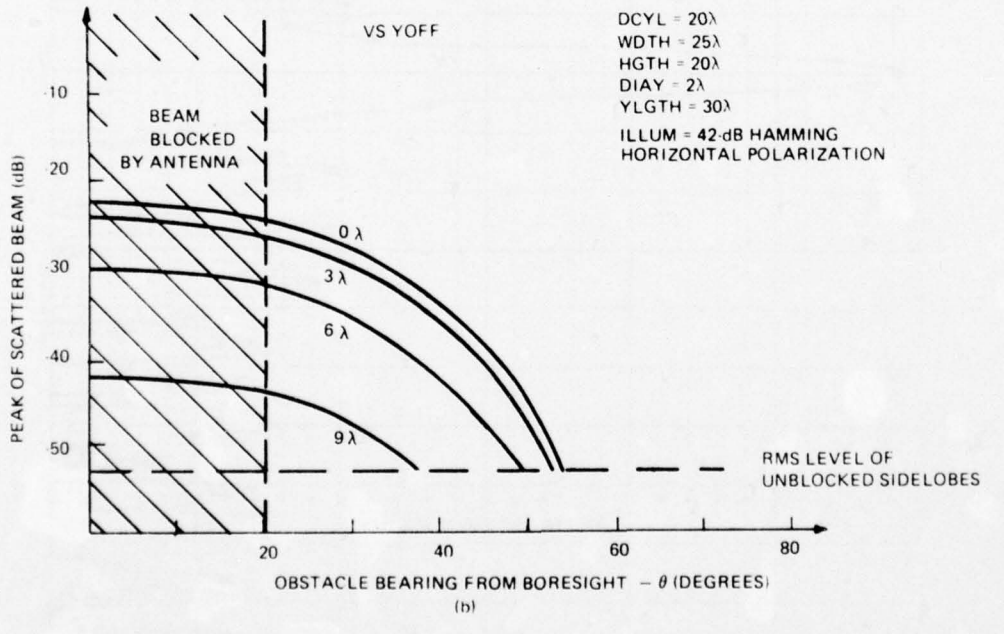

77-1070-V-42

Figure 44. Horizontal Cylinder Blockage Dependence on Cylinder Diameter and Vertical Offset

approximately the same as the rms blocked sidelobe level due to a vertical cylinder at a bearing of zero degrees.

Figure 44(a) reveals the effects of varying the cylinder diameter. Note that the dependence results from the blockage of the vertical aperture by a horizontal cylinder. In other words, the peak level of the scattered beam should vary in a manner closely related to the blockage of a horizontal aperture by a vertical cylinder, as shown in figure 37(a). As one would expect, the bearing at which the antenna no longer blocks the scattered beam is not dependent on the cylinder diameter. Note also that the bearing at which the blockage effects of the cylinder become negligible is not dependent on the cylinder diameter either.

The effects of varying the vertical offset of the cylinder, shown in figure 44(b), are similar to the effects of varying the cylinder diameter. This was expected, since both variables are used only in determining the blockage of the vertical aperture.

The effects of changing the length of the cylinder, however, are quite different, as seen in figure 45(a). As the length is increased, the angular region over which the cylinder is illuminated by the entire aperture of the antenna increases. As a result, the peak level of the scattered beam remains approximately the same over a larger angular region before finally beginning to fall off. Consequently, the bearing at which the blockage effects become negligible also increases. As in the case of varying the cylinder diameter or the vertical offset, the angular region over which the antenna blocks the scattered beam is not dependent on the cylinder length.

Varying the distance between the antenna and the cylinder results in a similar type of dependence as varying the length of the cylinder, as shown in figure 45(b). Increasing the distance between the antenna and the cylinder is somewhat equivalent to decreasing the length of the cylinder, with one exception. For larger distances between the cylinder and the antenna, the

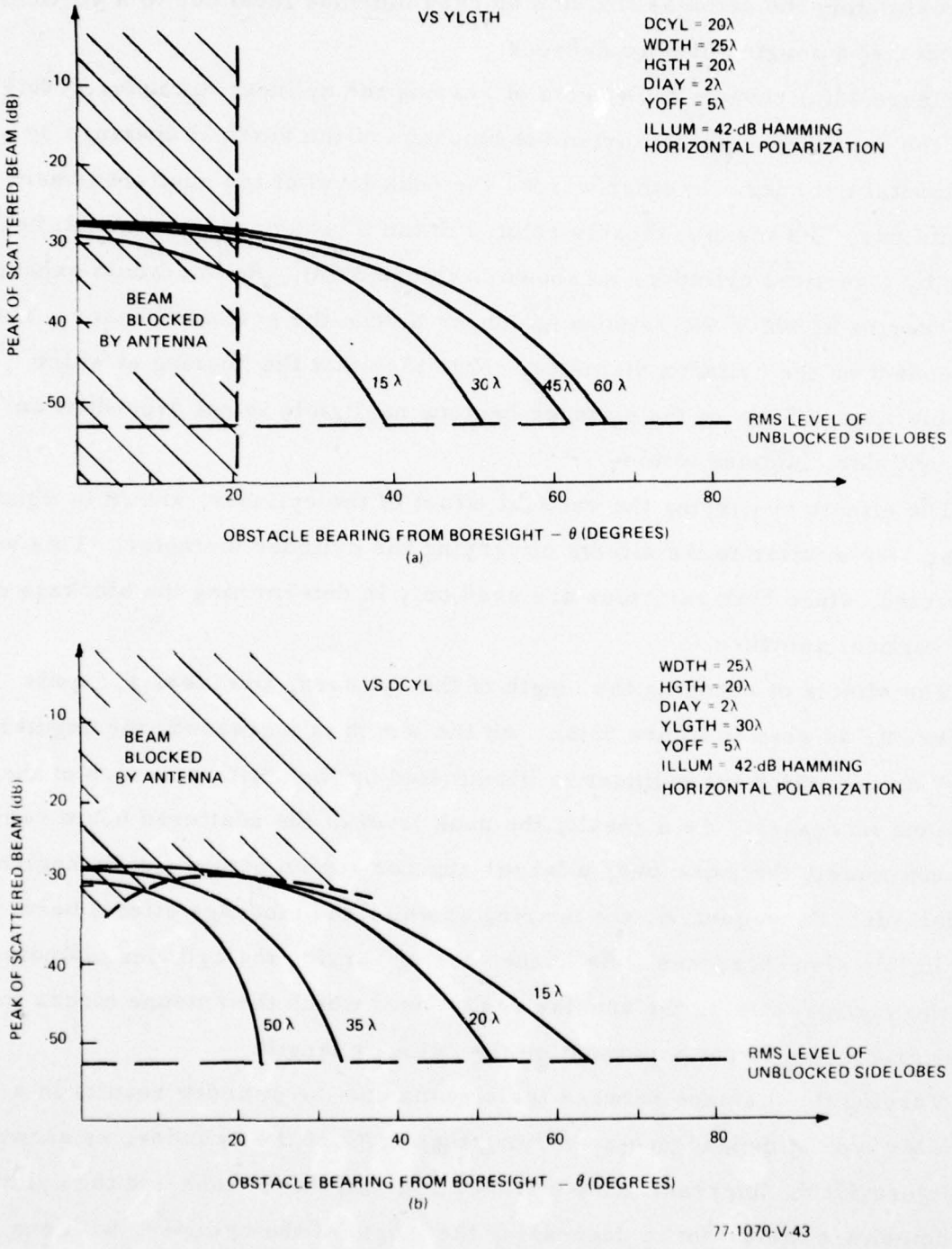

Figure 45. Horizontal Cylinder Blockage Dependence on Cylinder Length and Distance

angular region over which the antenna blocks the scattered beam becomes smaller.

When the blocked antenna is vertically polarized, the results presented in the graphs for horizontal polarization will be approximately 3dB lower. Note that this effect is just the opposite of the result obtained for blockage by a vertical cylinder, as expected.

4.3 FLAT PLATE BLOCKAGE

A number of representative configurations of plate and antenna have been computed to show some general trends in plate blockage. Generally, the parameter which describes the resulting pattern most concisely is the rms sidelobe level, in dB. This parameter is plotted as a function of bearing angle to the blocking plate for different plate widths, separation heights, ranges, and distributions.

In general, the configuration assumed has a 20 wavelength square antenna and blocking plate. They are separated by 100 wavelengths and are the same heights. The plate is perpendicular to the line between antenna and plate. This corresponds to a fixed obstacle as seen when the antenna rotates. Variations from this configuration are indicated on each plot. The computer program computes rms sidelobe level and prints it out, relative to the unblocked peak. In the plots presented here, the sidelobes are referenced to the resultant pattern beam peak.

The effect plate blockage has on different distribution functions is of interest. Figure 46 shows this for -20 dB, -40 dB, and -60 dB Taylor distributions, with 4 equal sidelobes ($\bar{n} = 4$). The curves are similar in some respects to those obtained with the cylindrical obstacle presented earlier. With the plate, the aperture is completely blocked when the plate is at boresight. The rms sidelobe level does not begin to improve appreciably until the trailing corners of the plate clear the mid-aperture projection. Once past this point, the rapid taper of the low sidelobe distribution becomes significant and the rms sidelobe level improves rapidly for the low sidelobe

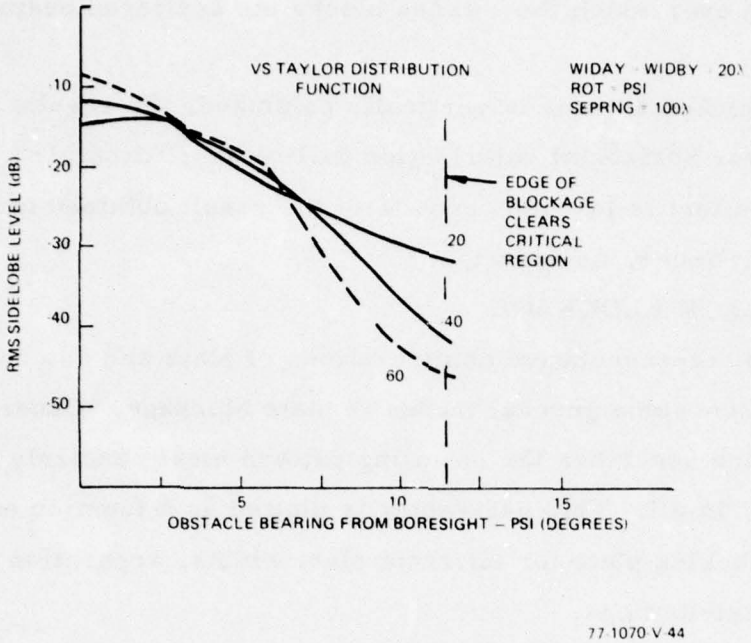

Figure 46. Plate Blockage Dependence on Aperture Illumination

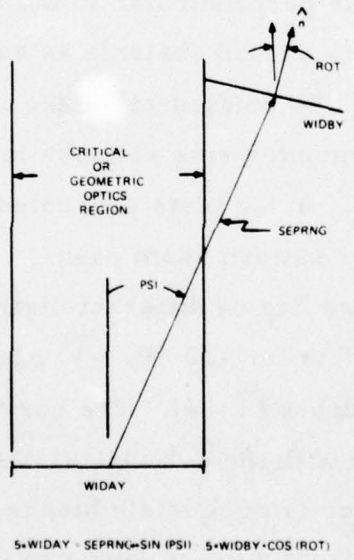

Figure 47. Blocking Plate Clearing Critical Region

distribution. As the plate clears the "critical region", the rms sidelobe level approaches the unblocked level. Clearing the "critical region" in the general case is shown in figure 47. The bearing angle, θ, at which this occurs for the specific case described is found by an iterative solution to the transendential equation

$$10 = 100 \sin \theta - 10 \cos \theta,$$

The solution of which is 11.42 degrees.

Changing blocker width causes the interesting curve shown in figure 48(a). Of interest is the fact that the narrow blockage is worse at boresight. This peaking at 0 degrees bearing angle is because the pattern of the blockage region is so broad, it spreads into the sidelobe region, whereas the wider obstacle pattern is about the same shape as the antenna pattern, consolidating most of its effect within the main beam. The narrower obstacle moves out of the "critical region," described earlier, and thus approaches the unblocked rms sidelobe level at smaller bearing angles.

Figure 48(b) shows the effect of rotating the plate about its own axis. Worthy of note is the high rms sidelobe level at a bearing angle (PSI) of 12 degrees, with the plate rotated (ROT) to 6 degrees. In this configuration, the second bounce off the antenna caused a large sidelobe which shows up in the poor rms sidelobe level.

Offsetting the heights of the plate and antenna shows no surprises in figure 49(a). At 10 wavelengths height separation, the plate is blocking half the antenna. As the blockage shields less of the aperture, the rms sidelobe level improves with the rate of improvement increasing at the mid-blocked condition. At boresight, 10 wavelength height separation, the blockage pattern is very similar to the antenna pattern, but the peak has improved. Thus, the rms sidelobes improve temporarily.

As a function of range in figure 49(b) the rms sidelobe level is degraded out to the "critical angle" which is greater for close obstacles.

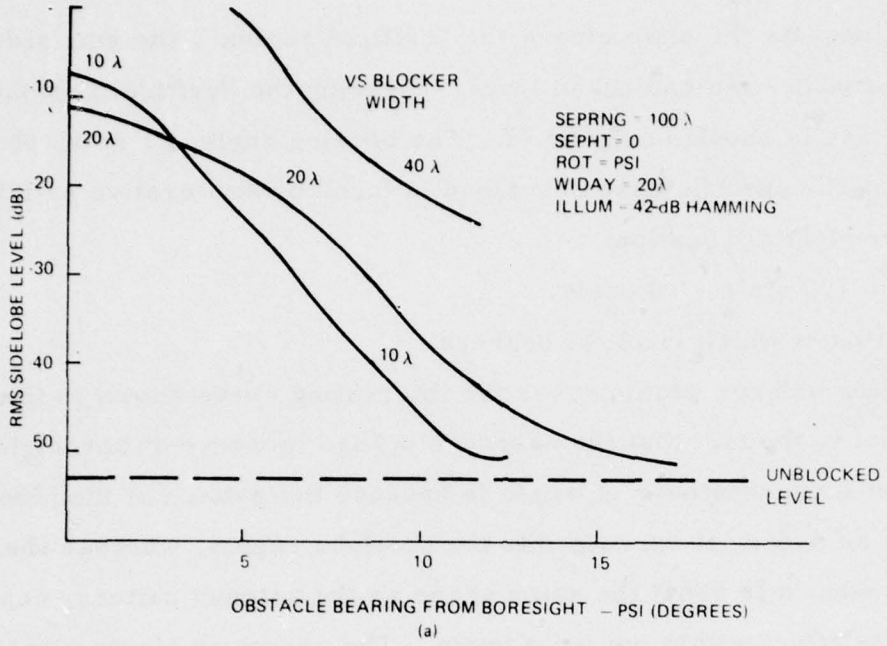

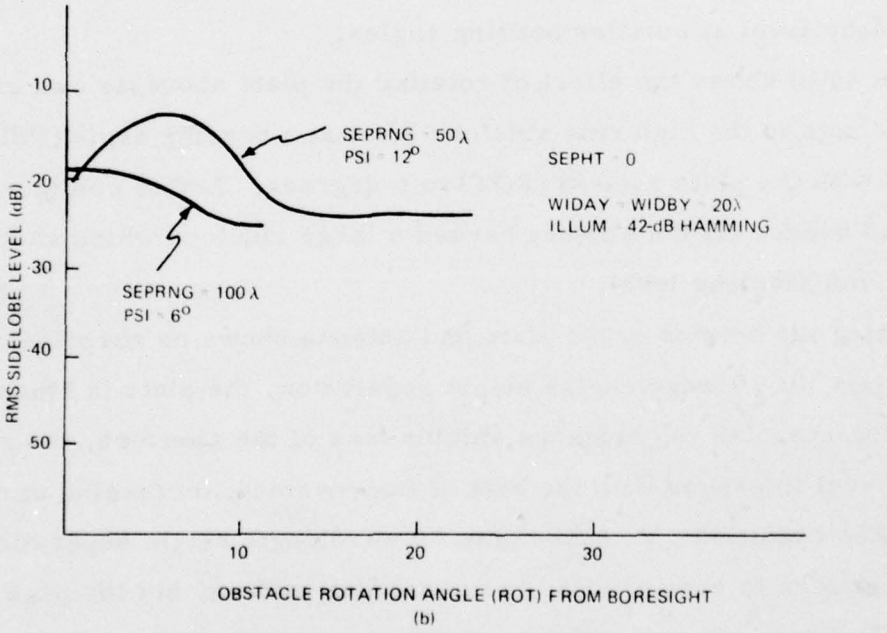

77 1070 V 46

Figure 48. Plate Blockage Dependence on Plate Width and Bearing

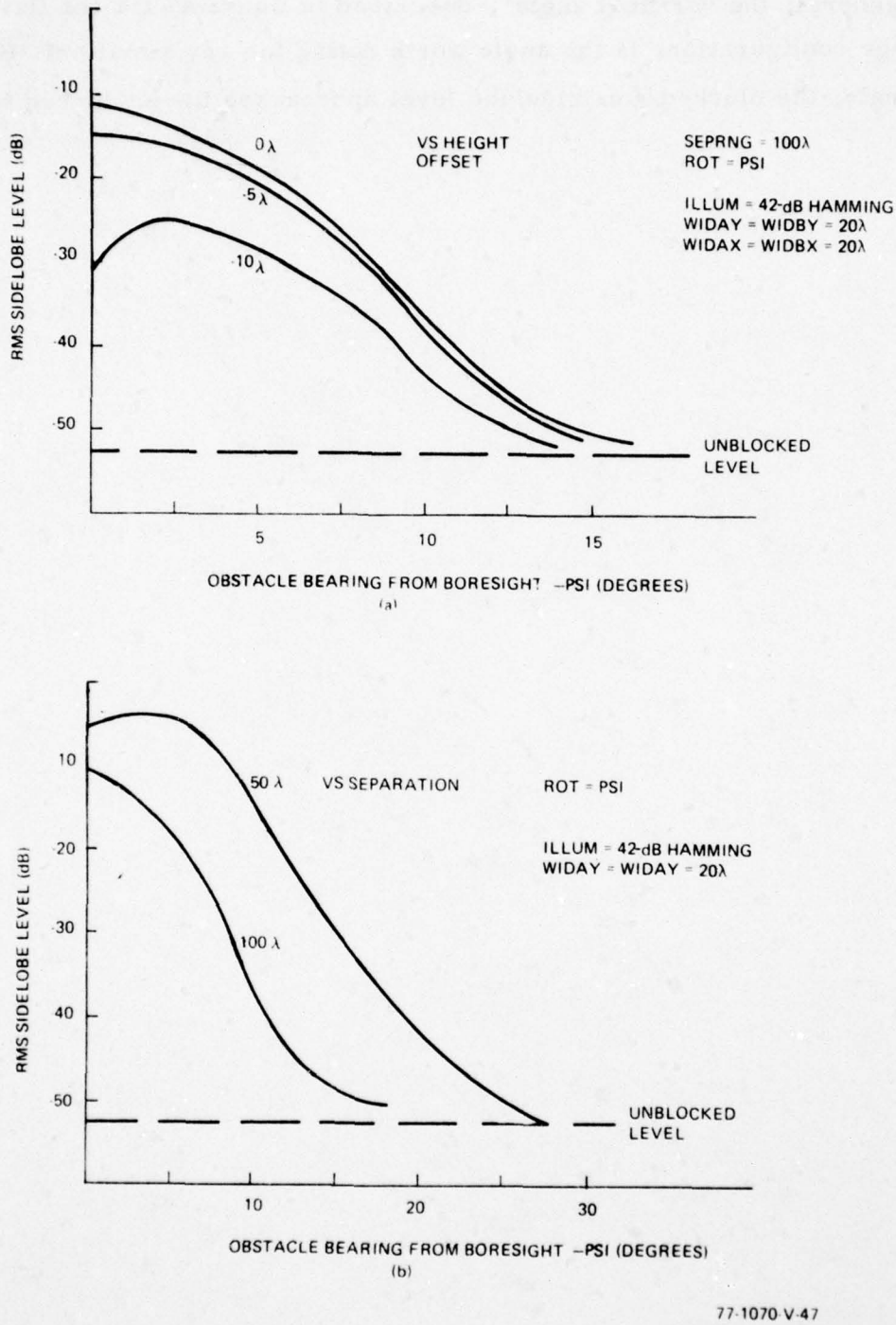

Figure 49. Plate Blockage Dependence on Vertical Plate Offset and Separation

In general, the "critical angle", described in figure 47 for the flat plate blockage configuration, is the angle worth noting for any situation. Beyond this angle, the blocked rms sidelobe level approaches the unblocked level.

5. CONCLUSION

The results of this study, summarized in Section 4, have shown conclusively that an ultra low sidelobe antenna does maintain its superiority over a conventional antenna when placed in a shipboard environment. Not only is the ULSA far superior to its counterpart outside the critical region, when the obstacles are not illuminated, but it also recovers from the effects of the blockage more rapidly than the conventional antenna. This phenomenon is due to the sharply peaked illumination function of the ULSA. By concentrating more of the total power in the center of the aperture, the illumination projected onto the obstacle decreases much faster for an ULSA than it does for a conventional antenna, as the antenna rotates past the obstacle.

As a result, the superior ECCM charteristics of the ULSA are maintained everywhere except in the critical region which spans approximately 70 degrees of the full 360 degrees of rotation for a typical shipboard configuration. Within this region, the two types of antennas will exhibit similar ECCM characteristics. In other words, 80 percent of the time, the radar will receive the full benefits of an ultra low sidelobe antenna, while during the remaining 20 percent of the time, the reduced capability of the system will be no worse than if a conventional antenna was being used.

The analytical phase of the study has produced several computer programs capable of analyzing the blockage effects of three basic shapes -- vertical cylinders, horizontal cylinders, and flat plates -- on the sidelobe structure of an arbitrary antenna. Using these programs, a complex shipboard environment can be successfully evaluated by reducing the actual blockage configuration to a combination of these basic obstacle shapes. The blockage effects of these obstacles can then be analyzed individually to provide quantitative information for a composite blockage analysis.

6. RECOMMENDATIONS

The analytical tools developed during this study have been shown to be valid models in determing the effect of blockage by (1) a vertical cylinder, (2) a horizontal cylinder, and (3) a flat plate. These tools can be used in several ways to learn more about the problems associated with near field blockage of antennas.

The computer programs could be used very effectively to perform a detailed blockage analysis for all the antennas on a particular class of ship already in service. Besides providing a quantitative analysis of the blockage effects for each antenna, recommendations could be made for decreasing the blockage, along with accurate estimates of the resulting system improvement. More specifically, selected "problem sites", known to have serious blockage problems, could be analyzed to determine what steps should be taken to improve the performance of the antenna.

Since structural changes to existing ships are not easily negotiated, perhaps a more practical use of these computer programs would be in the area of new ship design. Using these analytical tools, the locations of the various antennas can be optimized by considering all the antennas at once, rather than siting each antenna separately--a method which usually results in one antenna with insignificant blockage, while the rest are subjected to a maze of obstacles.

Another way in which these programs could be used to more clearly understand the problems associated with near field obstacles would be to expand the programs to include the capability of evaluating parameters other than sidelobe levels, such as cross polarization levels, beam deflection, gain reduction, and changes in beamwidth. Alternatively, new programs could be

developed to analyze other types of obstacles frequently encountered in a shipboard environment.

Perhaps the most challenging way in which the analytical tools developed during this study could be used would be to investigate blockage reduction techniques.

For example, a limited amount of work has been reported in the literature concerning the use of dielectric coatings to reduce the scattering from a cylinder. The model used to describe the infinite cylinder is ideal for considering coatings on the surface of the cylinder, since this is equivalent to adding another boundary condition which must be met by the incident and reflected waves. Thus, the existing computer program could be expanded to include the effects of dielectric coatings without affecting the existing capabilities of the program. An optimum dielectric constant and thickness would be determined for the particular blockage configuration of interest.

To see what the effects of a dielectric coating might be, a thin layer of X-band absorber was wrapped around the 2λ diameter vertical dylinder during the blockage measurements described in Section 2. The effect of this change is shown in figure 50. Coating the cylinder with absorber reduced the level of the scattered energy from the cylinder, and as a result, two changes occur in the blocked pattern. First, the large fluctuations in the sidelobe levels, caused by the reradiation of the scattered energy by the antenna, are significantly reduced. Secondly, the average sidelobe level of the blocked pattern decreases significantly, especially in the far out angles from boresight.

The significant improvement in the blocked sidelobe level of figure 50 seems to indicate that dielectric coatings could possibly be very useful in decreasing the effects of blockage from infinite metallic cylinders. A combined experimental and analytical study in this area would generate results which could be used to significantly reduce the blockage effects of existing sites.

77-1070

95/96

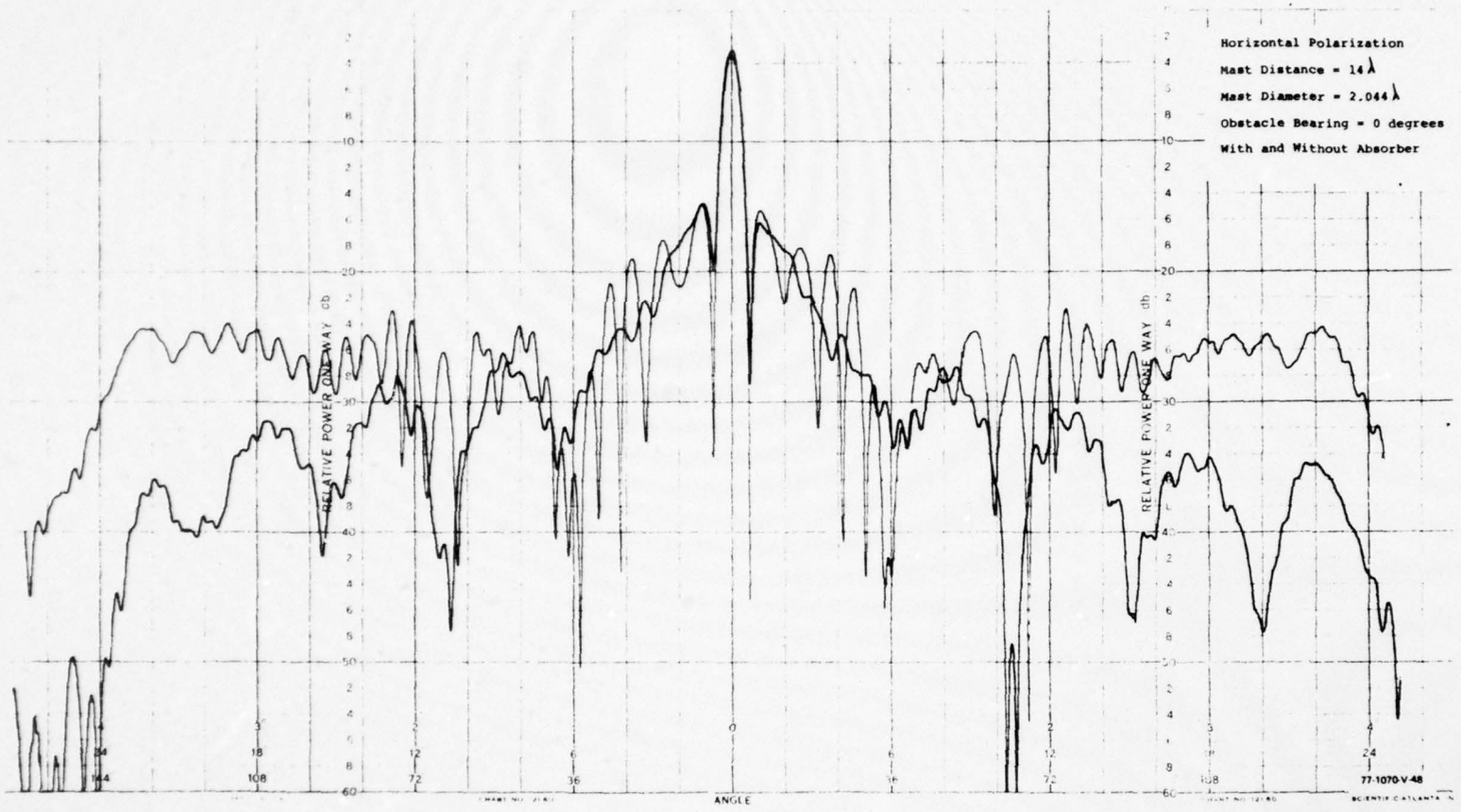

77-1070

Figure 50. Blockage Reduction Due to Absorber

AD-A069 984 WESTINGHOUSE DEFENSE AND ELECTRONIC SYSTEMS CENTER B--ETC F/G 9/5
NEAR FIELD BLOCKAGE OF AN ULTRA LOW SIDELOBE ANTENNA (ULSA). PA--ETC(U)
DEC 77 S G WINCHELL, D DAVIS N00173-77-C-0106

UNCLASSIFIED 77-1070-PT-1 NL

2 OF 2
AD
A069984

END
DATE
FILMED
7-79
DDC

REFERENCES

1. Abramowitz, M., and Stegun, I. A. (Eds.) "Handbook of Mathematical Functions", Dover, N. Y., 1959, Section 9.1.
2. Hissink, A. J., "Radar Antenna with Near-Field Cylindrical Obstruction", Proceedings of the I. E. E. E., vol. 118, No. 2, Feb. 1971, pp 293-300.
3. Hissink, A. J., and Gladman, B. R., "Rapid Generation of Bessel Functions Required for Solutions to Engineering Problems", Electronics Letters, 1970, 6, pp. 265-267.
4. Silver, S., Microwave Antenna Theory and Design, MIT Radiation Laboratory Series, Vol 12, McGraw Hill Book Co., N. Y., 1949, pp 190-192.

APPENDIX A
MEASURED BLOCKAGE PATTERS

I. HORIZONTAL POLARIZATION

* A. UNBLOCKED PATTERN (G) Note: (G) indicates gain measurement.

B. MAST BLOCKAGE PATTERNS

1. 1.022λ Dia. Mast

* a. 14λ Away: 0 (G), 10, 20, 40, 60, 80 Deg.

* b. 50λ Away: 0, 10, 20, 40, 60 Deg.

* c. 100λ Away: 0, 5, 10, 20, 30 Deg.

* d. 135λ Away: 0, 5, 10, 15, 20 Deg.

2. 2.044λ Dia. Mast

* a. 14λ Away: 0(G), 10, 20, 40, 60 Deg.

b. 50λ Away: 0, 10, 20, 30, 40 Deg.

c. 100λ Away: 0(G), 5, 10, 20, 30 Deg.

d. 135λ Away: 0(G), 5, 10, 15, 20 Deg.

3. 2.862 Dia. Mast

* a. 14λ Away: 0(G), 20, 30, 40, 60 Deg.

b. 50λ Away: 0, 20, 30, 40, 60 Deg.

c. 100λ Away: 0(G), 10, 20, 30, 40 Deg.

d. 135λ Away: 0, 5, 10, 15 Deg.

C. MAST/YARDARM BLOCKAGE PATTERNS

1. 1.022λ Dia Mast/0.409 Dia Yardarm, 14λ Away

* a. Yardarm on Boresight: 0(G), 10, 20, 40, 60 Deg.

b. Yardarm up to Aperture Edge: 0, 10, 20, 40, 60 Deg.

2. 1.022λ Dia. Mast/0.409λ Dia. Yardarm, 50λ Away

* a. Yardarm on Boresight: 0, 10, 20, 40, 60 Deg.

b. Yardarm up to Aperture Edge: 0, 10, 20, 40, 60 Deg.

3. 1.022λ Dia. Mast/0.409λ Dia. Yardarm, 100λ Away

* a. Yardarm on Boresight: 0, 5, 10, 20, 30 Deg.

b. Yardarm up to Aperture Edge: 0(G), 5, 10, 15, 20 Deg.

4. 1.022λ Dia. Mast/0.409λ Dia. Yardarm, 135λ Away

* a. Yardarm on Boresight: 0, 5, 10, 15, 20 Deg.

b. Yardarm up to Aperture Edge: 0, 5, 10, 15, 20 Deg.

5. 2.044λ Dia. Mast/0.818λ Dia. Yardarm, 14λ Away

a. Yardarm on Boresight: 0, 20, 40, 60, 80 Deg.

6. 2.044λ Dia. Mast/0.818λ Dia. Yardarm, 50λ Away

a. Yardarm on Boresight: 0, 10, 20, 30, 40 Deg.

b. Yardarm up to Aperture Edge: 0, 10, 20, 30, 40 Deg.

7. 2.044λ Dia. Mast/0.818λ Dia. Yardarm, 100λ Away

a. Yardarm on Boresight: 0, 5, 10, 20, 30 Deg.

b. Yardarm up to Aperture Edge: 0, 5, 10, 20, 30 Deg.

8. 2.044λ Dia. Mast/0.818λ Dia. Yardarm, 135λ Away

a. Yardarm on Boresight: 0, 5, 10, 15, 20 Deg.

b. Yardarm up to Aperture Edge: 0, 5, 10, 15, 20 Deg.

9. 2.862λ Dia. Mast/1.226λ Dia. Yardarm, 14λ Away

a. Yardarm on Boresight: 0, 20, 30, 40, 60 Deg.

b. Yardarm up to Aperture Edge: 0(G), 20, 30, 40, 60 Deg.

10. 2.862λ Dia. Mast/1.226λ Dia. Yardarm, 50λ Away

a. Yardarm on Boresight: 0, 20, 40, 60 Deg.

b. Yardarm up to Aperture Edge: 0, 20, 30, 40, 60 Deg.

11. 2.862λ Dia. Mast/1.226λ Dia. Yardarm, 100λ Away

a. Yardarm on Boresight: 0, 10, 20, 30, 40 Deg.

b. Yardarm up to Aperture Edge: 0(G), 5, 10, 15 Deg.

12. 2.862λ Dia. Mast/1.226λ Dia. Yardarm, 135λ Away

a. Yardarm on Boresight: 0, 5, 10, 15 Deg.

b. Yardarm up to Aperture Edge: 0, 5, 10, 15 Deg.

D. FLAT PLATE BLOCKAGE PATTERNS (19.62λ X 19.62λ)

1. 50λ Away

* a. On Boresight: 0, 10(G), 20, 30 Deg.

* b. 1/2 Aperture Down: 0, 10, 20, 30 Deg.

* c. 1 Aperture Down: 0, 10, 20, 30 Deg.

2. 100λ Away

* a. On Boresight: 0, 10, 20, 30, Deg.

b. 1/2 Aperture Down: 0, 10, 20, 30 Deg.

c. 1 Aperture Down: 0, 10, 20, 30 Deg.

3. 135λ Away

* a. On Boresight: 0, 5, 10, 15, 20 Deg.

b. 1/2 Aperture Down: 0, 5, 10, 15, 20 Deg.

c. 1 Aperture Down: 0(G), 5, 10, 15 Deg.

E. COMPOSITE BLOCKAGE PATTERNS

* 1. 2.044λ Dia. Mast/0.818λ Dia. Yardarm (on Boresight) located 14λ Away, With 19.62λ X 19.62λ Flat Plate located 50λ Away & 1 Aperture Down: 0(G), 10, 20, 30, 40, 50, 60 Deg.

* 2. 2.044λ Dia. Mast/0.818λ Dia. Yardarm (up to Aperture Edge) located 50λ Away, with 19.62λ X 19.62λ Flat Plate located 135λ Away & 1 Aperture Down: 0, 10, 15, 20, 25, 35 Deg.

F. CROSS POLARIZED PATTERNS (Transmit Vert. /Receive Horiz.)

* 1. Unblocked (G)

* 2. 1.022λ Dia. Mast, 14λ Away: 0 Deg. (G)

* 3. 1.022λ Dia. Mast/0.409λ Dia. Yardarm (up to Aperture Edge) located 14λ Away: 0 Deg.

4. 1.022λ Dia. Mast/0.409λ Dia. Yardarm (up to Aperture edge) located 100λ Away: 0 Deg. (G)

5. 1.022λ Dia. Mast, 100λ Away: 0 Deg.

6. 2.044λ Dia. Mast, 14λ Away: 0 Deg. (G)

7. 2.044λ Dia. Mast/0.818λ Dia. Yardarm (up to Aperture edge) located 14λ Away: 0 Deg.

8. 2.044λ Dia. Mast/0.818λ Dia. Yardarm (up to Aperture edge) located 100λ Away: 0 Deg.

9. 2.044λ Dia. Mast, 100λ Away: 0 Deg. (G)

10. 2.862λ Dia. Mast, 14λ Away: 0 Deg. (G)

11. 2.862λ Dia. Mast/1.226λ Dia. Yardarm (up to Aperture edge) located 14λ Away: 0 Deg. (G)

12. 2.862λ Dia. Mast/1.226λ Dia. Yardarm (up to Aperture edge) located 100λ Away: 0 Deg. (G)

13. 2.862λ Dia. Mast, 100λ Away: 0 Deg. (G)

14. 19.62λ X 19.62λ Flat Plate located 50λ Away

    a. On Boresight: 0 Deg. (G)

    b. 1/2 Aperture Down: 0 Deg.

    c. 1 Aperture Down: 0 Deg.

II. VERTICAL POLARIZATION - Refer to list of patterns for horizontal polarization. Any conditions marked with an * were taken in vertical polarization also.